FEATURE EXTRACTION AND CLASSIFICATION OF RADIOGRAPHIC WELD IMAGES

Ph. D. Thesis

by

JAYENDRA KUMAR

**DEPARTMENT OF ELECTRICAL ENGINEERING
INDIAN INSTITUTE OF TECHNOLOGY ROORKEE
ROORKEE – 247667 (INDIA)
DECEMBER, 2018**

FEATURE EXTRACTION AND CLASSIFICATION OF RADIOGRAPHIC WELD IMAGES

A THESIS

Submitted in partial fulfilment of the
requirements for the award of the degree

of

DOCTOR OF PHILOSOPHY

in
ELECTRICAL ENGINEERING

By

JAYENDRA KUMAR

DEPARTMENT OF ELECTRICAL ENGINEERING
INDIAN INSTITUTE OF TECHNOLOGY ROORKEE
ROORKEE – 247667 (INDIA)
DECEMBER, 2018

i

INDIAN INSTITUTE OF TECHNOLOGY ROORKEE
ROORKEE

<u>CANDIDATE'S DECLARATION</u>

I hereby certify that the work which is being presented in the thesis entitled "**FEATURE EXTRACTION AND CLASSIFICATION OF RADIOGRAPHIC WELD IMAGES"** in partial fulfilment of the requirements for the award of the Degree of Doctor of Philosophy and submitted in the Department of Electrical Engineering of the Indian Institute of Technology Roorkee, Roorkee, is an authentic record of my own work carried out during a period from July, 2011 to December, 2018 under the supervision of Dr. S. P. Srivastava, Professor and Dr. R. S. Anand, Professor, Department of Electrical Engineering, Indian Institute of Technology Roorkee, Roorkee.

The matter presented in this thesis has not been submitted by me for the award of any other degree of this or any other Institution.

(JAYENDRA KUMAR)

This is to certify that the above statement made by the candidate is correct to the best of our knowledge.

(S. P. Srivastava)   **(R. S. Anand**)
Supervisor   Supervisor

The Ph.D. Viva-voce Examination of **Mr. Jayendra Kumar**, research Scholar, has been held on ……………………..

Chairman, SRC   **Signature of External Examiner**

This is to certify that the student has made all the corrections in the thesis.

Signature of Supervisor(s)   **Head of the Department**
        Date:

ABSTRACT

In the present scenario of industrialization, welding has become one of the prominent features for any development. Welding is defined as the process of joining the two materials so that the bonding exists between the materials. The welding process gives a permanent joint to the material which is joined together, but it also affects the properties of the constituents. Any kind of deficiency in the welding process gives rise to weld defects. The process of welding generates many flaws such as gas cavity, lack of penetration, porosity, slag, crack, lack of fusion, worm hole, and undercut.

Welded material should be inspected accurately in order to ensure the quality of the design and operation. Reliable welding guarantees safety and reliability. The weld defects are captured by the traditional X-ray imaging. Interpretation of the radiographic weld image is a tedious task and also, it is difficult to distinguish and calibrate a large number of defects. Hence, there exists a need for detection of welding flaws so that the defects can be eradicated and serious damage is averted.

Non – Destructive Inspection is one of the important aspects which are responsible for identifying the weld defects. It is widely used since it detects flaws without damaging the property of the objects. With the advent of computer technology, recent research exerts on finding a technological solution for accurate identification and classification of welding defects. The research for the development of an automatic or semi-automatic system for weld flaws (defects) classification using radiographic images of weld joints has grown considerably in the last decades. Image processing is one of the recent approaches which is being used for the identification and classification of weld defects. But, still there exists a need for an optimal algorithm that holds valid for the entire radiographic weld image database with better classification accuracy. In the present work, an algorithm has been designed to accurately classify weld defects.

The first objective proposed was to develop a weld image database for multi flaws weld images. The second objective was to improve the quality of the radiographic weld images by using noise removal and other pre-processing techniques. Further, the images are segmented to get the information of the interest from the whole images, which was the third objective. The fourth and main objective was to extract the texture features using various basic texture feature extraction techniques, multi-resolution texture feature

extraction techniques and hybrid texture feature extraction techniques on segmented images for classifying them with the support vector machine (SVM) and artificial neural network (ANN) classifier into 9 different categories.

For the purpose of development and validation of the algorithm, an image dataset is a primary requirement. In the present work, the image database has been created from Welding research laboratory, Department of Mechanical and Industrial Engineering, Indian Institute of Technology Roorkee, Roorkee. The images were radiographic in nature and were not in good quality. It is indeed a cumbersome process to analyze a radiographic image to identify the welding flaws. There were in all 79 radiographic images with 8 types of flaws and one without flaws. There were 08 images from gas cavity, lack of penetration consists of 20 images, 16 images have been captured from porosity, 16 images of slag, crack had 11 images, lack of fusion consists of 07 images, wormhole consists of 02 images, and undercut consists of 03 images. Also, 05 images were considered having no defect. The radiographic films obtained from the laboratory were scanned with a high-resolution scanner to convert it in images.

Pre-processing is the first phase of image analysis. The purpose of pre-processing is to improve the quality of the image being processed. Since the images are acquired by the scanner for digitizing so they are in RGB format. Further, they are converted from RGB to gray scale in order to reduce the computational time. All the images obtained were of different sizes. The images were resized according to their region of interest for further processing. Radiographic images have generally salt and pepper noise, impulse noise, random noise etc. caused by natural interventions and sometime during scanning process electronics noise is usually added in these images.

In the present work, the median filter has been used to remove the noise in radiographic weld image and it removes the noise very efficiently here without affecting any relevant information. Afterward, the contrast enhancement has been done by Contrast-limited adaptive histogram equalization method. It enhances the dynamic range of the image-pixel gray level and enhances the contrast.

For Image Segmentation which is a key step in image processing for image analysis, and is essential for the extraction of image features especially for geometrical features. Hence, for getting better accuracy for classification, after pre-processing the images were segmented with various segmentation techniques such as gray threshold,

edge detection, horizontal edge detection using an integral filter, contrast and horizontal response using an integral filter and multilevel thresholding. Thresholding is the simplest method of image segmentation. It was used for changing a gray scale image to binary images. Edge detection algorithms seek to detect and localize edges without any input or interference from humans.

The proposed technique focuses to extract the texture features from the raw image and the segmented images to classify the database into 9 different categories of flaws. Feature extraction is a method of extracting information present in the images. It reduces the amount of resources required to define a large set of data accurately. Features have been extracted using gray level co-occurrence matrices, gray level run length matrices, local binary pattern, uniform local binary pattern, rotation invariant local binary pattern, rotation-invariant uniform local binary pattern, local binary pattern - histogram Fourier features, completed local binary pattern, adaptive local binary pattern, uniform adaptive local binary pattern, rotational invariant adaptive local binary pattern, rotational invariant uniform adaptive local binary pattern and binary Gabor pattern respectively.

Feature extraction has been carried using full feature vector data of the above techniques and also reduced feature vector data. The LBP variants were used for the above purpose. In order to address the issue of image rotation effect, LBPri has been used. Also, LBPu2 is used to reduce the uniformity present in an image pattern. To overcome the disadvantages of the rotational invariant LBPri, the LBPriu2 is used. A detailed description of the result is presented in the chapter.

Further to improve the classification accuracy of radiographic weld flaws DWT based feature extraction techniques have been proposed, where DWT decomposed sub-images have been processed with LBP variants and BGP texture feature extraction to get the tentative features. As DWT has the property to emphasize the directional information of the images, the texture features obtained from these directional sub-images further help to the enrichment of feature vector data, which in turn help in better discrimination of the radiographic weld Images. Amongst, the proposed DWT based texture feature extraction techniques, DWTBGP has yielded the best classification accuracy using ANN with 92.40% using 70/30 ratio of randomly divided database.

The classification accuracy of flaws present in radiographic weld Images, hybrid texture feature extraction techniques has also been proposed where, segmented images

have been processed with GLCM, LBP, LBPu2, LBPri, LBPriu2 and their respective combinations. The proposed hybrid local binary pattern variant texture feature extraction techniques have fetched better classification results.

Eventually, the thesis is concluded with a summary of the work presented in the thesis and also focuses on the scope of future work. An attempt has been made in the thesis to classify the weld images accurately with relatively higher classification accuracy.

ACKNOWLEDGEMENTS

I cannot close these prefatory remarks without expressing my deep sense of gratitude and reverence to my dear parents and mother in law for their blessings and endeavor to keep my morale high throughout the period of my work. I have no words to express the appreciation of my wife Dr. Anumeha, one who inspired me to do research, who stood by me at every moment, keep encouraging me in the low moment and keeping myself free from almost all the liabilities of home issues during my work. Words can hardly explain the cooperation, immeasurable support, and patience of my cute sons Avanish and Abhinav. They boosted me up, made me smile and encouraged me to do hard work. I want to express my sincere thanks to all those who directly or indirectly help me at various stages of this work.

In the end, I bow my head in front of "ALMIGHTY" especially Mahakaleshwar Bholenath, Ujjain and Maa Mahakaali, Jahangira, Sultanganj for blessing me so that I can complete my Ph.D. program.

(JAYENDRA KUMAR)

CONTENTS

LIST OF FIGURES

LIST OF ACRONYMS

1D	One dimensional
2D	Two dimensional
ANN	Artificial neural network
BGP	Binary Gabor pattern
CA	Classification accuracy
CLBP	Completed local binary pattern
CLBP^{u2}	Completed uniform local binary pattern
DWT	Discrete wavelet Transform
DWTCLBP	Discrete wavelet transform based completed local binary patterns
DWTCLBP^{u2}	Discrete wavelet transform based completed uniform local binary pattern
DWTLBP	Discrete wavelet transform based local binary patterns
DWTLBP-HF	Discrete wavelet transform based local binary patterns histogram Fourier features
DWTLBP^{ri}	Discrete wavelet transform based rotation invariant local binary pattern
DWTLBP^{riu2}	Discrete wavelet transform based rotation invariant uniform local binary patterns
DWTLBP^{u2}	Discrete wavelet transform based uniform local binary patterns
FOS	First-order statistics
FFDV	Full feature vector data
FS	Feature selection
FVDN	Feature vector data normalization
GLCM	Gray level co-occurrence matrix
GLRLM	Gray level run length matrix
IDL	Image decomposition level
KNN	K nearest neighborhood
LBP	Local binary pattern
LBP-HF	Local binary pattern histogram Fourier features
LBP^{ri}	Rotation invariant local binary pattern
LBP^{riu2}	Rotation invariant uniform local binary pattern
LBP^{u2}	Uniform local binary pattern
LDA	Linear discriminant analysis
MLP	Multilayer perceptron

MLP-BP-ANN	Multilayer perceptron back- propagation artificial neural network
MRLBP	Multi-resolution local binary pattern
mRmR	Minimal redundancy-maximal relevance
MSB	Most significant bit
NN	Nearest neighbourhood
NoF	Number of features
PC	Principal component
PCA	Principal component analysis
RBF	Radial basis function
RDD	Random divided database
ROI	Region of interest
SVM	Support vector machine
WT	Wavelet transform

CHAPTER 1: INTRODUCTION

This chapter presents the basics of the welding process, non-destructive testing, types of welding defects and the requirement to identify the different defects. At last, the objective of the presented work and organization of the thesis are outlined.

1.1 Overview

Welding is an efficient and economical process to join metals together which is achieved by adding some additional molten joining material on the melting part of the materials to be joined. It forms a strong bond when the molten material is cooled. In industries, It plays a major role for the purpose of construction, joining and repairing of steel beams, reinforcing rods in buildings, bridges, spacecraft, pipelines, nuclear containers, etc. During the process of welding, a number of different types of discontinuities can be present, which may arise due to material inconsistencies, the error produced by the operator, or other factors beyond the operators' control. Irrespective of the source of error, the detection of discontinuities is critical. An unacceptable weld extremely reduces the bond between two materials and may cause failure. With the stress for use of X-ray images modality for examining structure-function relationships, many new challenges have come up, and to meet the same, the development of X-ray (radiographic) imaging has to accelerate even faster. This would be further driven by the fast development of digital computer technology, new methods of extracting in vivo functional and dimensional information, and the persistent approach in establishing localized flaws and development of defects in the weldment.

The manual interpretation of radiographic NDE weld images depends upon the level of expertise of the specialist and is usually a time-consuming process as well as subjective. Image processing plays a vital role to interpret these images with an aim to spot the flaws in the weldment. A semi-automatic system can be introduced by employing different image processing techniques that would provide a consistent system when compared to classical methods. It would also be supportive in drawing a conclusion by employing the use of manipulating tools. The present work has been an effort in the direction of automating the inspection process. [1-7].

1.2   Types of Welding

There are various types of welding process out of which six welding processes [8] are discussed as given below

1.2.1   Arc welding process

Arc welding is the process in which the joining of the metal takes place by the arc developed between the base metal and the electrode. The base metal is connected to the power supply by one end and the other is connected to the electrode. The electrode may be consumable or non-consumable depending upon the weldment to be prepared. The arc usually produces a high temperature i.e. up to 30,000 degrees Celsius.

The process uses a consumable electrode are like shielded metal arc welding, submerged arc welding, gas metal arc welding also known as MIG, electro gas welding and electro slag welding.

The process does not require any consumable electrode or simply non-consumable electrode is tungsten arc welding (TIG), atomic hydrogen welding and plasma arc welding.

1.2.2   Resistance welding process

Resistance welding is the process in which the metal is joined by the heat produced due to the presence of resistance of the two metals being used. It is a type of pressure welding technique in which the pressure is applied between the metals so that its electrical resistance is changed that liberates the heat that is high enough to join the two metal pieces. It does not use any kind of filler metal. It is also of different types like resistance spot, seam welding, etc.

1.2.3   Solid state welding process

It is the process in which the joining of the metal takes place below the melting temperatures of the two metals to be joined. There is no need for the metal to be filled. The compression may or may not be applied for joining the metals. There is a various process that is included in it as ultrasonic, forge and hot pressure welding, diffusion bonding, and friction welding. They are widely used in mechanical industries like in aerospace and marine industries.

1.2.4 Radiant energy welding process

It is the process in which the joining of the metal takes place due to the heat produced when a strong beam of electrons of electromagnetic radiations strikes at the base metal. It is carried out at low pressures or in vacuum pressure. It is two types, i.e., electron beam welding and laser beam welding techniques. It is utilized to produce a straight weld and there exists a high gap between the metals. It gives a clean weld after the completion process.

1.2.5 Thermit welding process

Thermit welding is the process in which the heat is liberated from an exothermic reaction that tends to take place between a metallic oxide and metallic reducing agents. The commonly used metallic oxides are aluminium oxide and iron oxide with a suitable reducing agent that can develop a temperature up to 2400 degrees Celsius which is helpful in the process of welding. It is also known as exothermic welding. It is basically used to join two dissimilar metals..

1.2.6 Oxy fuel gas welding process

It is the type of welding procedure that involves the heat is produced by the reaction of oxygen gas with any fuel gas. There are various fuel gases, but the most common fuel gas is acetylene. So, this process is also known as the oxy-acetylene welding process. The heat generated is so high that the flame temperature reaches up to 3400 degrees Celsius which is high enough to melt the metal and joining of the metal to take place.

In all the welding processes stated there is some type of flaw that takes place in the material. The flaw may arise due to various reasons maybe it is the mistake of the worker, dissimilar properties of the components to be joined, environmental factors, the heat may not be sufficient to join the metals. These all reasons tend to arise the flaws, or we can say defects in the welding.

Also when the weld is completed, the base metal is very hotter at the point of the weld and subsequently along the length away from the point of fusion, the particles have different grain sizes and temperatures. These all properties create a temperature variation or simply a temperature gradient. In various cases, the gradient can result in various defects or we can say flaws.

1.3 Application of Welding

- It is used in various industries like automobile, aeronautical industries for joining the parts of the materials..

- Different method of welding also has different implications like different fields of operation.

1.4 Welding Defects or Flaws

Instead of a smooth joint, sometimes, due to various reasons, during the process of welding, weldments are not joined properly. It results in producing different types of flaws in weldments. The principal welding defects or flaws may be classified as given in [7-8].

1.4.1 Gas cavity

It is the cavity formed in the workpiece due to the entrapment of gases due to the shrinkage of the material at the time of solidification.

1.4.2 Porosity

These are the pores that are formed on the surface of the workpiece due to the trap of the gases. It is basically caused as the gas evolved during the welding process, which does not get enough time for the escape during the solidification process or simply the escape time for the gases is very short.
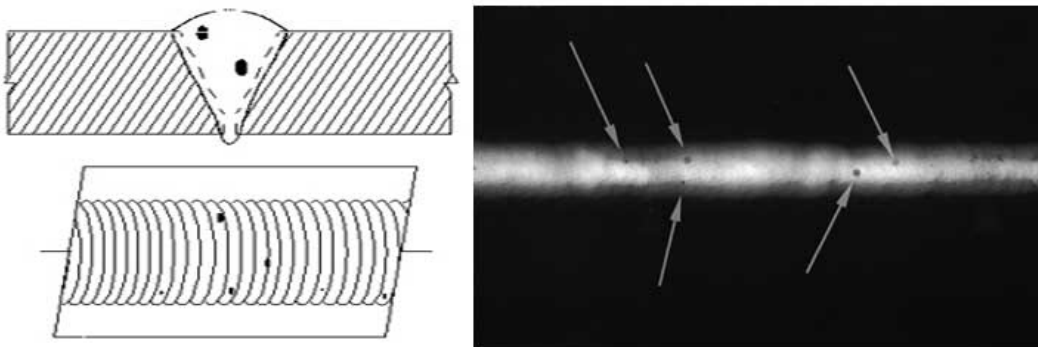
Fig.1.1: Porosity

1.4.3 Lack of fusion

It is the lack of joining of the in the base metal and the weld metal. It is the lack of penetration of the weld metal into the base metal. It is mainly caused by a faulty welding technique, improper use of filler metal on the base metal.

4
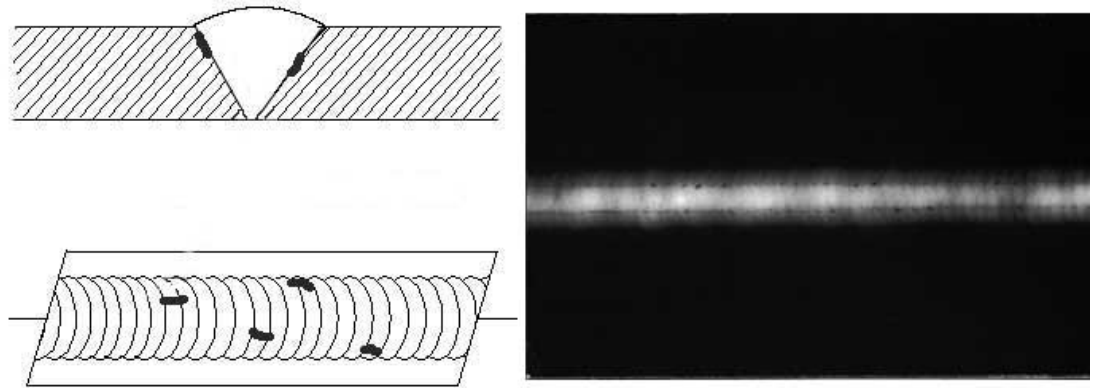
Fig.1.2: Lack of fusion

1.4.4   Lack of penetration

It is the process in which the incomplete penetration of the metal occurs on the workpiece. This may result in the natural stress rising at the point of fusion of the two metals and may develop a crack afterward.
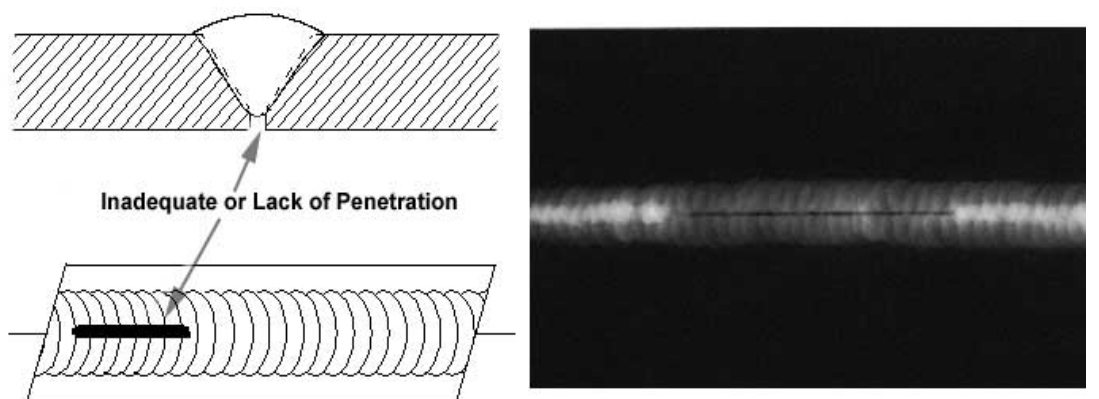
Fig.1.3: Lack of penetration

1.4.5   Wormhole

It is the long tube-like cavities that are formed in the base metal due to the gas entrapped in the metals during the solidification or the cooling of the weld bead. It may be a single or multiple that depends upon the type of the base metal taken. It is caused basically by the irregular workpieces having varied holes on the surface.

1.4.6 Slag inclusion

These are generally the oxides that are trapped in the weld zone. If the shielding during the welding process is not good, the environmental pollutants may also be a part of the slag. These can be prevented by using the correct amount of shielding gases, cleaning the weld surface after the welding process, proper designing of the joint in which the weld has to take place.
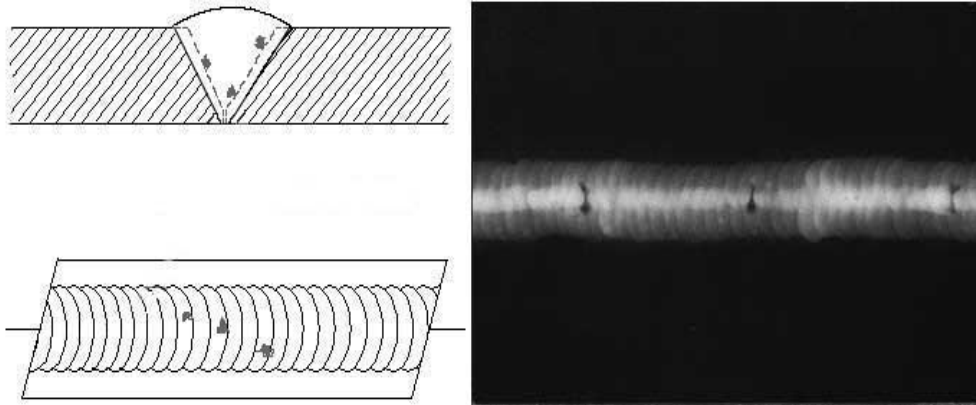
Fig.1.4: slag inclusion

1.4.7 Undercut

An undercut is usually a groove formed near the two metals joining or near the weld and is due to the non-uniform feed of the filler metal.
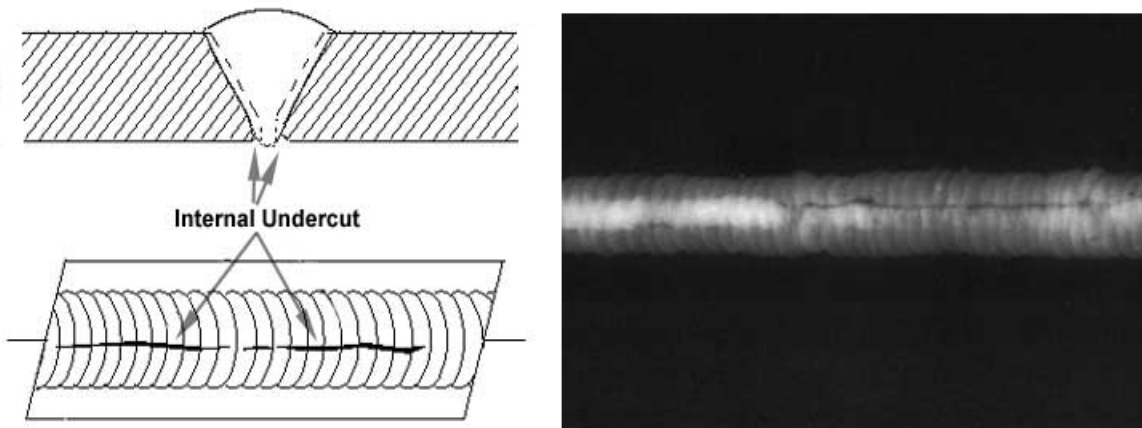
Fig.1.5: Undercut

1.4.8 Crack

The crack is caused on the surface of the workpiece. The crack may be formed in the longitudinal or in the transverse direction. These are generally formed on the surface of the material at the time of the solidification process. These are mainly formed in the workpiece that has irregular grain structures.
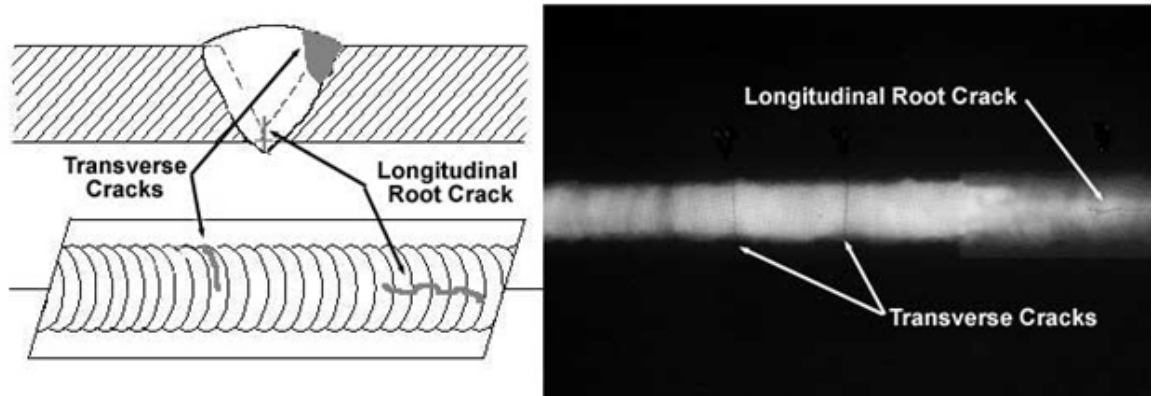
Fig.1.6: Crack

1.5 Testing of Materials

The materials can be basically tested by two types namely destructive and non-destructive testing which is summarized below:

1.5.1 Destructive Testing of Materials

In the destructive testing of material, the material is tested under the load till failure is traced out. The permanent deformation and rupture are caused by the material in it. It is used to test the materials performance and its ability under different loads and dynamic conditions. It is easier to carry out and large information is extracted from it. The test is carried on a large scale and a number of objects where the cost of destructing of material is negligible [9].

1.5.2 Non Destructive Testing of Materials (NDT)

It is the testing of the material in which the material is tested without undergoing permanent damage or deformation. It is the most widely used technique in the industry as well as in research work. NDT has different methods like eddy current, radiographic,

liquid penetration, ultrasonic testing. It has applications in various fields like mechanical engineering, civil engineering, system engineering and medicine [10].

The testing of the materials helps to determine the various properties like strength, hardness, toughness, and various others. The properties mentioned have a significant impact on the usage of the material. So, the testing of the material plays an important role in determining the materials for the application purpose.

1.6 Detecting Flaws Using NDT

It is essential to inspect the manufactured components to detect the presence of any defects or degradation during production, post-production or in-service. Non-destructive testing or evaluation (NDT or NDE) is carried out for protection, proper management, and grave management. It is usually achieved throughout the various phases of manufacture and in service. NDT examination has the advantages of improved speed during inspection and dependability, sensitivity to flaws of any orientation, suited to high operating temperatures. In the last two decades, NDT sciences have witnessed revolutionary progress in radiographical imaging and computerized ultrasonic image processing.

As per the meaning, non - destructive examinations should be non - destructive and non–invasive. Several approaches, as well as techniques, have been established to substantial stages of complexity. They all require the process of apparatus and understanding of results by skilled, and qualified professionals.

It permits the examination without interfering with the use of the final product. Also, an outstanding equilibrium is established among the quality control and finance is established. The term "NDI" comprises many approaches that can be summarized as follows: -

1. Notice internal or external inadequacies
2. Determination of structure, composition, or material properties
3. Evaluation of the degree of geometric characteristics
4. Measurement of the amount of flaw development.
5. Depiction of Severity of the flaws.

It is used in any stage of design of the product's and making a procedure that comprises of a collection of materials, research and development, assembly, quality

8

control, and care. All kinds of difficulties and flaws can be observed in the expansion and use of mechanical devices, electrical equipment, hydraulic systems, etc. Several NDT methods are present to assist the researcher to inspect these dissimilar snags and various defects in an assortment of materials under varying circumstances [11 - 12].

Liquid penetrant (fluorescent inspection), magnetic particle inspection, eddy current testing, radiographic review, and ultrasonic inspection are the several non-destructive inspection methods that exist in the system today.
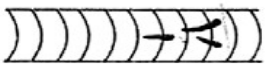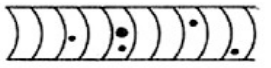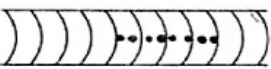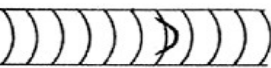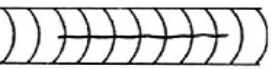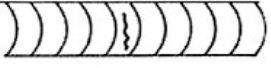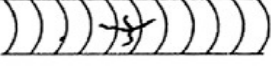
A brief discussion of these methods is presented below:

Expansions in image processing have widely extended the application and utility of NDI methods in the industry [13].

- ▪ **Penetrant Testing (PT)** is also known as Dye Penetrant Inspection (DPI), or Liquid Penetrant Inspection (LPI) or Fluorescent Penetrant Inspection (FPI). Surface breaking flaws can be disclosed by pouring out a coloured or fluorescent dye from the defected region in this method. The capability of a liquid to be drawn into a 'clean' surface breaking flaw by capillary action is the adopted technique for this testing. After a period of infiltration time, excessive surface infiltration is detached and a developer is applied. It results in the penetrant to reveal the flaw.

- ▪ **Eddy Current Testing (ET)** or **Electromagnetic Technique** It is used on conductive materials. Crack detection to the rapid sorting of small components for flaws, size variations, or material variation can be evaluated by this method. Aerospace, automotive, marine and manufacturing industries are the various areas where its use can be found. Eddy currents are induced into the specimen by an energized coil which is brought near the surface of a metal component that tends to oppose the original magnetic field by the current's setup magnetic field. The impedance of the coil in close nearness to the sample is affected by the introduction of the induced eddy currents in the specimen. When the eddy currents in the specimen change its pattern by the existence of the defector due to disparities in the materials, the impedance of the coil is changed. This alteration is measured and showed in such a way that specifies the type of flaws or state of the material.

- *Magnetic testing* also known as **MPI (Magnetic Particle Inspection)** is a technique that is used to find surface and near-surface flaws in steel and iron that belongs to ferromagnetic materials. The flaws are detected on the principle where magnetic lines of flux are distorted due to the existence of flaws in such a way that reveals its presence. The 'flux leakage' is used to detect the flaws. It follows the employment of fine iron particles for the area under inspection. Magnetic particle inspection is mainly used to find surface breaking flaws. It can also be detected to detect sub-surface flaws, but its quality reduces with the rise in depth of flaws.

Table 1.1: Real Images of Radiographs (Types of Weld Flaws in Cross-Section), British standard 1998 [14]

Description	Cross–section of weld	Radiogram
Worm hole		
Linear Slag Inclusion - |		
Gas Pore		
Porosity (Linear)		
Lack of side-wall fusion - (lack of root fusion)		
Lack of inter-run fusion		
Longitudinal Crack		
Traverse Crack		
Radiating Cracks		

- *Ultrasonic Testing* **(UT) -** It helps in mapping the defects and characterizing the three-dimensional coordinates of the defects which is essential to carry out analysis of defect dimensions and hence take a decision for reject/rework/acceptance. UT is a very reliable methodology to establish repeatability and reliability of defects being descaled.

- *Radiography testing* **(RT)** is the commonly used NDT method that notices the interior welding flaws. X-rays pass through metal and other substance that are opaque to ordinary light and thereby produces photographic records by the transmitted radiant energy [13]. Since dissimilar materials absorb X-ray to a different extent, penetrated rays indicate variations in intensity showing the internal structure of a weld. It records the varying degree of absorption of the radiation that penetrates the object on the conventional film radiography. This varying degree of absorption produces a latent image of the object that is inspected on a film that provides the internal details of the object (weldment, in this case). The amount of absorption depends on the thickness, density of the material as well as the absorbers' atomic number. Detectors such as radiography film or a fluorescent screen are used to record the variation in the intensity of the evolving beam as visual images or signals.

Industrial Radiography mainly focuses on recording images on film. Radiography consists of using the penetrations and differential absorption characteristics of radiation energy to examine materials for internet discontinuities. They are produced by high voltage x-ray machines, in which radioactive isotopes produce gamma rays such as Iridium 192 and Cobalt 60. These rays are placed near to the material to be reviewed and are made to pass through the material and are then taken on film. This film is then chemically treated a series of gray shades between black and white forms the end image. Thus, the obtained shadowed image of the object known as a radiograph.

1.7   Literature Review

A framework of classification is used to solve a multiclass problem. Information extraction from radiographic images is used for providing knowledge about it. It will

generate features as classes from the radiographic image, like length, breadth, dimension and so on. Information extraction results can be optimized well enough using multiple databases. The integration of spectral, spatial and structure parameters plays has a vital role in extraction.

The technological developments in the field are presented in a chronological overview of radiographic weld inspection, segmentation and classification methods for information extraction is presented below:

The application of image processing in the field of radiographic images has started from 1990 and still, it's a challenging work for computer vision applications.

In the beginning, Gayer A. et al. [15] developed a method for the automatic inspection of welding defects from real-time radiography which involved two-stage. First and foremost is a fast search, which locates faulty regions, and in the later stage, defects are located with more details. This has been attained by a consecutive similarity detection algorithm also known as the thresholding algorithm. Murakami K. [16] offered a simple algorithm that can automatically detect internal defects and classify them accordingly. The author has classified the types of flaws with the help of an expert system. Features have used the shape, position and intensity level of the defect pattern for the purpose of classification. However, the result attained from this technique is based on the types of defects. The system detects wormholes easily, but detecting cracks is difficult. At the same time, machine vision has been first applied for automatic inspection by Ker J. et al. [17]. Nockeman C. et al. [18] studied the reliability of radiographic weld detection using relative operating characteristics and show that it successfully differentiates between the inspection performance of various equipment or physical detection methods. Kato Y. et al. [19] proposed a computer-aided radiographic inspection expert system for recognizing different types of welding flaws. The identification rules were framed on the expert inspectors' views. The knowledge employed for defect identification is basically of two types: i.e. knowledge gained from a film (in terms of features considered) as well as the knowledge gathered from other than radiographic films.

Wu Z. et al. [20] have exploited histogram shape, object attribute or clustering behaviour, histogram entropy information, spatial context information and local adaptation for such purpose and developed a system using wavelet theory to detect multiscale

12

edges. A clarification system for automated visual inspection for quality evaluation of weldment was developed with the help of a pixel intensity scan by Cook G. E. et al. [21].

Hyatt R. et al. [22] has introduced a multistage method for flaw regions segmentation from the background radiographic images. The technique eliminates the overall background structure but preserves the details of weld defects. A double-threshold method for defects signature segregation was used for the filtered images. The author in [23] has introduced a concept for the extraction of welds from digitized radiographic images. The method was built on the opinion that the intensities of pixels in the weld area possess Gaussian distribution as compared with other areas in the image. This method held true only for segment linear welds. Later, in 1997, the author in [24] has used a multilayer perceptron (MLP) neural network-based process for the detection of a weld. It was applied for the purpose of segmenting both linear and curved welds. Further, the author in [25] has developed a technique that states that the welding flaws give rise to alterations in the overall line profile of a weld. The technique comprises of four parts such as pre-processing, curve fitting, profile-anomaly detection, and post-processing. The obtained result specifies that the technique is able to fetch fair detection and at the same time possess an acceptable false alarm rate. Liao et al. [26] proposed another approach using fuzzy clustering methods. Twenty-five features were selected for each line of the radiographic image. The results showed that fuzzy K-NN outperformed fuzzy c-means.

Further, the authors in [27] have employed fuzzy classifiers, specifically fuzzy K-NN and fuzzy c-means, for classifying the weld patterns. It was used for the segmentation of curved welds and was capable of detecting varying weld flaws in one radiographic image. In the same year, Laggoune H. et al. [28] developed a system of image processing for the geometry characterization of fusion zone based on edge detection using the wavelet transform for multistate edge detection which is based on an algorithm using generalized Canny having good signal to noise ratio.

The author in [29] has developed a human visual inspection method that can identify 60-75% of the signification defects. It has inferred that human inspection of the gas pipeline is hard and problematic job when a great number of welds are involved and identified. Therefore, automation helps to lower the cost of the process and also improves the quality of the inspection. Elewa I. M. et al. [30] assessed the welding defects in

13

radiographs of the gas pipeline using computer vision and developed an algorithm to identify different types of welding defects in radiographic images.

Mery D. et al. [31] used a texture feature for the automatic detection of welding defects. They segmented potential defects edges using Laplacian of Gaussian edge operator. The features of potential defects are extracted next. The features vectors provided by edge detection algorithm, in this case, were based on two features of texture i.e. occurrence matrix and 2D Gabor function.

Siqueira M. H. S. et al. [32] used a radiographic test to evaluate the classification accuracy of the different types of weld defect such as undercut, lack of penetration, porosity, slag inclusion, crack or lack of fusion. For this, the authors have used non-linear pattern classifiers and have used neural networks. The results pointed to an estimated accuracy of around 80% for the classes of defects analyzed. Few filtering aspects were also used to improve the quality of radiographic image quality. Wang Xin et al. [33] compare adaptive wavelet thresholding achieved by using a median filter and it was found that adaptive wavelet thresholding can improve observation of defects better. Silva R. R. et al. used geometrical features for defect classification with nonlinear classifiers and prove that the quality of the features is more important than the quantity [34].

The authors in [35] have introduced a flaw detection algorithm in radiographic weld images by incorporating morphological approach based on pixel characteristics. Valavanis I. et al. [14] proposed a technique for weld defect detection and classification. This uses texture measurements as well as the geometrical features which were given as inputs to the SVM, ANN, and k-NN classifier and found that the accuracy very much depends on the number of features extracted for classification. As reported, the accuracy is very low in the case of cracks, lack of fusion and non-defects. Here only six types of flaws were introduced. The author in [36] proposed a comparison based survey for the suitability of feature extraction methods employed for tungsten inclusion and hotspot detection from weld thermographs. Further, the authors have introduced a knowledge-based model for image interpretation but still, the accuracy is not up to the mark. Jebarani Sargunar P. N. J. et al. [9] developed the Gaussian mixture model (GMM) classifier for weld defects. Vilar R. et al. [37] has defined a system for weld defects classification by using adaptive-network-based fuzzy inference system.

14

Zapata J. et al. [38] has developed a system to notice, recognize and classify welding defects in radiographic images. Further, the performance was evaluated for two neuro-classifiers based on an artificial neural network (ANN) and an adaptive-network-based fuzzy inference system (ANFIS). The accuracy was 78.9% for the ANN and 82.6% for the ANFIS. This methodology was tested on 86 radiograph images that consist of 375 defects having five types of flaws.

In the above context, the present work has contributed in the direction for the application of image processing methods for extracting information in radiographic images. Till date, several research works are underway for detection, feature extraction, and classification of all the relevant information. The proposed work aims to improve the process of automated information extraction systems.

Wang G. and Lion T.W. have used Fuzzy k-nearest neighbor, multi-layer perceptron neural network classifiers and bootstrap method for classifying 6 defect types by extracting 7 features [39] and 12 features. [40]. Also, Gray level Peak value was considered for trough and slant-concave fitted line profiles of weld images. For further increasing the classification accuracy using the sequential forward search strategy and the random search strategy approach. Also, Ant colony optimization (ACO)-based algorithms, nearest mean, k-nearest neighbor, fuzzy k-nearest neighbor, and center-based nearest neighbor were employed [25] − [41]. Further, the author in [42] has employed the use of An adaptive-network-based fuzzy inference system (ANFIS) where 5 defect types were identified by extracting reducing the features to 04. [37]. Further, Senthil Kumar et al. used CCD camera-based images for their defect classification. In this work, the Gray level value was considered for classifying four defect types. They employed the use of Artificial neural network (ANN) with back propagation (BP) [43] and also ANN with differential evolutionary algorithm (DEA) [44] separately thereby achieving accuracy of 90% - 95%.

Further, the author in [45] has detected feature point index in weld defects by using Support vector machine (SVM) technique and Hough transform. Also, 04 features were extracted by using in the defect information such as area, perimeter, width and minimum bounding rectangle using the neighborhood boundary chain code (BCC) algorithm [46]. Acceptance decision algorithms (ADA) was developed by E.S Gadelmawla et al. in [47] to identify 11 defect types and 3 shape defects with only 03 features in gas pipeline weld

images. Also, Fuzzy pattern recognition EM and FCMI algorithms using the Average grayscale level and variance of the detected area [48 - 49]was developed.

R.R. da Silva et al. [50-52] has used a Hierarchical and non-hierarchical linear classifier using a neural network technique for detecting 5 types of defects such as lack of fusion, undercuts, slag inclusion, porosity and lack of penetration using six different features. The authors have also used nonlinear pattern classifier with neural networks, statistical interference techniques with random selection data with (Bootstrap) and without repositioning for classifying 5 defects by extracting 4 and 5 features respectively.

A multi-layer perceptron (MLP) neural network-based algorithm was fed to 25 extracted features for identifying 6 weld defects in [53]. Several feature extraction techniques were employed by gathering the information about Local entropy, Joint entropy and Relative entropy using 2-D histogram and grey level histogram in [54]. Background Subtraction Method (BSM), and Region Growing Method (RGM) was used for weld defect identification in [55].

With the advancement of technology and the use of several concepts, decision tree, and multi-layer perceptron's for surface quality analysis was used in [56]. The decision tree and mixed fuzzy rule formation for defect detection of car body panel weld defects were done in [57 - 61]. Here, both neural network, Bayesian classifier [62] and SVM have been used as classifiers in order to increase accuracy. Pattern recognition using a vision system and neutral network using Shape matching properties for correction of defects have been extensively used in [63 - 65]. Signal processing transforms such as Hilbert Transform [66] and Cimmino's and Simultaneous Algebraic Reconstruction Technique [67] have been used for identifying defects.

1.8   Research Gap

The following research gaps have been identified.

1. Radiographic weld images are low contrast, dark and contain high noise. It becomes difficult to detect the defects properly with the noise in images. Hence, image enhancement is a noteworthy part of automated defects detection in weld images. As presented in the state of art, the transform-based filters are mostly used to remove the noise in weld images. It removes the impulse noise effectively.

However, it is less efficient to preserve the sharp transition of the defects and degrades the resolution. Also, it is not effective to remove other types of noises.

2. Image features play a key role in the classification of weld flaws. Geometrical features are widely used for classification of weld flaws whereas, texture feature has not been much explored till now. There is a scope to extract texture features using various texture feature extraction techniques such as Gray level co-occurrence matrix (GLCM), Local Binary Pattern (LBP) and its variants.

3. There are less works reported in the literature, concentrated on weld flaws classification using ANN, SVM, and ANFIS. In a recent published paper, the accuracy has not been up to the mark and also not all types of weld defect have been addressed. The accuracy of weld flaws classification gets affected, especially between cracks and lack of fusion [14]. Hence, there is a scope to classify all possible weld defects flaws for the particular data set containing all types of flaws.

1.9 Objectives of the Thesis

Based on the research gaps, the following objectives were defined for carrying out the present research work.

1. Create a weld image database for multi flaws weld images.
2. Improving the quality of the radiographic weld images by noise removal and other preprocessing techniques
3. Appropriate application of image segmentation techniques for proper Identification of the flaws.
4. Extracting the various texture features of the images with and without segmentation and classifying them with the different classifiers in order to classify the different weld flaws present in radiographic images into 9 different categories as per the database with improved accuracy..

1.10 Organization of the Thesis

The first chapter gives an introduction to welding. A brief description has been presented. It also includes a brief description of the types of welding defects, NDT technology and the motivation for carrying out the present work. Also, a glance of the

literature reviewed for carrying out the research work is presented with research gaps and the research objectives for carrying out the research work. In the present work, the image database has been obtained from Welding Research and NDT laboratory, Department of Mechanical and Industrial Engineering, Indian Institute of Technology Roorkee, Roorkee.

In the subsequent chapter, pre-processing, and the contrast enhancement techniques have been carried out for improving the image quality for analysis. Further, feature extraction using Gray level co-occurrence matrices, Gray level run-length matrices, Local binary pattern, Uniform local binary pattern, Rotation invariant local binary pattern, Rotation Invariant Uniform Local Binary Pattern, Local binary pattern histogram Fourier features, Completed local binary pattern, Adaptive local binary pattern, Uniform Adaptive local binary pattern, Rotational Invariant Adaptive local binary pattern, Rotational Invariant Uniform Adaptive local binary pattern and Binary Gabor pattern respectively have been discussed. Feature extraction has also been carried using full feature vector data of the above techniques and reduced feature vector data using Principal Component Analysis.

Further to improve the classification accuracy of radiographic weld flaws DWT based feature extraction techniques have been proposed: where DWT decomposed sub-images have been processed with LBP variants and Binary Gabor Pattern to get the tentative features for classification has been discussed in chapter no 3.

Chapter 4 deals with hybrid texture feature extraction techniques; where, segmented images have been processed with GLCM, LBP, LBPu2, LBPri, LBPriu2 and their respective combinations.

Eventually, it is concluded with a summary of the work presented in the thesis and also focuses on the scope of future work. An attempt has been made in the thesis to classify the weld images accurately with relatively higher classification accuracy.

CHAPTER 2:   TEXTURE FEATURE EXTRACTION TECHNIQUES

This chapter explores the various texture features extraction techniques for the classification of flaws in radiographic weld images. It gives a concise description of the various existing feature extraction techniques for the proposed database.

2.1   Texture Feature Extraction Techniques

Texture features [68-76] plays a vital role in the classification of the image database. In the present work, some widely used texture feature descriptors [77, 68] are employed and their effectiveness for the classification of weld flaws images has been studied. The following are the texture feature extraction techniques discussed in this chapter.

1. Gray level co-occurrence matrices (GLCM)
2. Gray level run length matrices (GLRLM)
3. Local binary pattern (LBP)
4. Uniform local binary pattern (LBPu2)
5. Rotation invariant local binary pattern (LBPri)
6. Rotation Invariant Uniform Local Binary Pattern (LBPriu2)
7. Local binary pattern histogram Fourier features (LBP-HF)
8. Adaptive local binary pattern (ALBP)
9. Completed local binary pattern (CLBP)
10. Binary Gabor pattern (BGP)

The brief description of each of the techniques is presented in the following subsections:

2.1.1   Gray level Co-occurrence Matrix (GLCM)

The GLCM was introduced by Haralick et al., [78] which has been extensively used to extract texture features of grayscale images. In this technique, a statistical descriptor, co-occurrence matrix is generated, which is a measure of how often a different combination of pixel gray values with specified distance and orientations occur in an image. The GLCM [79] based features offer an advantage compared to the texture information computed using the histogram, as they don't carry any information about the relative position of the pixels with respect to each other.

Consider entry in 'G' represents the number of times a pixel with gray level 'I' is adjacent to a pixel with gray level 'j'. The GLCM technique considers different spatial distance and 4 directions (i.e., 0°, 45°, 90°, and 135°) which is used to generate GLCM matrices. Thereafter, second-order statistical texture features are computed from the GLCM matrices. In total, 18 features of GLCM have been investigated here, which consist of 13 features proposed by Haralick et al. [78] and 5 features proposed by Soh and Tsatsoulis [80], and are listed in Table 2.1. The detailed mathematical description of each of the features is available in [78, 80, 81].

A simple image below describes the GLCM feature extraction process in Fig. 2.1.
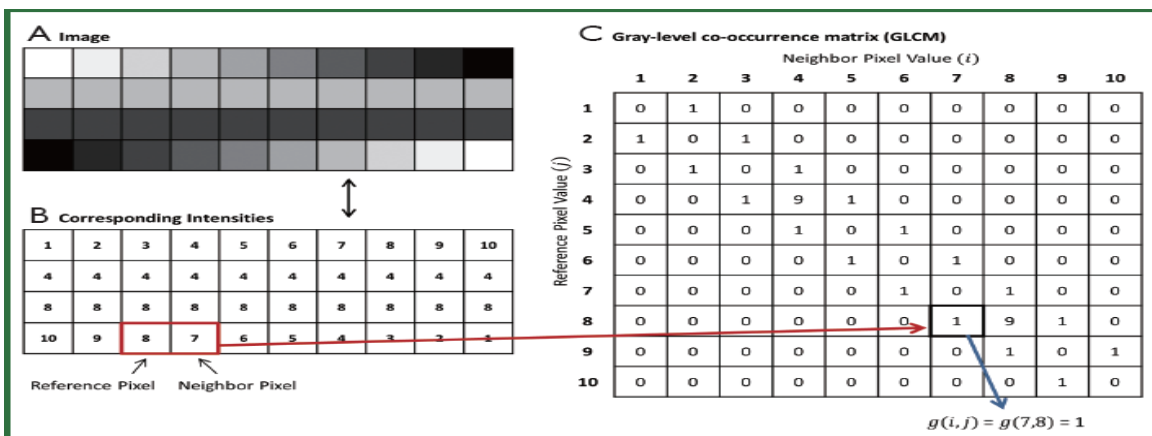
Fig. 2.1: GLCM feature extraction process

Table 2.1: Second-order statistical texture features calculated from GLCM.

Sr.no.	Features	Sr.no.	Features
1	Angular second moment (f1)	10	Difference variance (f10)
2	Contrast (f2)	11	Difference entropy (f11)
3	Correlation (f3)	12	Information measure of correlation1 (f12)
4	Sum of squares(variance) (f4)	13	Information measure of correlation2 (f13)
5	Inverse difference moment (f5)	14	Autocorrelation
6	Sum average (f6)	15	Dissimilarity
7	Sum variance (f7)	16	Cluster shade
8	Sum entropy (f8)	17	Cluster prominence
9	Entropy (f9)	18	Maximum probability

2.1.2 Gray Level Run Length Matrix (GLRLM)

A higher-order statistical texture feature measure technique known as Gray level run length matrices was proposed by Galloway [82]. It generates 2D matrices having elements, where 'L' is number of gray level; 'R' stands for the longest run. Each element of GLRLM matrices has information about number of times the original image has run of length 'j' of gray level intensity 'i' in the given direction. The statistical texture features of higher order computed from GLRLM matrices are listed in Table 2.2.

Table 2.2: statistical texture features calculated from GLRLM.

Authors	Sr. No.	Features
Galloway	1	Short runs emphasis (SRE)
	2	Long runs emphasis (LRE)
	3	Gray level non-uniformity (GLN)
	4	Run length non-uniformity (RLN)
	5	Run percentage (RP)
Chu *et al.*,	6	Low gray level runs emphasis (LGRE)
	7	High gray level runs emphasis(HGRE)
Albregtsen	8	Short run low gray-level emphasis (SRLGE)
	9	Short run high gray-level emphasis (SRHGE)
	10	Long run low gray-level emphasis (LRLGE)
	11	Long run high gray-level emphasis (LRLGE)

2.1.3 Local Binary Pattern (LBP)

The LBP is an overwhelming texture descriptor strategy for image analysis because of its discriminative information representation capacity (Ojala et al., 1994 [83-84]). The application zones where LBP has appeared potential object identification, face recognition, demographic classification, and so on. It is viewed as a simple, yet computationally productive [84-87]. A circular neighborhood of variable size was proposed in [88] to conquer the deficiency of the original LBP operator of neighborhood measures that can't catch the predominant texture features in huge scale structures.
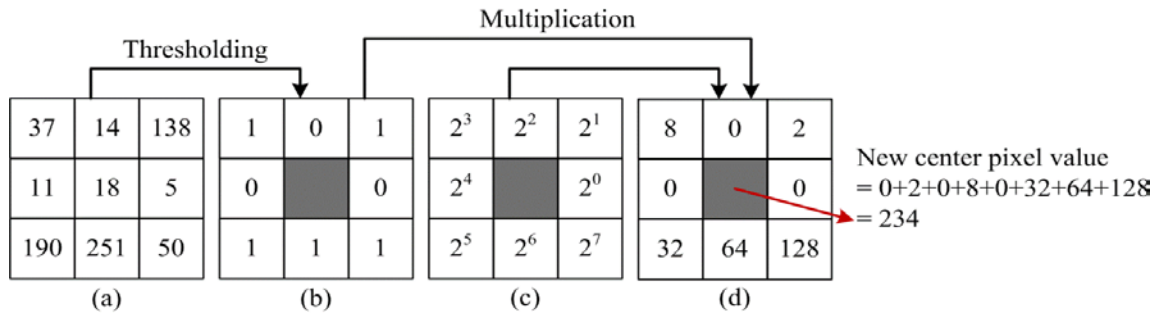
Fig. 2.2: The LBP computation process

a) 3×3 local window image, (b) thresholding,(c) weight and d) new center pixel value (decimal).

The LBP of an image with centre pixel coordinates (x, y) is given by [88]:

$$LBP_{P,R}(x,y) = \sum_{p=0}^{P-1} s(g_p - g_c))2^p$$

where, g_c and g_p, are the gray value of the centre pixel and its p neighbors, respectively. Also, $s(z) = \begin{cases} 0, & z < 0 \\ 1, & z \geq 0 \end{cases}$ it signifies a thresholding function.

In $LBP_{P,R}$, P represents a number of sampling points on the roundabout neighborhood, while R the resolution of the spatial goal of the area. Bilinear interpolation is connected to pixel values if the sampling points are not part of integer coordinates. The LBP operator produces a 256-dimensional texture descriptor for a given image. The pictorial representation of the calculation of new center pixel value for LBP is shown in fig 2.2.

2.1.4   Uniform Local Binary Pattern (LBP^u2)

The LBP designs are said to be uniform examples if at most 2-bit wise transition (1 to 0 or 0 to 1) is accounted for in the circular binary pattern of LBP [88]. The histogram includes a separate bin for uniform patterns and just a single bin is assigned to all the non-uniform patterns. For a given pattern of P bits, P(P-1)+3 bits are generated. The decrease in the non-uniform pattern is because of the way that in com natural images the LBP patterns are generally uniform. Further, uniform patterns of texture represent about 90% of the whole pattern with (8, 1) neighborhood and near 70% for (16, 2) neighborhood [89]. The LBPu2 produces 59-dimensional surface descriptors.

22

2.1.5 Rotation Invariant Local Binary Pattern (LBP^{ri})

The rotation of an image results into various LBP codes. To address the issue of the image rotation impact, LBP^{ri} has been proposed [88, 90, 91]. In this way, to make every one of the adaptations of parallel codes the equivalent, the LBP codes are turned back to reference pixel position to invalidate the result of interpretation of a pixel location. The LBP$_{P,R}^{ri}$ is created by circularly turning the fundamental LBP code and considering the pattern which has a base an incentive as given by [88, 90,91]:

$$LBP_{P,R}^{ri} = \min_{i}\left\{ROR\left(LBP_{P,R},i\right)\right\}$$

where, $i = 0, 1, 2, \ldots, P-1$. The circular bit-by-bit right shift activity is performed on x (a P-bit number) for i times by the function $ROR(x, i)$. The LBP$_{P,R}^{ri}$ descriptor produces in general 36-bin histograms for each image due to 36 different, 8 bit rotation invariant codes [90, 91].

2.1.6 Rotation Invariant Uniform Local Binary Pattern (LBP^{riu2})

The LBP$_{P,R}^{riu2}$ was proposed to reduce the disadvantage of LBP$_{P,R}^{ri}$ (poor performance because of crude quantization of angular space at 45°) [90].

A pattern is known as "uniform" if the uniformity value $U \le 2$, and defined as:

$$U(x) = \sum_{p=0}^{P-1} F_b\left(x \oplus ROR(x,1), p\right)$$

where, b stands for binary numbers. Given a binary number x, the circularly consecutive binary bits b are obtained by:

$$F_b(x,i) = ROR(x,i)\cdot\left(2^b - 1\right)$$

The logical operators "XOR" and "AND" are denoted by '$\oplus$' and '$\cdot$' (dot) operator, respectively and for a given bit sequence, i indicates the index of least significant bit (LSB). The rotation of uniform codes towards their minimum value generates $(P+1)$ patterns. Merely counting the number of one's in the "uniform" patterns, binary number generates LBP$_{P,R}^{riu2}$ pattern code. The other patterns are marked "miscellaneous" and grouped into a single value as given by:

$$LBP_{P,R}^{riu2} = \begin{cases} \displaystyle\sum_{p=0}^{P-1} s\left(g_p - g_c\right) , & U\left(G_P\right) \leq 2 \\ P+1 & , otherwise \end{cases}$$

The $LBP_{P,R}^{riu2}$ produces 10-bin histograms.

2.1.7   Local Binary Pattern Histogram Fourier features (LBP-HF)

A rotation invariant LBP-HF protects the most discriminative qualities is obtained by taking the discrete Fourier transform (DFT) of [92, 93]. It is developed comprehensively for the whole image contrasted with other histogram-based invariant texture descriptor strategies which have standardization of rotation in the neighborhood region. The LBP-HF's are invariant to cyclic moves along the rows of input histogram, and are said to be invariant to the rotational movement of an input image [92]. The DFT is utilized to build the features as given by [92, 93]:

$$H\left(n,u\right) = \sum_{r=0}^{P-1} h_l\left(U_P\left(n,r\right)\right) e^{-i2\pi ur/P}$$

where, $H\left(n,u\right)$ corresponds to the DFT of the nth row of LBP^{u2} histogram $h_l\left(U_P\left(n,r\right)\right)$. It produces 38-bin histograms for a given texture image.

2.1.8   Adaptive Local Binary Pattern (ALBP)

In the year 2010, an adaptive local binary pattern that enhances images classification efficiency by minimizing the variations of the oriented mean and standard deviation of absolute local difference $\left|g_c - g_p\right|$ was introduced by Guo *et al.*, [94]. A weight parameter $\left(w_p\right)$ given below is introduced to minimize the overall directional differences $\left|g_c - w_p * g_p\right|$ along diverse orientations. The objective function for ALBP [94]is expressed by:

$$w_p = \arg\min_w \left\{ \sum_{i=1}^{N} \sum_{j=1}^{M} \left|g_c\left(i,j\right) - w.g_p\left(i,j\right)\right|^2 \right\}$$

where, N and M are the number of rows and columns of the image, respectively. For each of the orientations $2\pi p / P$ of entire image, a weight factor w_p is approximated. The expression for ALBP is then given by

$$ALBP_{P,R} = \sum_{p=0}^{P-1} s\left(g_p * w_p - g_c\right)2^p, \ s(x) = \begin{cases} 1, x \geq 0 \\ 0, x < 0 \end{cases}$$

2.1.9 Complete Local Binary Pattern (CLBP)

The completed local binary pattern (CLBP) enhances the significant texture feature extraction capability of LBP proposed by Guo et al. [95]. Fig 2.3(a) shows 3×3 block of an image having centre pixel value 34. The local difference, sign component and magnitude components are illustrated in Fig 2.3 (b), (c) and (d) respectively.
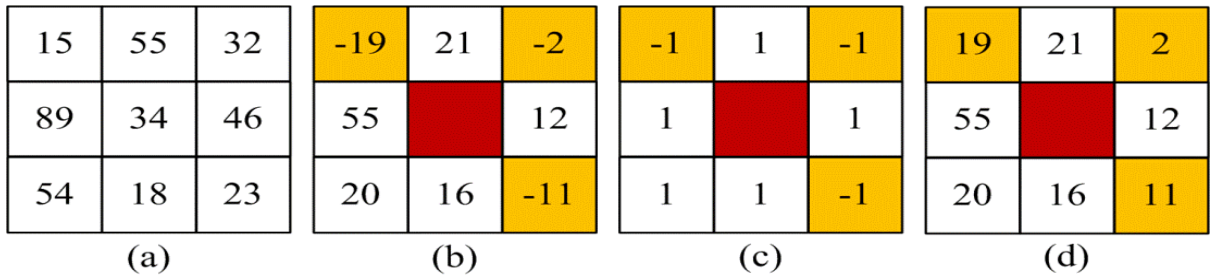
Fig.2.3: CLBP computation process

(a) 3×3 block of image, (b) local difference ($g_p - g_c$) (c) sign component, and (d) magnitude component.

The structure of CLBP is depicted in Fig 2.4. In CLBP, two components namely local difference and centre gray level are obtained from the gray scale image. The sign (*S*) and magnitude (*M*) components of local difference is produced by employing local difference sign-magnitude transform (LDSMT) as given by [95]:

$$d_p = g_p - g_c = s_p * m_p, \ and \begin{cases} s_p = sign\left(d_p\right) \\ m_p = \left|d_p\right| \end{cases}$$

where, m_p and $s_p = \begin{cases} 1, d_p \geq 0 \\ -1, d_p < 0 \end{cases}$ are magnitude and sign of d_p, respectively. The CLBP Sign (*CLBP_S*) and CLBP Magnitude (*CLBP_M*) operator portrays the complementary components of image's local structure. Also, the CLBP Centre (*CLBP_C*)

operator is created by altering centre pixel into binary code using global thresholding [93]. Here, *CLBP_S*, and *CLBP_M* operator are concatenated to shape the CLBP histogram.
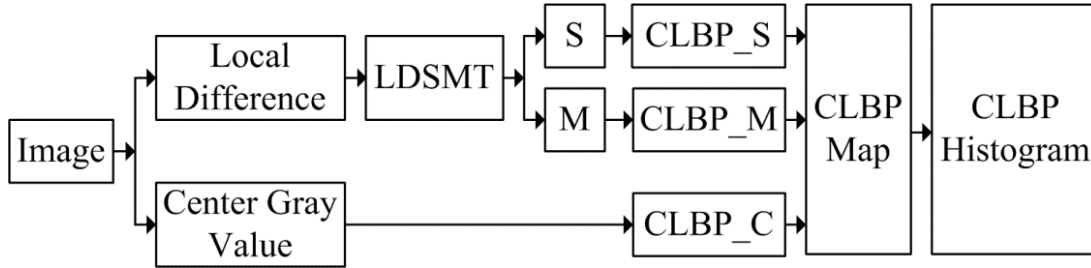
Fig.2.4: Structure of CLBP

2.1.10 Binary Gabor Pattern (BGP)

Binary Gabor pattern (BGP) is robust and efficient descriptors for texture classification [96]. The BGP employs J Gabor filters (g_0 to g_{j-1}) with J different orientations. The texture image is convolved with these J Gabor filters. The radius of the filter mask is represented by R. For a circular image patch p having radius R is centred at location x on the image. Multiplying image patch p pixel-wise with J filters and later summing up all the elements produces a response vector $r = \{r_j : |j = 0, 1, \ldots, J-1\}$. A binary vector $b = \{b_j : |j = 0, 1, \ldots, J-1\}$ is produced by binarising 'r'. The BGP is then expressed by:

$$BGP = \sum_{j=0}^{j} b_j \cdot 2^j$$

For a given 2^J binary patterns (b has J elements), the BGP operator generates 2^J output values. The rotation invariant binary Gabor pattern (BGP_{ri}) is defined by:

$$BGP_{ri} = \max\{ROR(BGP, j) | j = 0, 1, \ldots, J\}$$

where, $ROR(x, j)$ performs circular bitwise right shift operation on x (*J*-bit number) for *j* number of times.

26

2.2 Feature Dimensionality Reduction by Principal Component Analysis (PCA)

With the high-dimensional features, the computational prerequisite of classifier rises and the characterization accuracy may not be enhanced because of high-dimensional features. Along these lines, a feature dimension reduction strategy [97, 98] is required to change the information from high-dimensional space to low-dimensional space. The undertaking of feature dimensionality decreases to hold the best subset of features of the full feature dataset [99,100]. The dimension of feature vector information can be decreased by PCA (include dimensionality decrease).

PCA is one of the widely used linear transformation technique [101]. The PCA decreases data dimensions by registering a couple of symmetrical straight mixes of the first dataset features with maximal change. The PCA includes ascertaining the Eigenvalues and Eigenvectors of the covariance matrix of the original feature matrix. The Eigenvectors described by largest Eigenvalue are known as the first principal component (PC). The second PC is orthogonal to the first PC with the second largest difference, etc. The first several PC's have the most part of the variance, which is sufficient to represent the original data without losing significant information of the data.

2.3 Classifier

Three classifiers, namely, Neural Network and two variants of SVM, viz., linear and radial basis function (RBF) kernel have been used here for weld flaws classification. These classifiers are briefly explained in the following subsections:

2.3.1 Artificial Neural Network

A neural network [90] is defined as the set of organized elements better known as neurons. Each connection has weight associated with it. It basically consists of three or more layers [102]. The first layer is the input layer which feds data into the network. The intermediate layer also knows as the hidden layer has the weights associated with it. The neurons in the hidden layer collect the weighted inputs and compute the outputs by the given transfer function hidden layer is fed to the subsequent layer until the desired output is achieved. In the present work, the Levenberg–Marquardt algorithm is employed. The network performance parameters mean square error "mse" was used for the purpose of classification and mean square error with regularization "msereg" was used for the purpose of location.

In recent times artificial neural networks (ANNs) has become popular and helpful model for classification, clustering, pattern recognition and prediction in many disciplines. ANNs are one type of model for machine learning (ML) and has become relatively competitive to conventional regression and statistical models [77, 68].. It is an iterative technique that locates the minimum of a multivariate function which is given in the form of a sum of squares of non-linear real-valued functions [103]. The present work employs the use of Cascade Forward and Feedforward methods for the purpose of classification.

Feed forward networks possess one or more hidden layers of sigmoid neurons followed by an output layer of linear neurons. Multiple layers of neurons with nonlinear transfer functions allow the network to learn the relationship between input and output vectors which may be nonlinear and linear in nature. The previous network includes a weight connection from the input to each layer and from each layer to the successive layers and thus forms a cascade connection [104].

2.3.2 Support Vector Machine

The SVM, an effective and robust supervised classifier, gives excellent generalization performance and has been fruitfully applied to several pattern recognition problems in signal and image processing [105-112]. It was at first proposed as binary classifier [113,102]. Let (x_i, y_i) for $i = 1, 2, 3,...,l,$ represents a particular set of instance-label pairs, $x_i \in R^n$, $y_i \in \{+1,-1\}$, then the SVM binary classifier predicts a label y, in y_i for a given testing instance x. The optimization problem for binary classification is defined as follows [114]:

$$\min_{w} \frac{1}{2} w^T w + C \sum_{i=1}^{l} \xi\left(w; x_i, y_i\right)$$

Subject to constraint,

$$y_i\left(w^T x_i + b\right) - 1 \geq 0, \forall i$$

where, $\xi\left(w; x_i, y_i\right)$ is a loss function capacity and C (nonnegative) is a punishment parameter (cost factor). The binary class SVM is stretched out for multiclass classification utilizing methodologies, for example, "one against one", "one against all", and "directed acyclic graph" [115]. Further, a multiclass SVM classifier proposed by

28

Crammer and Singer [116] includes taking care of single optimization issue as it were. The linear SVM and RBF kernel SVM (nonlinear) are quickly depicted here.

(a) Linear SVM

Nowadays, linear classifier is a prefessrd choice as it works directly on the given data space. The linear SVM classifier is ideal for a dataset having massive features and is sparse in nature. It is viewed as an effective and appreciates quicker training and testing technique [117, 118]. The multi-class SVM proposed by Crammer and Singer [116] has been used in linear SVM classifier, here. The decision function for p class is expressed by [114]:

$$f(x) = argmax_{p=1,2,\ldots,P} \left(w_p^T x_i \right)$$

(b) Radial Basis Function Kernel SVM

At the point when the training set is indistinguishable in the original space, the original data x_i are mapped into a high dimensional space $\Phi(x_i)$, in which mapped data are linearly divisible. The articulation for decision rule is given as [119]:

$$f(x) = sgn\left(\sum_{i=1}^{l} \alpha_i y_i k\left(x_i, x_j \right) + b \right)$$

where, $k(x_i, x_j)$ is a kernel function and α_i imply the Lagrange multipliers (for dual optimization problems) which depicts the optimal isolating hyperplane. The radial basis function a standout amongst the most famous kernel function and is given by [119]:

$$K\left(x_i, x_j \right) = e^{\left(-\gamma x_i - x_j^2 \right)}, \gamma > 0$$

where, γ is the kernel parameter.

2.4 Weld Flaws Image Database

In order to accurately identify and classify the weld defects, an algorithm has been developed and tested on the database. The database of radiographic weld defects images is not available in the open domain for research purposes. Although, data sets used by researchers are very small in all the reported research work. Here, also the initiatives have taken for prepare of self-database of weld flaws for analysis, feature extraction, and classification purpose.

The image database has been prepared by researcher himself, after weld defects radiographic films prepared in the welding research laboratory of the department of Mechanical and Industrial Engineering, Indian Institute of Technology Roorkee. For preparing the digitized images of the radiographic film of weld flaws, a high resolution, and high color depth HP Scanjet G3110 photo flatbed scanner has used here. This scanner is capable of inefficient scanning of the negative and radiographic film due to its high resolution and high color depth. Although, the images are radiographic in nature and are not in quality. It is indeed a cumbersome process to analyze a radiographic image to identify the welding flaws. Also, it should be kept in mind that the quality of images is one of the major criteria for obtaining accuracy in classification.

There are in all 79 radiographic images with 8 types of the flaws and one without any flaw. Table 2.3 gives the detail description of the nature of the image and total no of images corresponding to each defect and in Fig 2.5, one image of each flaw from the database has been shown.

In the present work and in the consequent chapters' effort has been made that the algorithm effectively works with the features extracted by different methods.

Table 2.3: Description of Image Database

S. No	Nature of Image	No. of. Images
1	Gas Cavity	08
2.	Lack of Penetration	20
3.	Porosity	07
4.	Slag	16
5.	Crack	11
6.	Lack of Fusion	7
7.	Wormhole	2
8.	Undercut	3
9.	No Defect	5
Total No. of Images		79

Gas cavity(GC)	Lack of penetration(LOP)
Porosity(PO)	Slag inclusion(SI)
Crack(CR)	Lack of fusion(LOF)
Worm hole(WH)	Undercut(UC)
Non defect(ND)	
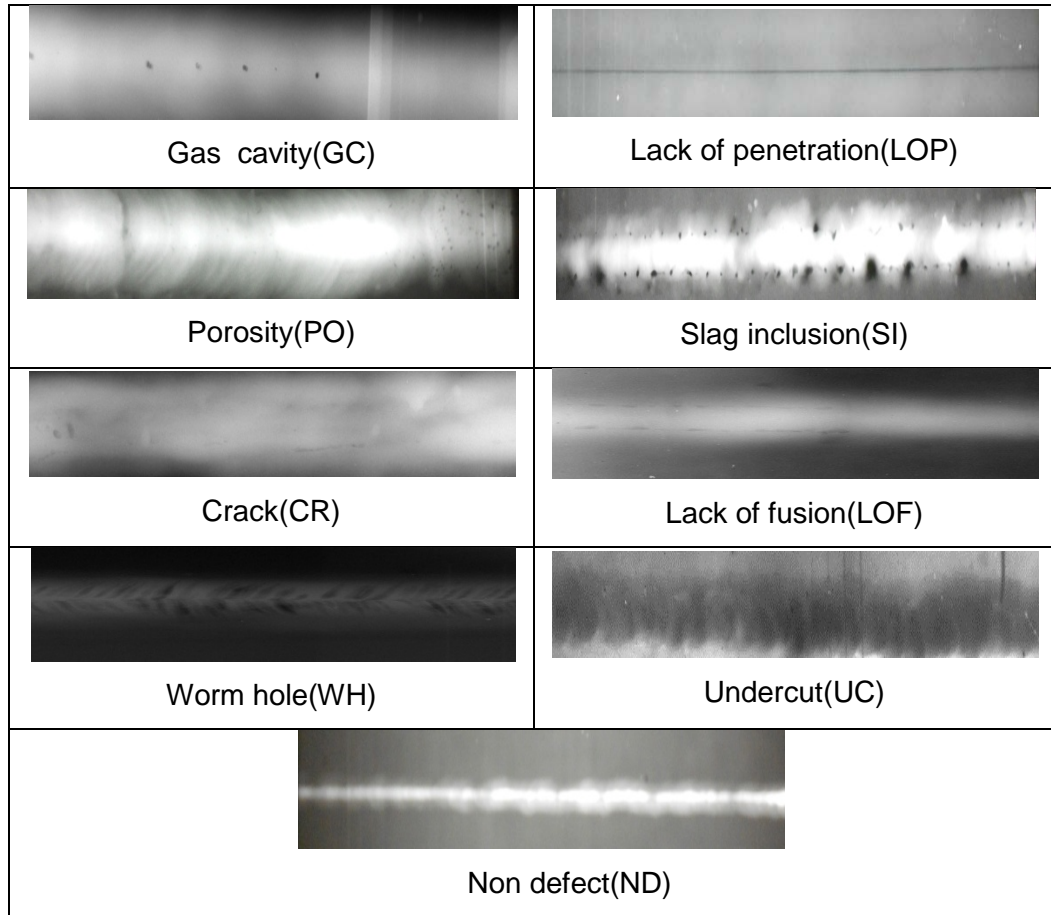
Fig.2.5: Digitize images of radiographic weld flaws.

2.5 Methodology

The methodology adopted for the present algorithm is explained below in detail:'

2.5.1 Procedural Steps

Brief descriptions of these procedures are described below:

1. The weld flaw images if available in RGB is converted to grayscale in order to reduce the computational time during feature extraction. The expression for RGB to grayscale conversion is given by

$$G_{luminance} = 0.2989 \times R + 0.5878 \times G + 0.1140 \times B$$

where, $G_{luminance}$ represents grayscale image achieved by considering luminance information only and eliminating the hue and saturation information of colour image. The R, G and B signify red, green and blue components of colour image, respectively.

2. The grayscale images are then processed by the median filter of 3x3 mask size to remove the noise contents from the image.

3. The state-of-the-art texture feature extraction techniques are utilized to extract the texture features of grayscale weld flaws images.

4. The extracted features are then normalized in the range 0 to 1, before applying to the classifier as input. The normalization is done using the equation

$$F_{Norm} = \left(\frac{F - \min(F)}{\max(F) - \min(F)} \right)$$

where, F_{Norm}: normalized feature vector data, and F: original feature vector data.

5. The normalized features data is given to different classifiers for classifying the images database into 9 categories.

6. It can be verified form the classification accuracy that which combination of texture feature extraction technique and classifier is best.

The above procedural steps in form of block diagram has been shown below in Fig. 2.6
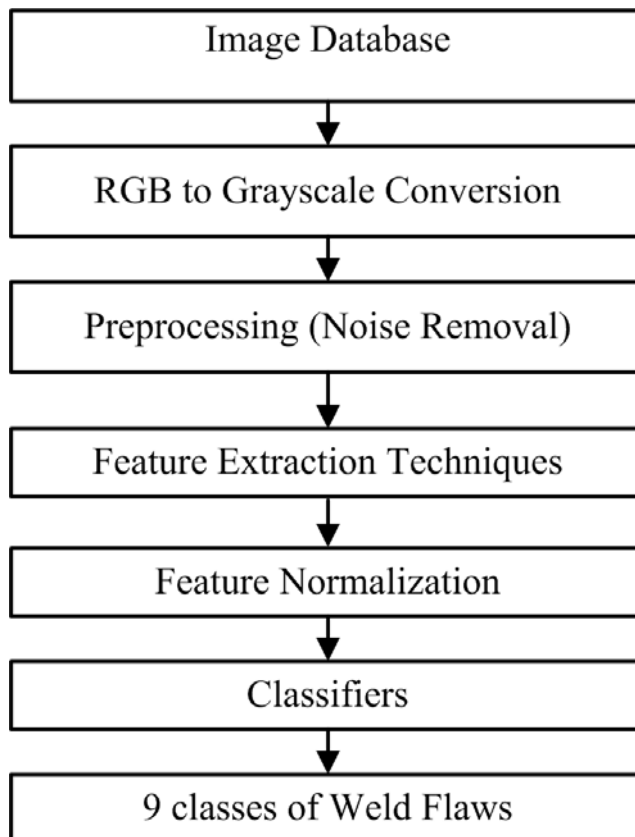

Fig.2.6: Weld flaw image classification using texture feature extraction technique.

2.5.2 Performance Evaluation of Feature Extraction Techniques

The performance evaluation of the texture feature extraction techniques has been examined by dividing the data randomly to achieve the classification accuracy. The approach is discussed in the following subsections:

Here, the extracted features dataset is divided randomly [105] into fixed training and testing subsets for each class. In the presented work, the examination has been carried out with two different proportions of training and testing datasets as given below:

1. 80% data for training and 20% data for testing (80/20)
2. 70% data for training and 30% data for testing (70/30)

2.6 Experimental Results and Discussion

The experimental work presented in this section investigates the efficacy of the various texture feature extraction techniques for the classification of radiographic images of the weld flaws database into 9 classes with the help of classifiers. The three classifiers used in this work are ANN, linear SVM, and RBF kernel SVM classifiers.

2.6.1 Parameter Selection

The GLCM technique generates 18 features in each direction for a given neighborhood distance. The neighborhood distance (d) in the range 1-10 has been investigated and d=2 has been selected as it yields the best result. Further, these features are calculated in four directions (0°, 45°, 90°, and 135°).

The P and R parameter values are considered as 8 and 1, respectively, for all the variants of LBP (LBP, LBP^{u2}, LBP^{ri}, LBP^{riu2}, LBP-HF, $CLBP^{u2}$, $ALBP^{u2}$, $ALBP^{ri}$ and $ALBP^{riu2}$) because these values have yielded fast and accurate feature extraction as represented by [120]. Further, for texture images, uniform patterns account for approximately 90% of all patterns when using the (8, 1) neighborhood and these patterns account for around 70% in the (16, 2) neighborhood. The use of LBP^{riu2} having $P = 8$ and $R = 1$ has also reported the best result compared to (P, R) pair values of (16, 2) and (24, 3) [88]. Furthermore, the R parameter is usually chosen small because the correlation between pixels decreases with distance, and a lot of the texture information can be obtained from local neighborhoods[121].

For linear SVM classifier, the optimum value of C has been selected by searching in the range (10^{-4}, 10^{-3},…, 10^{+5}), whereas the optimum value of C and gamma $\left(\gamma\right)$ has been selected by using grid search method in the range (10^{-4},10^{-3},…,10^{+5}) for RBF kernel SVM classifier [122]. The tolerance of termination criteria $\left(\xi\right)$ value has been tested in the range (0.1, 0.01, 0.001, and 0.0001) and found that ξ = 0.001 gives the best trade-off between classification accuracy and computational time. Also, the bias (b) parameter value has been selected as 1 for SVM implementation.

2.6.2 Experimental Results

Table 2.4: Classification accuracy achieved by full feature vector data for different proportions of training and testing data of RDD using three classifiers.

| Texture feature extraction techniques | % Classification accuracy achieved by classifiers for different proportions of training and testing data | | | | | |
| | LSVM | | RBF kernel SVM | | ANN | |
	80/20	70/30	80/20	70/30	80/20	70/30
GLCM	59.49	58.22	59.49	56.96	86.07	86..07
GLRLM	56.96	55.69	58.22	56.96	82.08	81.01
LBP	54.43	54.33	60.76	59.49	83.54	82.28
LBP^{u2}	51.90	51.90	56.96	56.96	84.81	83.54
LBP^{ri}	45.57	45.57	53.16	53.06	84.81	83.54
LBP^{riu2}	48.10	46.83	56.96	55.69	83.54	82.08
LBP-HF	44.30	43.04	54.43	54.43	82.28	81.01
CLBP^{u2}	39.24	39.24	53.16	53.16	82.28	82.28
ALBP^{u2}	56.96	56.96	58.22	56.96	84.81	83.54
ALBP^{ri}	49.36	49.36	56.96	55.69	83.54	83.54
ALBP^{riu2}	50.69	50.69	54.43	54.43	82.28	81.01
BGP	59.49	56.96	64.55	63.29	**91.14**	**89.87**

The classification accuracy of the various texture feature extraction techniques has been computed using the earlier discussed classifiers, who have been selected on the basis of their general performance for pattern recognition and classification task. The

classification accuracy has been computed for full feature vector data (FFVD) and PCA reduced feature vector data. To evaluate the performance of various texture feature extraction techniques randomly divided database (RDD) selection has been adapted here.

2.6.3   Performance Evaluation of various Texture Feature Extraction Techniques

The classification accuracy obtained for full feature vector data and PCA reduced dimension feature vector data is discussed in the below subsections.

2.6.3.1   Full feature vector data (FFVD)

The classification accuracy achieved by various well known texture feature extraction techniques for different ratios of training and testing data is listed in table 2.4

Linear SVM classifier: Amongst the studied texture feature extraction techniques, full feature vector data (FFVD) of Binary Gabor pattern (BGP) technique and Gray level co-occurrence matrix (GLCM) shows best classification accuracy of 59.49%, at 80/20, proportions of training and testing data of randomly divided database (RDD) where as their classification accuracy at 70/30 proportions of training and testing data of RDD are 56.96% and 58.22% respectively. The Completed Local Binary Pattern (CLBP^{u2}) technique has resulted in the lowest classification accuracy. The classification accuracy achieved by other texture feature extraction techniques is also listed in Table 2.4 for comparison purposes. However, the classification accuracy of the Linear SVM classifier using feature vector data produced by all the above techniques is in a very lower range.

RBF kernel SVM classifier: The full feature vector data produced by Binary Gabor pattern (BGP) texture feature extraction technique has obtained the best classification accuracy of 64.55% and 63.29% for 80/20 and 70/30 proportions of training and testing data of RDD, respectively among all other techniques FFVD. Further, the feature vector data obtained by CLBP^{u2} texture feature extraction technique has given the worst classification accuracy of 53.16% for both 80/20 and 70/30 proportions of training and testing data of RDD. The classification accuracies achieved by other texture feature extraction techniques are also listed in Table 2.4. Here, it should be noted that the

classification accuracies of this classifier using all techniques FFVD are in between 53.16% to 64.55%, which is not acceptable.

ANN classifier: In the case of ANN classifier, again the BGP texture features with 216 features have achieved the best classification accuracy of 91.14% and 89.87% for 80/20 and 70/30 training and testing ratios of RDD. The second-best classification accuracy of 86.07% for both 80/20 and 70/30 training and testing ratios of RDD has been performed by GLCM with 72 features. Whereas, the performance of LBP and its variants are average. The classification accuracy achieved by other texture feature extraction techniques using ANN classifier is also listed in Table 2.4.
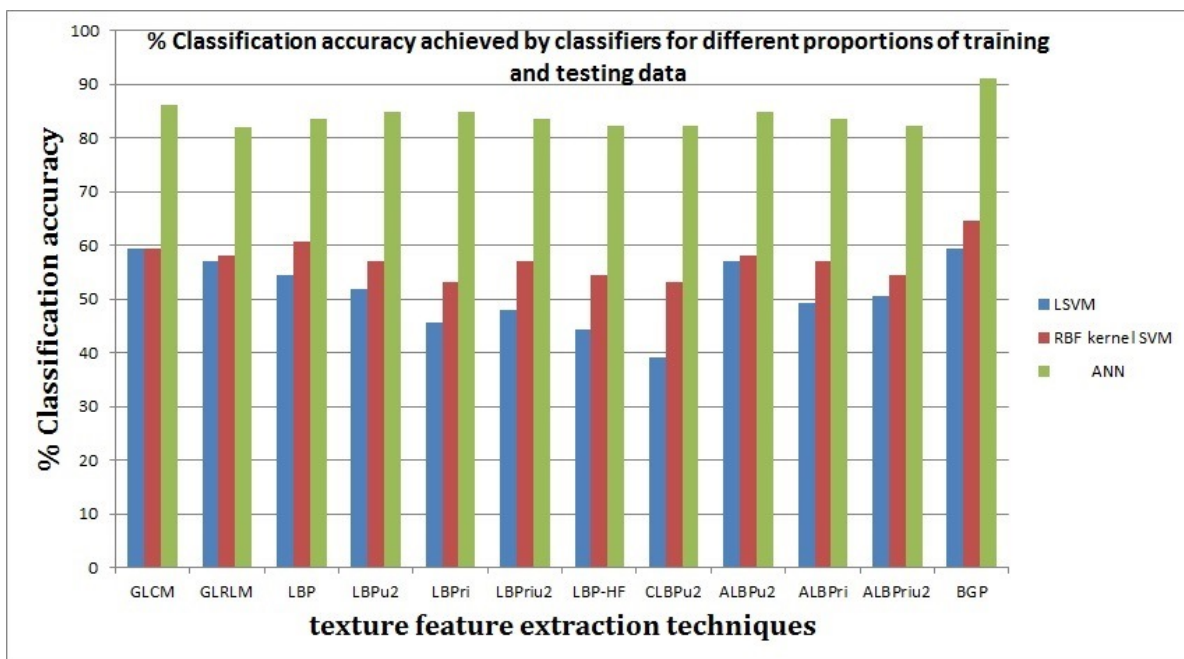

Fig.2.7: % Classification accuracy achieved by classifiers for 80/20 proportion of training and testing data of RDD.

Among all three classifiers, the performance of the artificial neural network (ANN) classifier is superior with full feature vector data of all the above texture feature extraction techniques.

2.6.3.2   The PCA dimensionality reduced feature vector data

The classification accuracy results obtained by the PCA based reduced feature vector data by linear SVM, RBF kernel SVM, ANN has been listed in Table 2.5 to Table 2.7 respectively.

Linear SVM classifier: Amongst the studied texture feature extraction techniques, full feature vector data (FFVD) of Binary Gabor pattern (BGP) technique and Gray level co-occurrence matrix (GLCM) shows best classification accuracy of 59.49%, at 80/20, proportions of training and testing data of random divided database (RDD) whereas their classification accuracy at 70/30 proportions of training and testing data of RDD are 56.96% and 58.22% respectively. The Completed Local Binary Pattern (CLBP^{u2}) technique has resulted in the lowest classification accuracy. The classification accuracy achieved by other texture feature extraction techniques is also listed in Table 2.5 for comparison purposes. However, the classification accuracy of Linear SVM classifier using feature vector data produced by all the above techniques is in very lower range.

Table 2.5: % Classification accuracy achieved by PCA reduced feature vector data for different proportions of training and testing data of RDD using linear SVM classifier.

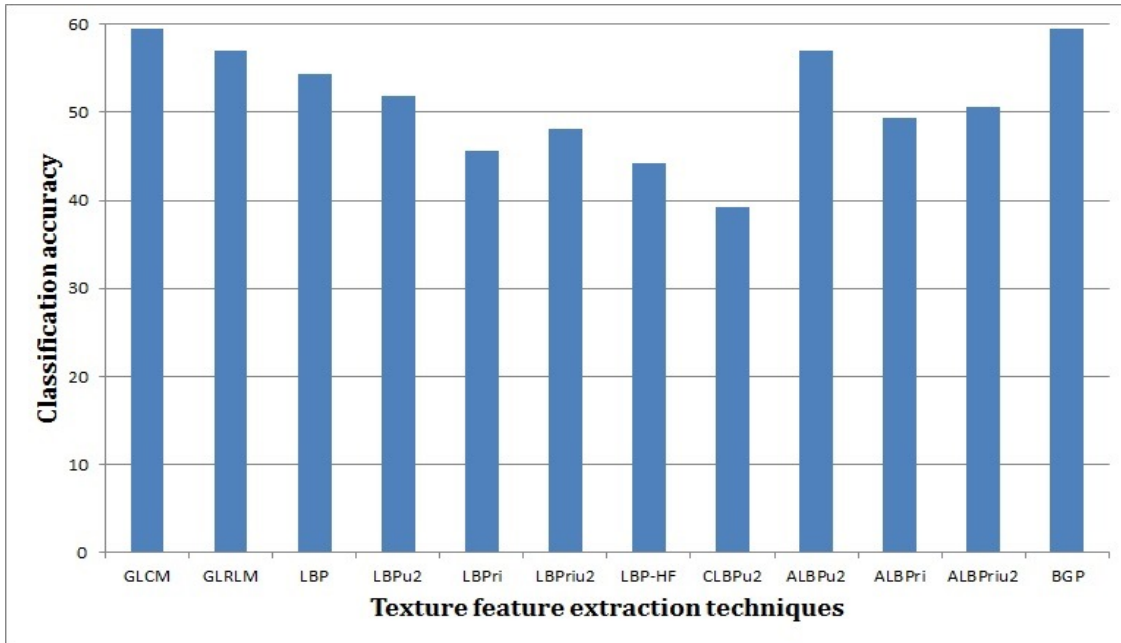| Texture feature extraction techniques	% Classification accuracy using linear SVM			
	NoF	80/20(RDD)	NoF	70/30(RDD)
GLCM	50	59.49	55	58.22
GLRLM	30	56.96	35	55.69
LBP	140	54.43	150	54.33
LBP^{u2}	50	51.90	50	51.90
LBP^{ri}	30	45.57	30	45.57
LBP^{riu2}	8	48.10	9	46.83
LBP-HF	35	44.30	35	43.04
CLBP^{u2}	110	39.24	105	39.24
ALBP^{u2}	45	56.96	45	56.96
ALBP^{ri}	25	49.36	25	49.36
ALBP^{riu2}	8	50.69	8	50.69
BGP	140	59.49	145	56.96

Fig.2.8: % Classification Accuracy achieved by different feature extraction techniques using Linear SVM.
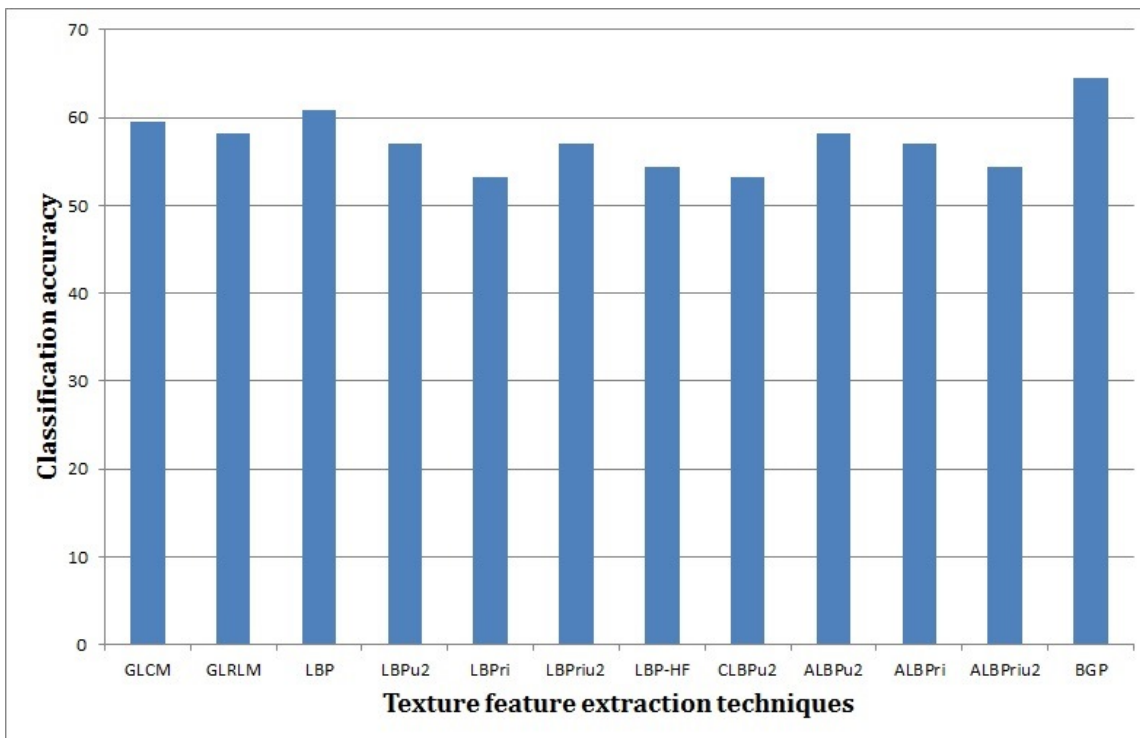

Fig.2.9: % Classification Accuracy achieved by different feature extraction techniques using RBF Kernel SVM.

Table 2.6: % Classification accuracy achieved by PCA reduced feature vector data for different proportions of training and testing data of RDD using RBF kernel SVM.

Texture feature extraction techniques	% Classification accuracy using RBF kernel SVM			
	NoF	80/20(RDD)	NoF	70/30(RDD)
GLCM	55	59.49	60	56.96
GLRLM	35	58.22	35	56.96
LBP	130	60.76	150	59.49
LBP^{u2}	40	56.96	50	56.96
LBP^{ri}	25	53.16	25	53.06
LBP^{riu2}	9	56.96	9	55.69
LBP-HF	30	54.43	35	54.43
$CLBP^{u2}$	100	53.16	105	53.16
$ALBP^{u2}$	40	58.22	45	56.96
$ALBP^{ri}$	30	56.96	25	55.69
$ALBP^{riu2}$	10	54.43	10	54.43
BGP	150	64.55	135	63.29

RBF kernel SVM classifier: The PCA reduced feature vector data of BGP technique has produced the best classification accuracy of 64.55% (150 features), 63.29% (135 features), for 80/20, and 70/30 training and testing ratios of RDD, respectively. Further, PCA reduced feature vector data of $CLBP^{u2}$ technique has achieved the worst classification accuracy of 53.16% (100 features), for same training and testing ratios of RDD.

ANN classifier: The PCA reduced feature vector data of BGP technique has produced the best classification accuracy of 91.14% (120 features) for 80/20 and 89.87% for 70/30 training and testing ratios of RDD respectively, whereas the second highest accuracy of 86.07% obtained by ANN classifier for both 80/20 and 70/30 ratio of randomly divided data set. It is observed that ANN classifier produced better classification accuracy for all feature extraction techniques. The accuracy of classification for the ANN classifier is in between 81.01% to 91.14% for all feature extraction techniques.

Fig.2.10: % Classification Accuracy achieved by different feature extraction techniques using ANN classifier.

Table 2.7: % Classification accuracy achieved by PCA reduced feature vector data for different proportions of training and testing data of RDD using ANN classifier.

Texture feature extraction techniques	% Classification accuracy using ANN			
	NoF	80/20(RDD)	NoF	70/30(RDD)
GLCM	60	86.07	55	86.07
GLRLM	35	82.08	35	81.01
LBP	200	83.54	150	82.28
LBP^{u2}	50	84.81	55	83.54
LBP^{ri}	30	84.81	25	83.54
LBP^{riu2}	10	83.54	9	82.08
LBP-HF	35	82.28	35	81.01
CLBP^{u2}	100	82.28	105	82.28
ALBP^{u2}	50	84.81	40	83.54
ALBP^{ri}	25	83.54	30	83.54
ALBP^{riu2}	10	82.28	10	81.01
BGP	120	**91.14**	120	**89.87**

40

It is observed that in most of the cases, the PCA reduced feature vector data of the BGP technique yields best classification accuracy amongst all texture feature extraction techniques presented here. The PCA reduced feature vector data of the GLCM feature extraction technique closely follows the results produced by the BGP feature extraction technique.

It is clearly visible from these figures that the PCA reduced feature vector data of the BGP texture feature extraction technique has established its superiority over other feature extraction techniques. It is worth noting that amongst all the three classifiers, the full feature vector data and the PCA reduced feature vector data both have given better performance with ANN for most of the texture feature extraction techniques considered in this discussion. However, RBF kernel SVM and linear SVM both give lower classification accuracy in comparison to ANN classifiers. Though PCA reduced feature vector data has achieved almost the same classification accuracy compared to full feature vector data, but these accuracies were obtained using a smaller number of feature vector data compared to full feature vector data, requiring less computation time in classification.

2.7   Summary

In this chapter, the effectiveness of the texture feature extraction techniques has been investigated for the successful classification of Radiographic weld Images into 09 categories with the help of three different classifiers namely Linear SVM, RBF Kernel SVM, and ANN. The efficiency of the state-of-the-art texture feature extraction techniques has been tested using two different randomly divided databases. Further, in this method, 02 cases are discussed (viz., FFVD and PCA reduced feature vector data).

It is evident from the result that GLCM outperforms GLDM. GLDM features use first-order statistics and are not very useful in weld defect flaw classification. GLCM captures second-order statistics so it enhanced the classifier performance. The features obtained from GLCM have the ability to locate more accurate classification boundaries due to combined features' ability to locate the classification boundaries more efficiently.

BGP has the merits of high classification accuracy, small feature size, and fast classification speed. Even though BGP has a slightly larger feature size and works a little slower when compared with LBP, its classification accuracy is remarkably better. Due to its appreciable size and the running speed, it is more suitable in real applications. The

best classification accuracy of 91.14% has been achieved by FFVD data of BGP texture feature extraction techniques using the ANN Classifier. The PCA reduced feature vector data of the same technique have the same result for 80/20 RDD. It is also evident that the PCA reduced feature vector does not affect the accuracy in most of the cases. However, the advantage of PCA reduced database is that it takes less time for classification. Also, ANN is capable of locating nonlinear classification boundaries. The higher performance of ANN may be due to its ability to locate nonlinear classification boundaries.

CHAPTER 3: WAVELET TRANSFORM BASED FEATURE EXTRACTION TECHNIQUES

This chapter explores the effectiveness of discrete wavelet transform (DWT) based local binary pattern (LBP) variants and binary Gabor pattern texture feature extraction techniques for classification of weld flaws using its radiographic images data base. The chapter starts with a concise description of the DWT, proposed DWT based texture feature extraction techniques for weld flaws classification and subsequent evaluation of the effectiveness of these techniques using ANN classifiers.

3.1 Introduction

The discrete wavelet transform (DWT) is nowadays established as a key operation in image processing. It is a multi-resolution analysis and it decomposes images into wavelet coefficients and scaling function. DWT has been utilized in a wide range of applications in signal and image processing like image analysis, object recognition [123], de-noising, segmentation, compression, biomedical imaging, fingerprint anti-spoofing [124] and texture feature extraction, etc. [125-135]. The DWT has gained popularity in image processing applications for efficiently providing spatial-frequency information [136-145].

The significant elements of 2D-DWT includes four critical elements, one scaling function $\varphi(x,y)$, and three wavelet functions ($\psi^H(x,y)$, $\psi^V(x,y)$ and $\psi^D(x,y)$), which are product of two one dimensional (1D) functions. The ψ^H, ψ^V and ψ^D wavelets are useful in the measurement of gray level variations in the horizontal, vertical and diagonal directions, respectively. The scaled φ and translated ψ basis functions are defined as follows [146]:

$$\varphi_{j,r,c}(x,y) = 2^{j/2}\varphi\left(2^j x - r, 2^j y - c\right)$$

$$\psi^i_{j,r,c}(x,y) = 2^{j/2}\psi^i\varphi\left(2^j x - r, 2^j y - c\right), \, i = \{H,V,D\}$$

The DWT expression to an image $f(x,y)$ of size $M \times N$ is given by:

$$W_\varphi\left(j_0, r, c\right) = \frac{1}{\sqrt{MN}} \sum_{x=0}^{M-1}\sum_{y=0}^{N-1} f\left(x, y\right) \varphi_{j_0, r, c}\left(x, y\right)$$

$$W_\psi^i\left(j, r, c\right) = \frac{1}{\sqrt{MN}} \sum_{x=0}^{M-1}\sum_{y=0}^{N-1} f(x, y) \phi_{j0, r, c}(x, y), \ i = \{H, V, D\}$$

In the above equation j_0 is an arbitrary starting scale. The $W_\varphi\left(j_0, r, c\right)$ coefficients

produce an approximation of image $f\left(x, y\right)$ at j_0 scale and $W_\psi^i\left(j, r, c\right)$ coefficients

provide diagonal, vertical and horizontal details at scale $j \geq j_0$.
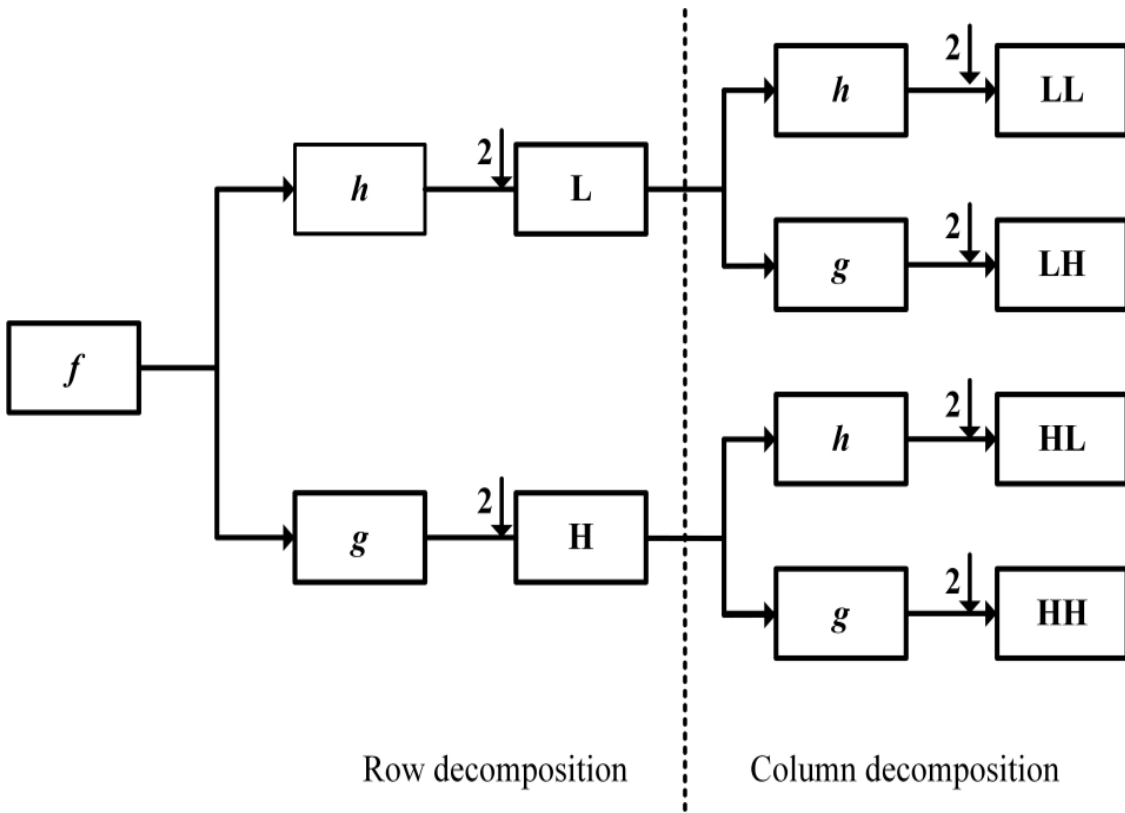
Fig. 3.1: 2D representation of the wavelet decomposition.

To perform a 2D-DWT, initial a one-level, 1-D DWT is applied along the rows of the image. Second, a one-level, 1-D DWT is applied along with the segments of the changed image from the initial step. The effect of these two arrangements of tasks is a changed image with four particular groups: (I) LL, (ii) LH, (iii) HL and (iv) HH. Here, L represents low-pass separating, and H represents high-pass sifting. The LL band relates generally to a down-sampled (by a factor of two) rendition of the first image. The LH band will, in general, protect limited even features, while the HL band tends to isolate localized high-

44

frequency point features in the image. At long last, the HH band will, in general, detach confined high-recurrence points includes in the picture. Additional levels of decomposition can extract lower frequency features include in the image; these extra dimensions are connected just to the LL band of the transformed image at the past dimension. A one-level, 2D-DWT deterioration is delineated in Fig:3.1.

A compactly supported orthogonal wavelet having a pre-allocated level of smoothness was structured by Ingrid Daubechies [147]. It has been utilized in several image processing applications [148]. Daubechies wavelet family is described by time invariance, delivers genuine number coefficients, deviated and has a sharp channel change band that is helpful in limiting the edge impacts between the recurrence groups. The fractal such as self-symmetry property encourages quick wavelet change in the calculation, likewise for a given help, it offers the most noteworthy number of vanishing minutes [147].

The necessity for the significant texture features depends on the accompanying realities. As the visual discernment assesses images on a different resolution in the meantime, the multi-resolution investigation capacity of DWT is useful in identifying features at a unique resolution, which is undetectable at any other resolution. Further, the LBP variations and BGP feature extraction techniques are notable for their capacity of removing substantial features of images. In this manner, the features acquired by consolidating DWT with LBP variations and BGP at a few dimensions of image decomposition separates unmistakable features. Moreover, joining these features together at a few dimensions of image decomposition enhances segregation ability of classifier for welding images.

3.2 Proposed Methodology

3.2.1 Procedural Steps

The algorithmic steps for the classification of weld flaw images are shown in figure below. The four steps i.e., pre-processing, texture feature extraction, feature dimension reduction and classification are involved in the proposed approach.
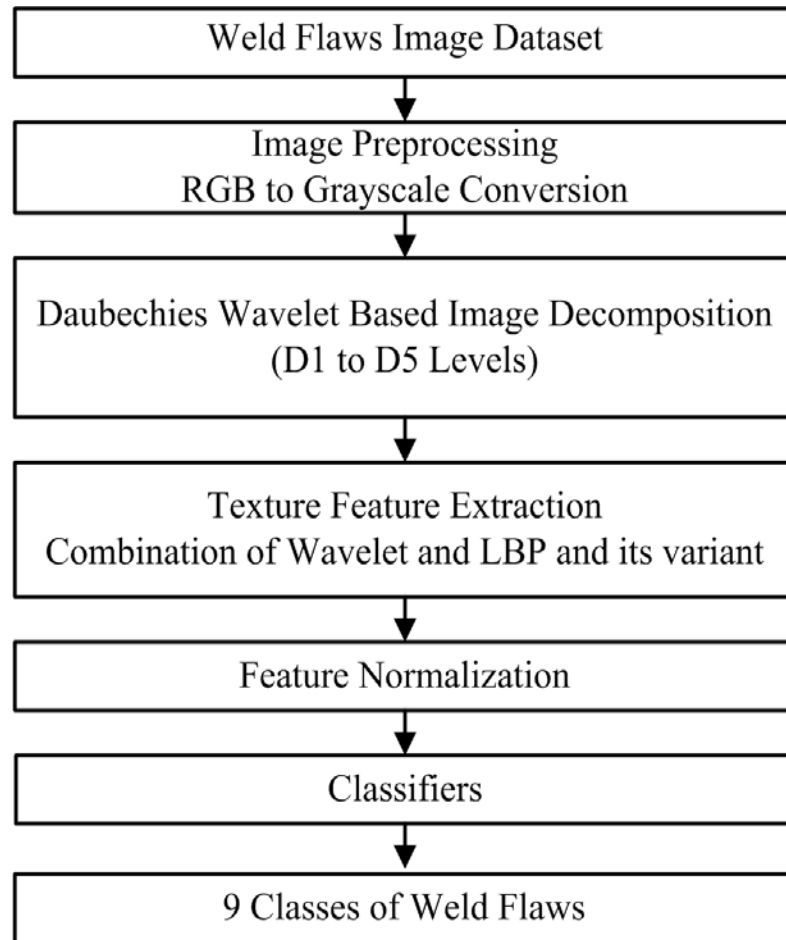
Fig. 3.2: Block diagram of proposed DWT based LBP variants-based texture features for weld images classification.

1. In the pre-processing step, the color (RGB) images are converted to the grayscale image to reduce the computation time and better performance as per earlier practice.

2. The second step is the texture feature extraction. The Daubechies wavelet (db2) has been utilized to decompose these grayscales to five different levels/scales (L1 to L5). The transformation is carried out to obtain significant features of the image at a unique resolution that is unnoticeable at any other resolution. The decomposition process divides a grayscale image into four identical quarter-size sub-images. Subsequently, texture features are extracted from each of the sub images at different levels (L1 to L5) of image decomposition. Here, seven texture feature extraction techniques namely LBP, LBPu2, LBPri, LBPriu2, LBP-HF, CLBPu2, and BGP are used. Thus, on the basis of the combination of DWT with different variants of LBP

and BGP, following DWT based local binary pattern variants-based texture feature extraction techniques are proposed here and they are listed below.

DWTLBP	DWT based local binary pattern
DWTLBPu2	DWT based uniform local binary pattern
DWTLBPri	DWT based rotation invariant local binary pattern
DWTLBPriu2	DWT based rotation invariant uniform local binary pattern
DWTLBP-HF	DWT based local binary pattern histogram Fourier features
DWTCLBPu2	DWT based uniform completed local binary pattern
DWTBGP	DWT based Binary Gabor pattern

3. Further, these texture feature vectors containing numerous ranges of values and therefore normalized in the range of 0 to 1. The feature vector data is normalized using equation as already used in the earlier chapter

$$F_{Norm} = \left(\frac{F - \min(F)}{\max(F) - \min(F)} \right)$$

where, F_{Norm}: normalized feature vector data, and F: original feature vector data.

4. The proposed texture descriptors deliver large complex features, which all may not be significant for discrimination of the weld images. Thus, for the reduction of feature vector size PCA is used in the third step.

5. In the last step, ANN algorithms have been utilized to classify the given weld flaws image in different classes. Further, the efficiency of the proposed DWT based LBP variants and BGP texture feature extraction techniques has been commented on the basis of the classification accuracy acquired through the classifiers.

The performance of the DWT based texture feature extraction techniques for classification of weld flaws images has been investigated employing randomly dividing the database with the training and testing ratio of 70/30 (i.e. 70% of data for testing, 15% for validation and 15 % for testing).

3.3   Experimental results and discussion

The experimental work presented in this section investigates the efficiency of the DWTLBP variants-based texture feature extraction techniques for the classification radiographic images of the weld flaws database into 9 classes with the help of classifiers. The classifiers used for the investigation are ANN classifiers only because from previous chapters it is clear that only the ANN classifier gives a good result on all feature vector data extracted from the weld flaws image database since it has been able to detect the boundaries of all the images.

3.3.1   Parameter selection

The selections of parameters for efficient implementation of various feature extraction techniques and classifiers have been discussed in chapter 2. The classification accuracy obtained by the DWT (with LBP variants and BGP) based texture feature extraction techniques for radiographic images of weld flaws have been computed using ANN classifiers. The analysis of the results is presented in a similar manner but only for the ANN classifier, because SVM classifiers are not producing satisfactory results in all previous cases. So, further experiments have been performed using only the ANN classifier for both full feature vector data and PCA reduced feature vector data in order to achieve good classification accuracy.

3.3.2   Performance Evaluation using Full Feature Vector Data (FFVD)

The percentage classification accuracy attained by the DWT based texture feature extraction techniques for grayscale radiographic images of weld flaws database is presented in Table below. The classification accuracy obtained by the proposed texture feature extraction techniques using the best performer classifier ANN is discussed below. The ANN classifier performs far better in all the previous cases.

From the below table, it is clear that in all the feature extraction techniques, it is noted that the percentage classification accuracy is maximum at the 3rd or 4th level of decomposition. When the images are further decomposed at a higher level, the accuracy reduces. So, it is clear indications of no further decomposition of images are required to achieve the goal.

48
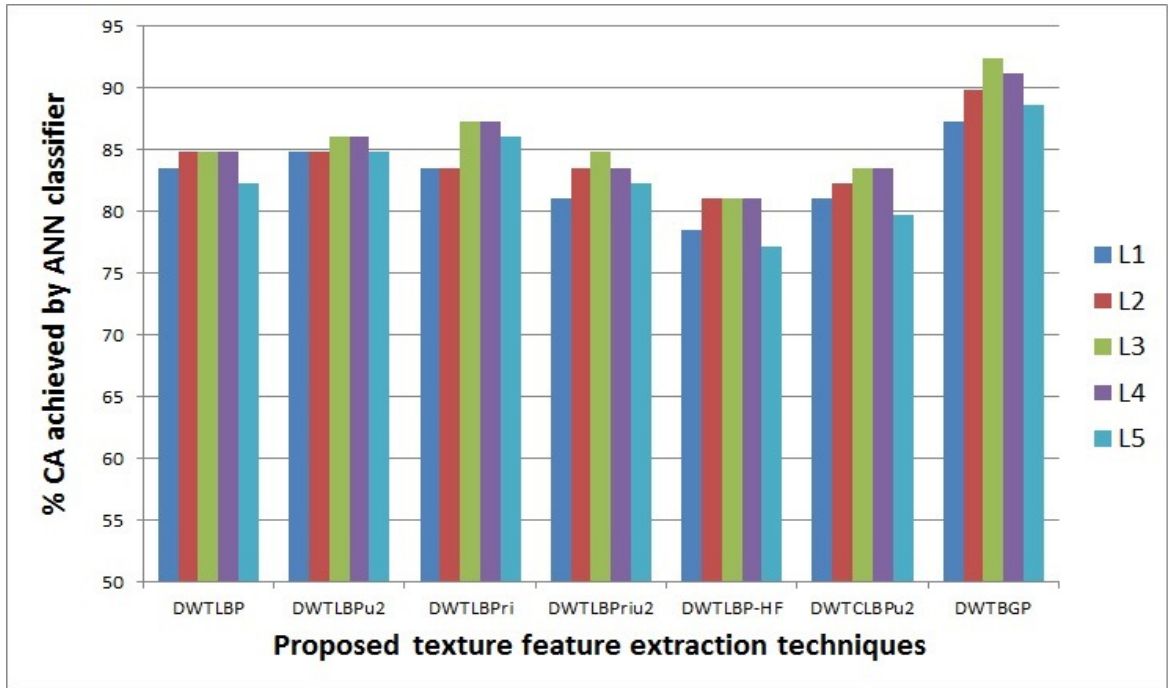
Fig. 3.3: %age Classification achieved by ANN Classification different levels of DWT Decomposition

The texture feature vector data of the DWTBGP feature extraction technique has given the best classification accuracy of 92.4% at third level of decomposition. In addition, the second-best classification accuracy of 87.34% has been achieved by texture feature vector data produced by the DWTLBPri texture feature extraction technique for third and fourth level of decomposition. The least classification accuracy of 81.01% has been achieved by using texture feature vector data produced by DWTLBPHF, among the proposed feature extraction techniques. All these classification accuracies are reported for texture feature vector data generated at the 3rd level or 4th Level of image decomposition. The same has been shown in figure 3.3. The detailed analysis is mentioned in Table 3.1 to 3.7.

Table 3.1: Maximum Classification accuracy at each level of DWTLBP.

Proposed techniques	IDL	Feature extraction time in seconds	NoF	% CA achieved by ANN classifier
DWTLBP	1	0.1630	1024	83.54
	2	0.2011	2048	**84.81**
	3	0.2168	3072	84.81
	4	0.2308	4096	84.81
	5	0.2433	5120	82.28

From table 3.1, it is evident that the combination of DWTLBP, 2nd, 3rd and 4th level image decomposition gives the classification accuracy of 84.81%.

Table 3.2: Maximum Classification accuracy at each level of DWTLBPu2

Proposed technique	IDL	Feature extraction time in seconds	NoF	% CA achieved by ANN classifier
DWTLBPu2	1	0.2569	236	84.81
	2	0.3038	472	84.81
	3	0.3275	708	**86.07**
	4	0.3402	944	86.07
	5	0.3494	1180	84.81

From table 3.2, it is evident that the combination of DWTLBPu2 3rd and 4th level image decomposition gives the classification accuracy of 86.07%.

Table 3.3: Maximum Classification accuracy at each level of DWTLBPri

Proposed technique	IDL	Feature extraction time in seconds	NoF	% CA achieved by ANN classifier
DWTLBPri	1	0.2615	144	83.54
	2	0.3149	288	83.54
	3	0.3400	432	**87.34**
	4	0.3595	576	87.34
	5	0.3758	720	86.07

From table 3.3, it is evident that the combination of DWTLBPri, 3rd and 4th level image decomposition gives the classification accuracy of 87.34%, thereby increasing the image classification accuracy.

Table 3.4: Maximum Classification accuracy at each level of DWTLBPriu2

Proposed technique	IDL	Feature extraction time in seconds	NoF	% CA achieved by ANN classifier
DWTLBPriu2	1	0.2508	40	81.01
	2	0.2950	80	83.54
	3	0.3198	120	**84.81**
	4	0.3283	160	83.54
	5	0.3332	200	82.28

From table 3.4, it is obvious that the combination of DWTLBPri 3rd level image decomposition gives the classification accuracy of 84.81%. The classification accuracy has reduced.

Table 3.5: Maximum Classification accuracy at each level of DWTLBP-HF

Proposed techniques	IDL	Feature extraction time in seconds	NoF	% CA achieved by ANN classifier
DWTLBP-HF	1	0.2662	152	78.48
	2	0.3216	304	**81.01**
	3	0.3488	456	81.01
	4	0.3694	608	81.01
	5	0.3862	760	77.21

From table 3.5, it is evident that the combination of DWTLBP-HF2ndand 3rdlevel image decomposition gives the classification accuracy of 81.01%, which has further decreased the image classification accuracy.

Table 3.6: Maximum Classification accuracy at each level of DWTCLBPu2

Proposed techniques	IDL	Feature extraction time in seconds	NoF	% CA achieved by ANN classifier
DWTCLBPu2	1	0.3037	472	81.01
	2	0.3724	944	82.28
	3	0.3947	1416	**83.54**
	4	0.4039	1888	83.54
	5	0.4257	2360	79.74

From table 3.6, it is evident that the combination of DWTCLBPU2 3rd and 4th level image decomposition gives the classification accuracy of 83.54%.

Table 3.7: Maximum Classification accuracy at each level of DWTBGP

Proposed technique	IDL	Feature extraction time in seconds	NoF	% CA achieved by ANN classifier
DWTBGP	1	0.1980	864	87.34
	2	0.2261	1728	89.87
	3	0.2456	2592	**92.40**
	4	0.2689	3456	91.14
	5	0.2985	4320	88.60

From table 3.7, it is evident that the combination of DWTBGP 3rd level image decomposition gives the maximum classification accuracy of **92.40%,** which has further increased the image classification accuracy and has given the best result.

Further, the time required by each of the above seven proposed DWT based texture feature extraction techniques for full feature vector data of a single image in the form of the bar chart is presented below in Fig. 3.4. The DWTBGP texture feature extraction technique has achieved best classification accuracy due to the merit of his feature of 92.4% at the third level of image decomposition, which required 0.2456 second of extraction time for individual images, which is much better than the time taken by other techniques except DWTLBP. The feature extraction time of DWTLBP is minimum (0.2011 seconds at 2nd level) but accuracy is 84.81 % only.
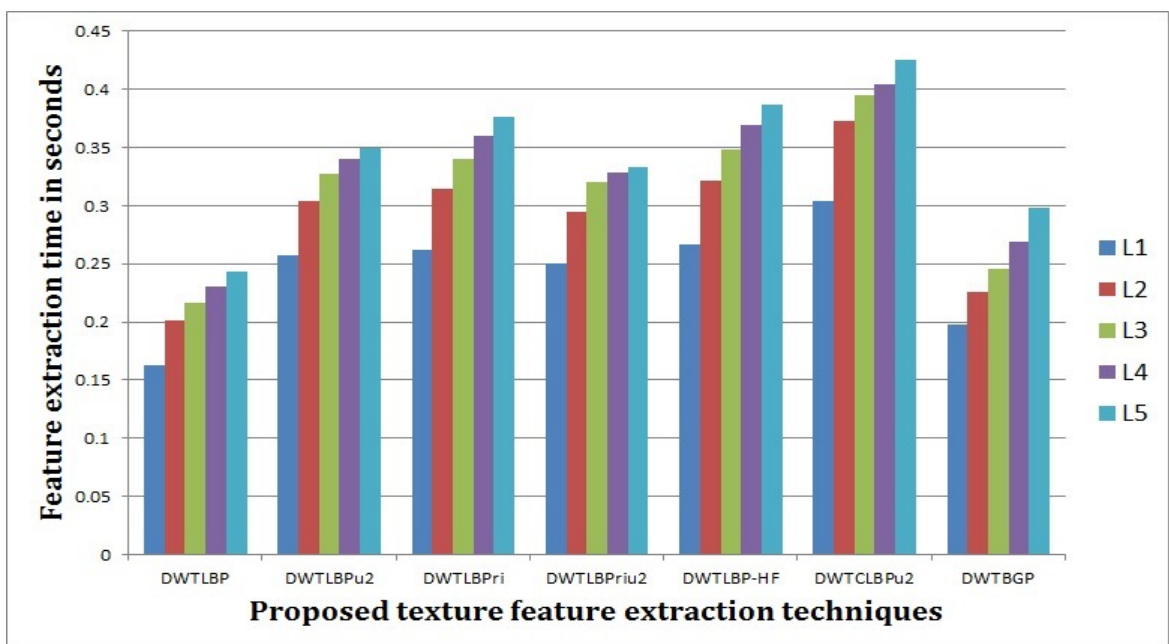
Fig. 3.4: Feature Extraction Time in Seconds for all the proposed feature extraction techniques.

3.3.3 Performance Evaluation using PCA dimensionality reduced feature vector data

In order to improve the classification accuracy of weld flaws using radiographic images of welding joints, PCA has been employed to reduce the dimensionality of full feature vector data. The performance of feature extraction techniques with PCA using different classifiers are listed in Tables below and have been succinctly discussed below. By employing PCA, results have been obtained with reduced features thereby, making the speed of operation and feature selection accurately.

Table 3.8: Classification accuracy at each level of DWTLBP after applying PCA

Proposed technique	IDL	Feature extraction time in seconds	NoF	% CA achieved by ANN classifier
DWTLBP	1	0.1630	300	83.54
	2	0.2011	250	**84.81**
	3	0.2168	300	84.81
	4	0.2308	400	84.81
	5	0.2433	250	82.28

From table 3.8, it is evident that the combination of DWTLBP after applying PCA 2nd and 3rdand 4thlevel image decomposition gives the classification accuracy of 84.81% respectively which is the same as the FFVD result. The advantage of PCA is that it gives good results at less number of feature vector sizes.

Table 3.9: Classification accuracy at each level of DWTLBPu2 after applying PCA

Proposed technique	IDL	Feature extraction time in seconds	NoF	% CA achieved by ANN classifier
DWTLBPu2	1	0.2569	200	84.81
	2	0.3038	400	84.81
	3	0.3275	350	**86.07**
	4	0.3402	450	86.07
	5	0.3494	400	84.81

From table 3.9, it is evident that the combination of DWTLBPu2 after applying PCA at 3rd and 4th level image decomposition gives the classification accuracy of 86.07% respectively, which is again the same to FFVD result but at only 350 number of feature vector size instead of 708 feature.

Table 3.10: Classification accuracy at each level of the DWTLBPri after applying PCA.

Proposed technique	IDL	Feature extraction time in seconds	NoF	% CA achieved by ANN classifier
DWTLBPri	1	0.2615	50	83.54
	2	0.3149	150	83.54
	3	0.34	200	**87.34**
	4	0.3595	250	87.34
	5	0.3758	150	86.07

From table 3.10, it is evident that the combination of the DWTLBPri after applying PCA at 3rd and 4th level image decomposition gives the classification accuracy of 87.34% respectively.

Table 3.11: Classification accuracy at each level of DWTLBPriu2 after applying PCA.

Proposed techniques	IDL	Feature extraction time in seconds	NoF	% CA achieved by ANN classifier
DWTLBPriu2	1	0.2508	30	81.01
	2	0.295	40	83.54
	3	0.3198	60	**84.81**
	4	0.3283	80	83.54
	5	0.3332	50	82.28

From table 3.11, it is evident that the combination of DWTLBPriu2 after applying PCA at 3rd level image decomposition gives the classification accuracy of 84.81% respectively.

From table 3.12, it is evident that the combination of DWTLBP - HF after applying PCA at 2nd, 3rd and 4th level image decomposition gives the classification accuracy of 81.01% respectively which has decreased the classification accuracy.

Table 3.12: Classification accuracy at each level of DWTLBP-HF after applying PCA.

Proposed techniques	IDL	Feature extraction time in seconds	NoF	% CA achieved by ANN classifier
DWTLBP-HF	1	0.2662	50	78.48
	2	0.3216	100	**81.01**
	3	0.3488	100	81.01
	4	0.3694	100	81.01
	5	0.3862	150	77.21

Table 3.13: Classification accuracy at each level of DWTCLBPu2 after applying PCA.

Proposed techniques	IDL	Feature extraction time in seconds	NoF	% CA achieved by ANN classifier
DWTCLBPu2	1	0.3037	200	81.01
	2	0.3724	150	82.28
	3	0.3947	250	**83.54**
	4	0.4039	200	83.54
	5	0.4257	400	79.74

From table 3.13, it is evident that the combination of DWTCLBPu2 after applying PCA at 3rd and 4th level image decomposition gives the classification accuracy of 83.54% respectively.

Table 3.14: Classification accuracy at each level of DWTBGP after applying PCA.

Proposed techniques	IDL	Feature extraction time in seconds	NoF	% CA achieved by ANN classifier
DWTBGP	1	0.1980	300	87.34
	2	0.2261	550	89.87
	3	0.2456	600	**92.40**
	4	0.2689	550	91.14
	5	0.2985	350	88.60

From table 3.14, it is evident that the combination of DWTBGP after applying PCA at 3rd level image decomposition gives the classification accuracy of 92.40% respectively. It is quite obvious from the results that even after reducing the feature vector length after applying PCA that the classification accuracy is the same as before applying PCA. Hence, PCA reduces the time of operation.

3.4   Summary

In this chapter, the DWTLBP variants and DWTBGP texture feature extraction techniques have been proposed to enhance the classification accuracy of radiographic weld images. In the proposed techniques, the DWT has been employed to decompose the image up to 5 different levels, followed by texture feature extraction with LBP variants and BGP. The resultant DWT sub-images coefficients obtained using the proposed methodology are distinct at each level and contain valuable information. Extracting texture features by variants of LBP from several level (L1 – L5) resolutions sub-images have increased the number of significant features. Combining the texture features of several levels (L1 – L5) generate significant feature vector useful in discrimination among the radiographic image of weld flaws.

The best classification accuracy of **92.4%** is obtained for DWTBGP texture features at the 3rd level of image decomposition using the ANN classifier. Further, reduction in feature vector dimensions is obtained using PCA and it is observed that the same result is obtained at a very less number of feature vector sizes after applying principal component analysis (PCA). In all the cases, the best result obtained at the third or fourth level of decomposition in both the cases i.e. with FFVD and PCA reduced vector data, and then after the result has been reduced for further decomposition level i.e. at fifth level. It should also be noted the application of PCA for feature reduction before applying classifier is beneficial because it very much reduces the time of execution.

CHAPTER 4: HYBRID FEATURE EXTRACTION TECHNIQUES

This chapter explores the effectiveness of the hybridization of segmentation and feature extraction to enhance the classification accuracy of weld flaws. The segmentation of the weld image database has been proposed here with many effective segmentation techniques for weld images. Then these segmented images have been used for GLCM and LBP variants of feature extraction techniques and their combination in presented at such a manner that the quality of feature vector should be improved. After the feature vector extraction, these hybrid features have been used in the different architecture of the ANN classifier to achieve the better classification accuracy of weld flaws.

4.1 Introduction

In the present scenario of industrialization, welding has become one of the prominent features for any development. Welding [149] is defined as the process of joining two materials in such a manner that the bonding exists between the materials. Welding is effectively used in building aircraft, turbines, industries, pipelines, etc. But the welding needs a proper environment and it should be carried out in accordance with the characteristics of the material. But the failure gives rise to weld defects.

In order to identify and classify the weld defects, there had been many researches. T. W. Liao, et al. [150] has proposed an automated radiographic NDT system for inspection of weld defects. The process involves two methods weld extraction i.e welds are extracted from radiographic images and an algorithm is developed to identify the flaws. This method was able to recognize only linear weld defects. Further, the author in [151] developed an algorithm for the identification of weld defects using curve fitting techniques. The database considered was only 24 images with 75 defects. S. V. Barai, Yoram Reich in [152] has used the concept of data mining namely insight and prediction for feature extraction of radiographic weld images. Also, he has proposed an idea to use these features to be fed to the neural network. The advantages of the concept were that better result was obtained due to the proper quality of the database.

With the advent of time, feature extraction techniques along with neural networks have found to have its effect in Image processing. In this regard, Ying Yin and Gui Y. Tian in [153] has done the inspection and evaluation of radiographic weld images by

optimizing the features such as geometrical shape, edge chain code, and geometric moment invariants. The best features were extracted and fed to the feed-forward back-propagation neural network for the classification of weld images. The author was successfully improving accuracy after feature optimization. Further, Rafael Vilar, Juan Zapata and Ramon Ruiz [42] introduced a system for the detection of weld defects using image processing, noise reduction, contrast enhancement, and thresholding for proper identification of the weld regions and appropriate classifications of weld defects. The geometrical features extracted were fed to an artificial neural network for classification. 86 radiographic images were considered. Even though results obtained were promising but it included a complex computer requirement.

The support vector machine has emerged as a proper classification tool. Ioannis Valavanis and Dimitrios Kosmopoulos [14] have developed a mechanism for the detection of flaws by extracting 43 texture and geometrical features. The features extracted were fed to Support Vector Machine, Neural Network, and k-NN classifiers. The computational time was significantly reduced but still, the accuracy was limited to 85.40%. Faiza Mekhalfa and Nafaa Nacereddine [154] proved the effective use of support vector machine over the traditional artificial neural network. The focus was on to develop an algorithm for successful weld image classification and which consumes less computational time. 344 images were considered with only 04 defects. The pixel size considered was 640 X 640.

The authors used geometrical features and compared the result with the Support vector machine and multilayer perceptron. A. Azari Moghaddam and L. Rangarajan [155] have proposed an algorithm to classify the weld defects using k nearest neighbor and support vector machine classification. The image databases considered only three different types of weld defects. The proposed algorithm was specially meant for lengthy defects.

In the present work, an attempt has been made to accurately identify and classify the weld defects. The image database has been pre-processed and segmented then the features have been extracted by GLCM, LBP, LBPri, LBPu2, LBPriu2, and combination of (LBP, LBPri, LBPu2, LBPriu2) and feed to the artificial neural network for classification.

4.2 Sample Image Database

In order to accurately identify and classify the weld defects, an algorithm has been developed and tested on the database. The image database has been obtained from Weld Testing and NDT laboratory, Department of Mechanical and Industrial Engineering, Indian Institute of Technology Roorkee. The images are radiographic in nature and are in not quality. It is indeed a cumbersome process to analyze a radiographic image to identify the welding flaw. Also, it should be kept in mind that the quality of an image is one of the major criteria for obtaining accuracy in classification. Detailed information about the image database is presented in Chapter - 2.

4.3 Image Pre-processing

In order to process the image for the purpose of testing of algorithm, all the raw digital imaged needs to be processed. For this purpose, following steps are involved:

4.3.1 Noise Removal

In the present work, the median filter has been used to obtain an efficient and reliable radiographic weld image. The electronics noise [157] is usually present in these images. The median filter is a non - linear method to de-noise the image. It removes noise by moving through the image pixel by pixel, replacing each value with the median value of the neighboring pixels. This pattern is known as "window" which slides, pixel by pixel over the entire image. The median is calculated by first sorting all the pixel values from the window into numerical order. Further, all the pixels are being replaced with the median value. It is useful as it removes relevant defects without decreasing image sharpness.

4.3.2 Contrast Enhancement

After the pre-processing technique, the contrast enhancement has been done by Contrast-limited adaptive histogram equalization method [158-159]. It enlarges the dynamic range of the image-pixel gray level and enhances the contrast. An enhancement function is applied over all neighborhood pixels from which transformation function is derived [159]. Fig.4.1 (a) shows the original radiographic image with gas cavity defect (b) shows the contrast-enhanced image and (c) reflects the histogram of the adaptive histogram equalization method.
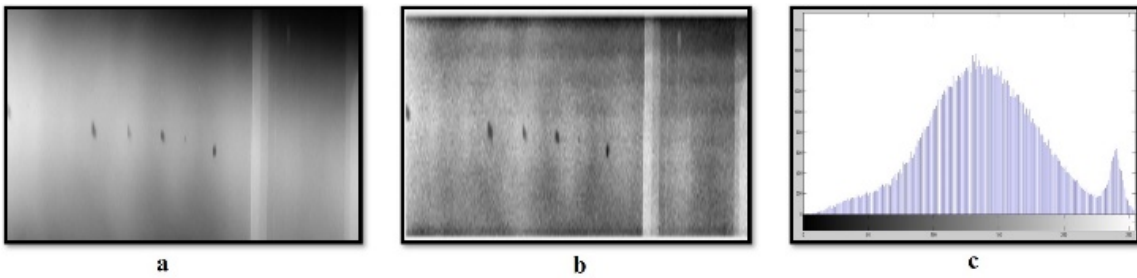
Fig. 4.1: Contrast enhancement of the radiographic image of the gas cavity

4.3.3 Image Segmentation

Image segmentation is a key step from image processing [149] to image analysis [160]. Since a qualified segmentation is the prerequisite and base of the consequent processing such as object extraction, parameter measurement and object recognition [150].

After pre-processing the radiographic images, the segmentation process is essential for the extraction of image features, especially for geometrical features. Hence, for getting better accuracy for classification, after pre-processing the images are segmented with various segmentation techniques such as Gray Threshold, Edge Detection, Horizontal edge detection using Integral filter, Contrast and Horizontal Response using Integral Filter and Multilevel Thresholding.

Gray Threshold is a straightforward and simple method. In this case, an optimal threshold is selected by the discriminant criterion, namely, so as to maximize the separability of the resultant classes in gray levels. The procedure is very simple, utilizing only the zeroth- and the first-order cumulative moments of the gray-level histogram.

Edges in digital images are defined as sharp intensity transitions. Edge-detection algorithms seek to detect and localize edges without any input or interference from humans. These algorithms are typically application based and may not produce the same results for a given image.

Pre-processing is the first phase of image analysis. The purpose of pre-processing is to improve the quality of the image being processed. It makes the subsequent phases of image processing like recognition of characters easier. Thresholding is the simplest method of image segmentation. It can be used for changing a grayscale image to binary images. Once computed a measure of edge strength (typically the gradient magnitude), the next stage is to apply a threshold to decide whether edges are present or not at an image point. The lower the threshold, the more edges will be detected and the result will be increasingly susceptible to noise and detecting edges of irrelevant features in the image. Conversely, a high threshold may miss subtle edges or result in fragmented edges.
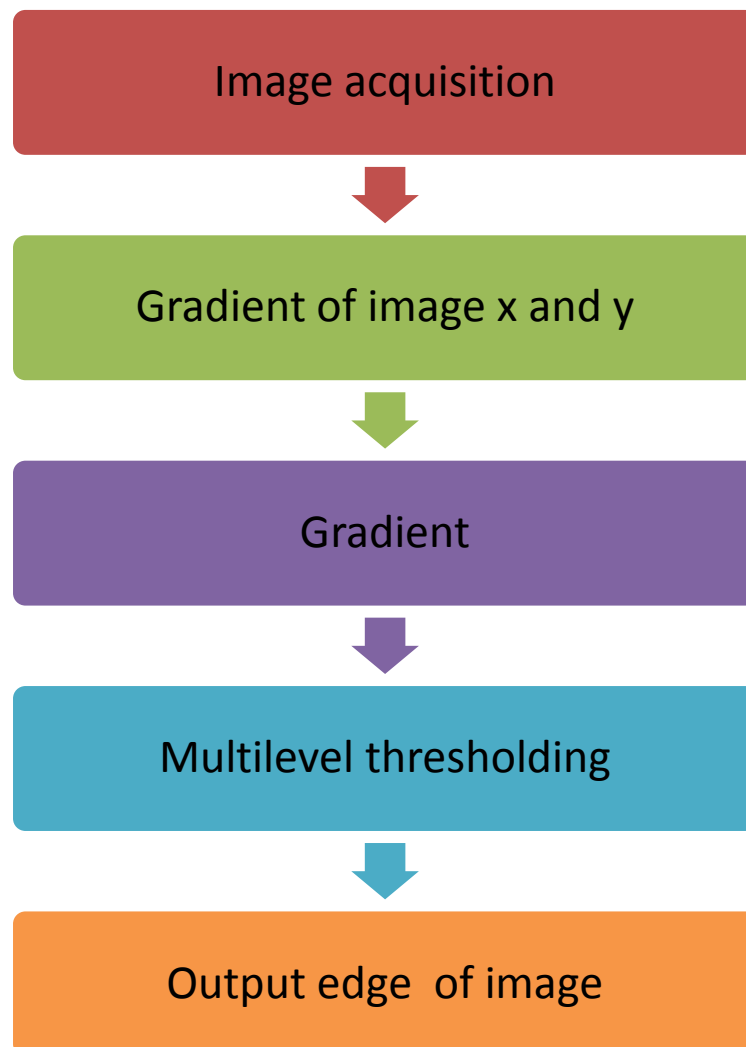
Fig. 4.2: Multilevel thresholding process

The process of multi-level thresholding works in five steps shown in Fig. 4.2. First step for the image acquisition, it is a process to eliminate noise from received test image, second gradient calculation along the x and y-axis, third block for gradient, the value of gradient helps to separate two different thresholds, forth for multi-level thresholding, at this stage different threshold level 3 and level 4 are calculated and find the best one, then got the output edge of image.

The reason for applying various segmentation threshold is because a particular segmentation technique gives the best result for particular types of weld flaws [158]. Hence, different types of combinations of segmentation techniques are applied to fetch better accuracy in classification.

Since Segmentation is the process of partitioning of the image and further analyzing it. The segmentation deals in the division of the image in the subdivisions. This subdivision of the image continues until the region of the interest of the required defect in welding is not solved.

It is not necessary that each segmentation technique fetch the best result for every type of defect. Each segmentation classifies the image differently and gives different results that are discussed in the next section.

The flow charts below denote the steps carried out in the segmentation process:
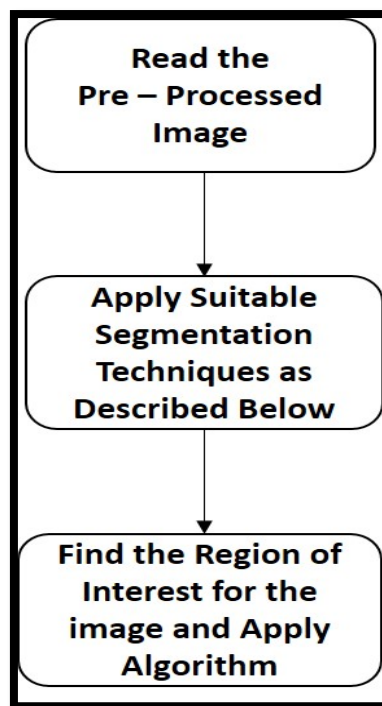
Fig. 4.3: Block diagram of Image Segmentation

There are various segmentation methods that are being followed as mentioned below:

4.3.3.1 Thresholding

It is the simplest and most commonly used segmentation technique in the image segmentation. It can be used to create a binary image. The threshold value or some specified value is given to the program below which all the pixels diminish and the higher value pixels are only shown, this is how thresholding technique works
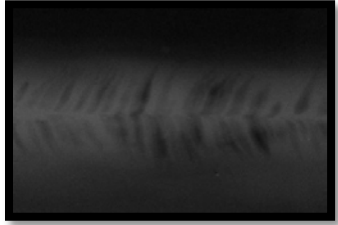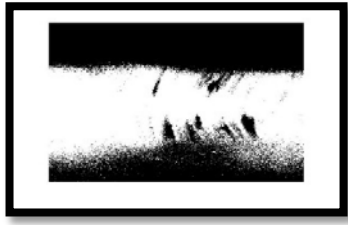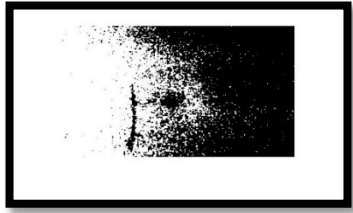
Nature of Flaw	Original Image	Segmented Image
Wormhole		
Gas Cavity		

Fig. 4.4: Segmented image after applying thresholding

4.3.3.2 Global Thresholding

The global thresholding is similar to the thresholding, the only difference is that it uses the Otsu method for thresholding.
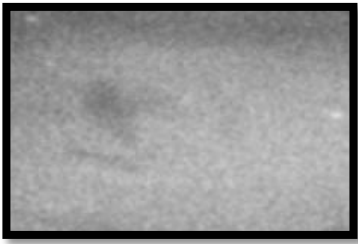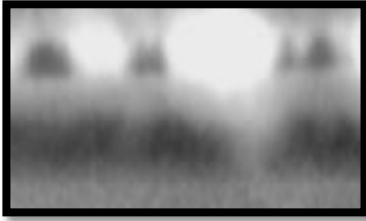
Nature of Flaw	Original Image	Segmented Image
Gas Cavity		
Gas Cavity		

Fig. 4.5: Segmented image after applying Global thresholding

4.3.3.3 Edge Detection

An edge is a boundary that separates the two regions of differing intensities in an image. The different techniques are being used for the edge detection. Some of the edge detection techniques are as follows:
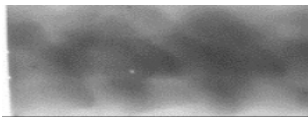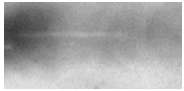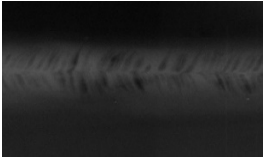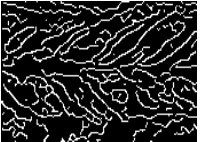
Sobel: It finds the edges at those points where the gradient of the image is maximum.

Laplacian of Gaussian: It finds the edges by looking for zero crossings after the filtration of the image.

Roberts: It finds edges at those points where the gradient of the image is maximum.

Prewitt: It finds edges at those points where the gradient of image is maximum as in Roberts.

Canny: It finds the edges by looking for the looking maxima of the gradient. It calculates the gradient using the derivative of Gaussian filter
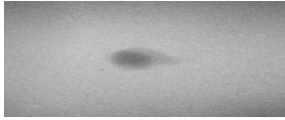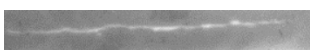
Nature of Flaw	Original Image	Segmented Image
Gas Cavity		
Lack of Penetration		
Porosity		
Slag		
Crack		
Lack of Fusion		
Wormhole		

Undercut		

Fig. 4.6: Images showing different intensities

4.3.3.4 Horizontal Edge Response

After applying the edge detection segmentation technique, the following images are obtained which are used for further analysis.

Nature of Flaw	Original Image	Segmented Image
Gas Cavity		
Lack of Penetration		
Porosity		
Slag		
Crack		
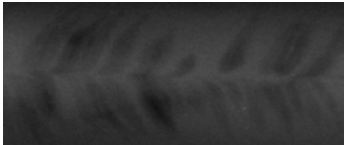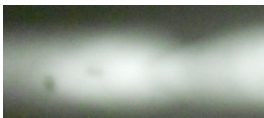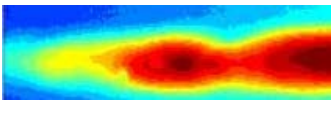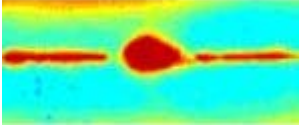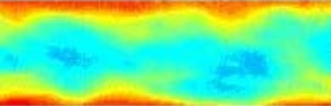
Lack of Fusion		
Wormhole		
Undercut		

Fig. 4.7: Images obtained after applying edge detection segmentation technique

4.3.3.5   Multi-Level thresholding

It is the thresholding method that implies Otsu's thresholding technique for segmentation purposes.

Nature of Flaw	Original Image	Segmented Image
Gas Cavity		
Lack of Penetration		
Porosity		
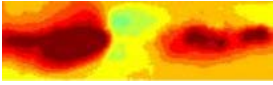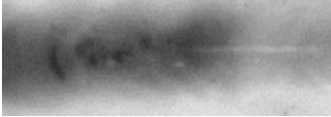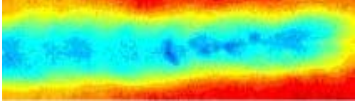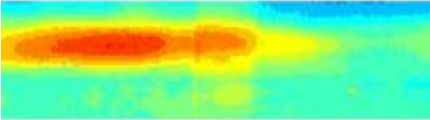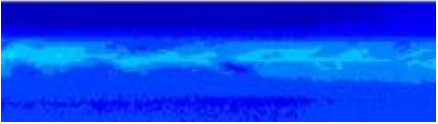
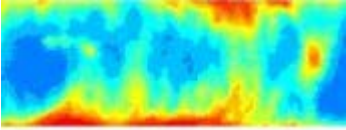|		
Slag		
Crack		
Lack of Fusion		
Wormhole		
Undercut		

Fig. 4.8: Images obtained after applying multilevel thresholding technique

4.4   Experiment – 1- (Image Segmentation + GLCM)

The methodology adopted for the identification and classification of welding defects have been explained in the flowchart given below in Fig. 4.9.
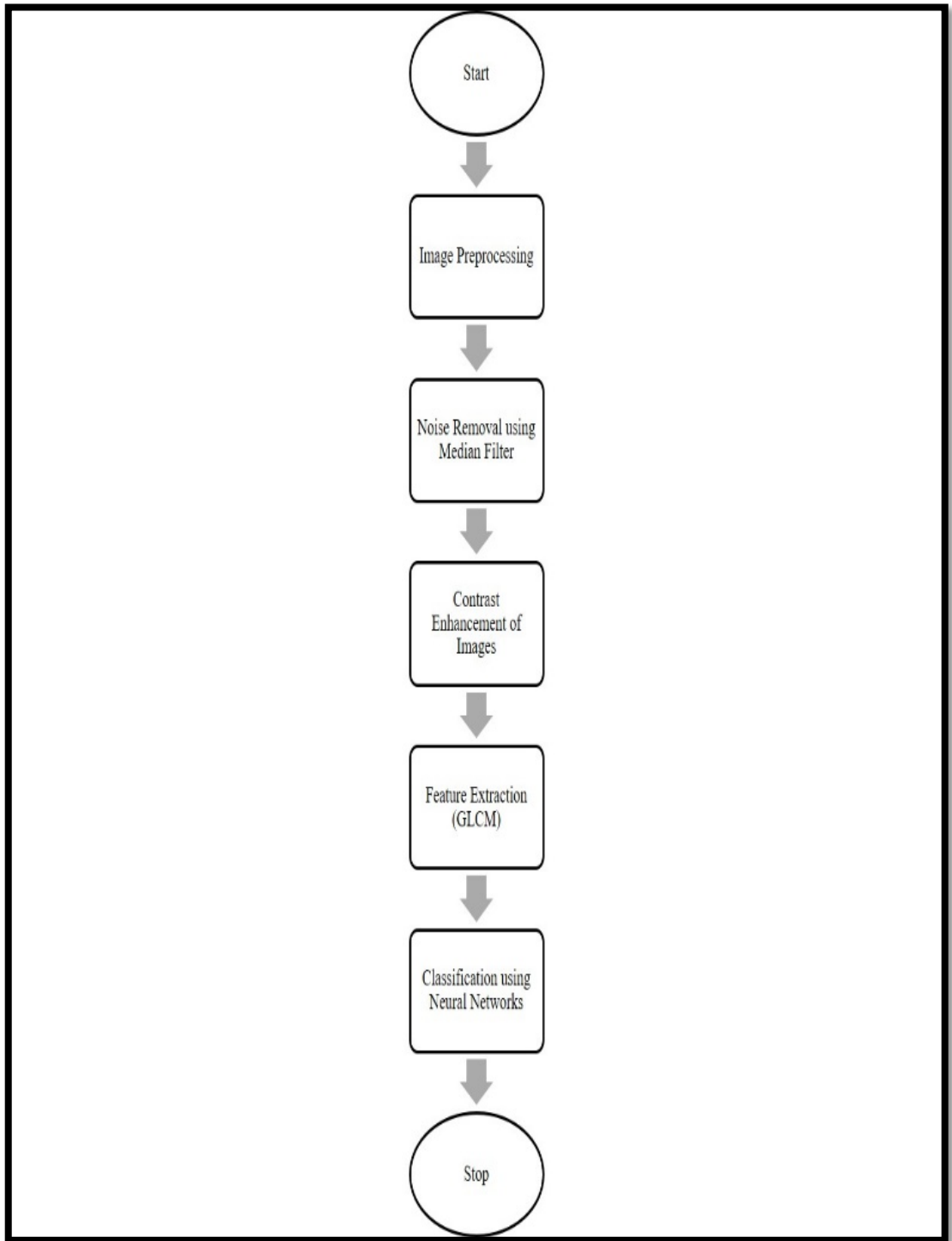
Fig. 4.9: Block diagram of Image Classification by Experiment - 1

The accuracy classification has been evaluated for both 8 and 64 level features extracted from GLCM and is shown in Table 4.1.

Table 4.1: Classification accuracy (%)

S. No.	No. of GLCM Features	Type of Neural Network	Classification Accuracy (in %)	No. of Neurons
1	8	Cascade Forward (cf)	**81**	75
		Feed Forward (ff)	79.7	64
2	64	Cascade Forward (cf)	**88.6**	58
		Feed Forward (ff)	87.3	60

The features obtained from the images have been fed to a neural network. As already discussed, Levenberg-Marquardt has been used for training. In this cascade forward and feed-forward architecture has been selected for analysis. The results were calculated for a range of 100 neurons. The optimal neuron for getting the highest accuracy has been depicted in table 4.2.

Table 4.2: % classification accuracy of GLCM (8 features)

No. of GLCM Features	Neural Network	Segmentation Techniques	Classification Accuracy (in %)	No. of Neurons
8	cf	Gray Thresh	72.2	99
8	cf	Contrast Enhancement	81	75
8	cf	Edge Detection	77.2	96
8	ff	Horizontal Edge Responses Using Integral Filter	77.2	98
8	ff	Contrast enhancement + horizontal response using integral Filter	78.5	95
8	ff	Multi-Level Thresholding	**83.5**	58

In table 4.3 cascade forward architecture has been selected for analysis. The results were calculated for a range of 100 neurons. For contrast enhancement techniques, an accuracy of 88.6 % at 58 neurons is obtained.

72

Table 4.3: % classification accuracy of GLCM (64 features)

No. of GLCM Features	Network	Segmentation Techniques	Maximum Accuracy (in %)	No. of Neurons
64	Cf	Gray Threshold	81	58
64	Cf	Contrast Enhancement	**88.6**	58
64	Cf	Edge Detection	79.7	58
64	Cf	Horizontal Edge Responses Using Integral Filter	82.3	72
64	Cf	Contrast Enhancement+Horizontal Response Using Integral Filter	83.5	92
64	Cf	Multi-Level Thresholding	84.8	89

In table 4.4 feed-forward architecture has been selected for analysis. The results were calculated for a range of 100 neurons. Here also, for the contrast enhancement technique, we obtained the maximum accuracy of 87.3%.

Table 4.4: % classification accuracy of GLCM (64 features)

No. of GLCM Features	Network	Segmentation Techniques	Maximum Accuracy (in %)	No. of Neurons
64	ff	Gray Thresh	82.3	96
64	ff	Contrast Enhancement	**87.3**	60
64	ff	Edge Detection	82.3	82
64	ff	Horizontal Edge Responses Using Integral Filter	83.5	84
64	ff	Contrast Enhancement + Horizontal Response Using Integral Filter	86.1	89
64	ff	Multi-Level Thresholding	82.3	51

It is observed from the above table that for 8 features with 75 neurons, 81% accuracy was observed for cascade forward. While the only 79.7% accuracy was achieved at 64 neurons, for feed-forward. Similarly, for 64 features using cascade feature at 58 neurons the optimal classification accuracy of 88.6% was obtained which is very promising as compared to the work in [161], where the accuracy classification is 86.1%. It

might be due to the pre-processing of the image where noise has been removed and also, contrast enhancement has been done.
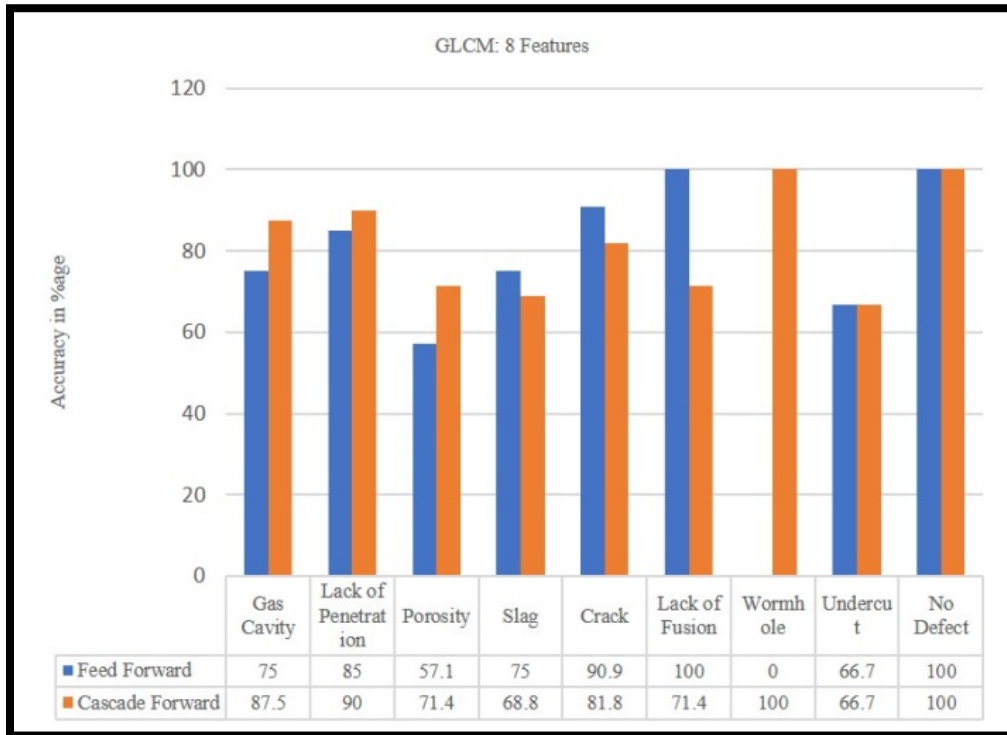

Fig. 4.10: Individual Classification Accuracy of each flaw with GLCM 8 Features

The individual classification accuracy of each type of flaws is shown in Fig. 4.10. It is observed that the Gas Cavity, Lack of penetration, porosity, wormhole, and no defect has been satisfactorily classified in Cascade Forward Neural Network. Also, the classification result in undercut defect is minimal with 66.7%. But one thing is acceptable that Cascade forward training is better than feed-forward training based on all the above result.

Further, the results have further been introspected to have knowledge about which type of defect was misclassified. Fig. 4.10 depicts the individual classification accuracy of each weld flaws with GLCM 8 features for both feed-forward and cascade forward neural network architecture.

Fig. 4.11 depicts the classification accuracy with GLCM 64 level features for both Feed-forward and Cascade Forward network.

	Gas Cavity	Lack of Penetration	Porosity	Slag	Crack	Lack of Fusion	Wormhole	Undercut	No Defect
■ Feed Forward	87.5	95	57.1	81.3	100	100	100	66.7	80
■ Cascade Forward	87.5	100	85.7	75	100	85.7	100	100	60
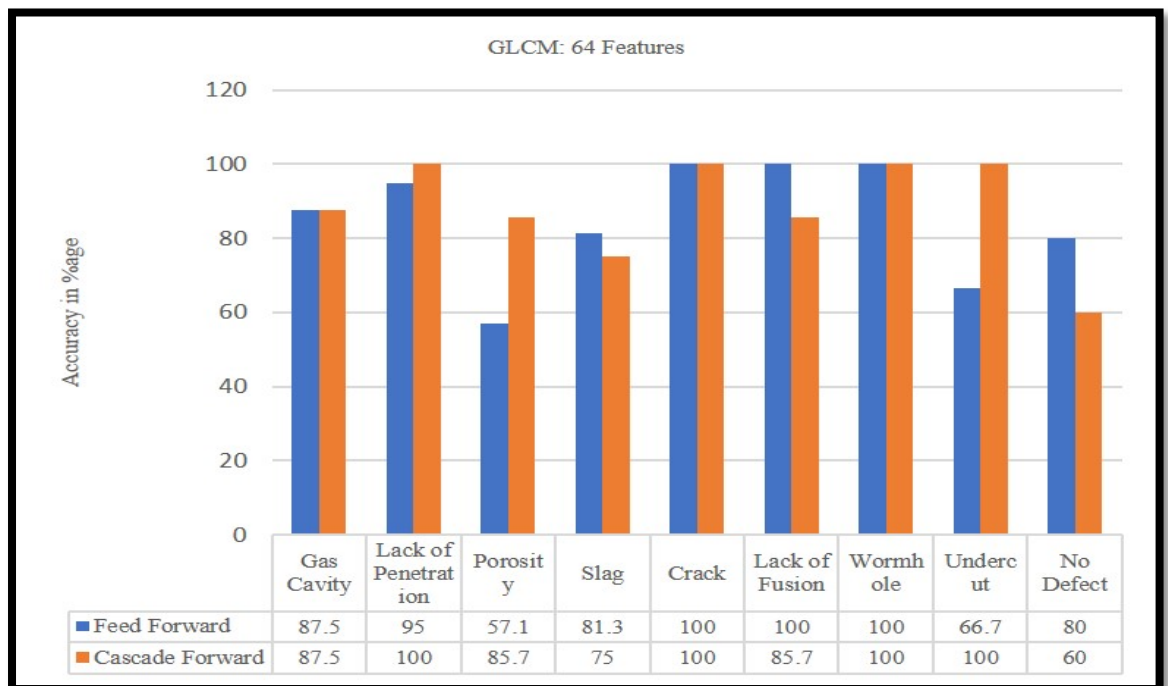
Fig. 4.11: Individual Classification Accuracy of each flaw with GLCM 64 Features

It has been observed in Fig. 4.11 that the classification results of GLCM 64 level features with training with cascade forward neural has found to be very promising. Almost all four types of flaws gas cavity, Lack of penetration, porosity, crack, wormholes, undercut has been classified at a better accuracy rate. The no defect types of images have been least classified. The slag defect has the least classification accuracy with 75% which is still better than feed-forward training and with 8 features of GLCM.

Based on the above observations, it is recommended that 64 features with cascade forward neural network yield better results.

4.5   Experiment – 2 (Image Segmentation + LBP Variants)

In the present paper, an attempt has been made to accurately identify and classify the weld defects. The image database has been pre-processed and segmented after that the features have been extracted by LBP, LBPri, LBPu2 and LBPriu2 and their different combinations and feed to Artificial neural network classifier in order to achieve better classification accuracy..

4.6 Algorithm

The methodology adopted for the identification and classification of welding defects have been explained in the flowchart given below:
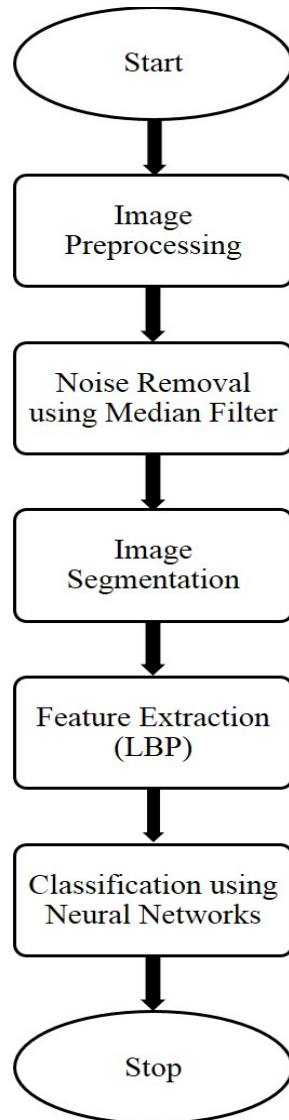

Fig. 4.12: Block diagram of weld flaws Image Classification

At first, from the different segmentation techniques, LBP features have been extracted to process the algorithm. 256 features of LBP have been considered. It is observed from Table 4.5 and Fig. 4.13, that Contrast Enhancement has the maximum accuracy of 86.1% at 72 neurons whereas by applying multilevel thresholding 83.5% accuracy is achieved. Edge Detection Method performs the least with 77.2% while gray Threshold gives 78.5%.

Table 4.5: % classification accuracy of LBP after segmentation

No. of Features	Segmentation Technique	% Classification Accuracy	No. of Neurons
256	Edge Detection	77.2	85
256	Contrast Enhancement	**86.1**	72
256	Gray thresh	78.5	98
256	Multi-Level Thresholding	83.5	58
256	Horizontal Edge Responses Using Integral Filter	79.7	19
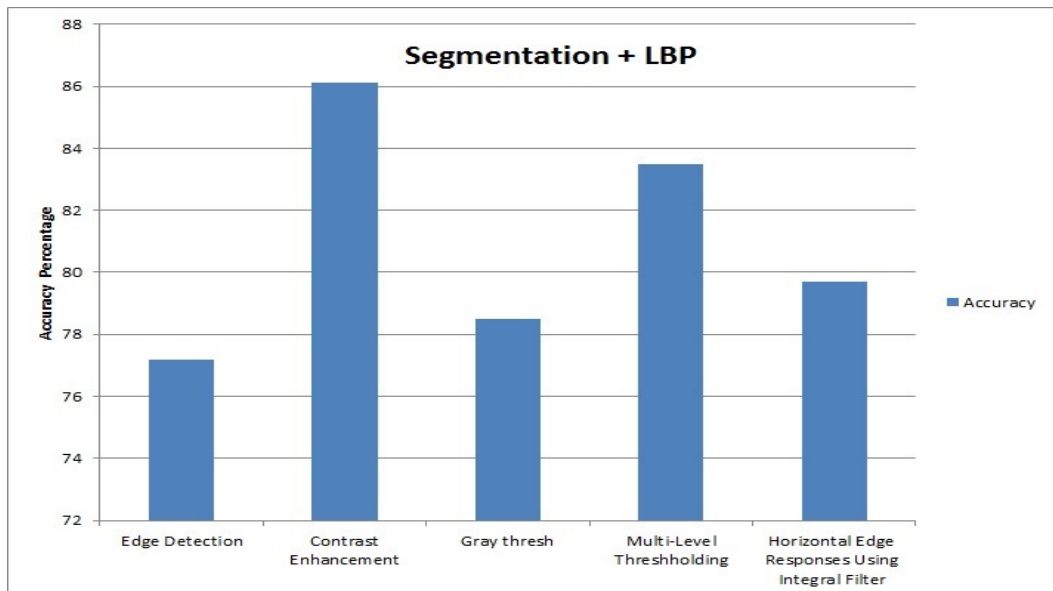
Fig. 4.13: classification accuracy of LBP after segmentation

Hence, it is observed that here contrast enhancement technique yields the maximum result and outperforms every technique with 86.1%. It is to be kept in mind that the experiment was carried out from 1 neuron to 100 neurons in order to analyze the effect for achieving better accuracy and the optimal neuron is presented in the table.

Now, the next attempt has been made to extracts LBPri features from different segmentation techniques. 36 number of LBPri features have been extracted to process the algorithm. It is observed from the Table 4.6 and Fig.4.14, that the accuracy of 83.5% was achieved by applying contrast enhancement whereas 84.8% accuracy is achieved by multi-level thresholding and Horizontal Edge Responses using Integral Filter at 40 and 33 neurons respectively. Edge Detection Method performs the least with 73.4% while gray

Threshold gives 79.7%. Hence, it is observed that multi-level thresholding and Horizontal Edge Responses using the Integral Filter technique yields the maximum result and outperforms every segmentation technique for LBPri feature extraction. The number of neurons gives the exact neuron in which the maximum accuracy was achieved. It is to be kept in mind that the experiment was carried out from 1 neuron to 100 neurons in order to analyze the effect for achieving better accuracy and the optimal neuron is presented in table 4.6.

Table 4.6: % classification accuracy of LBPri after segmentation

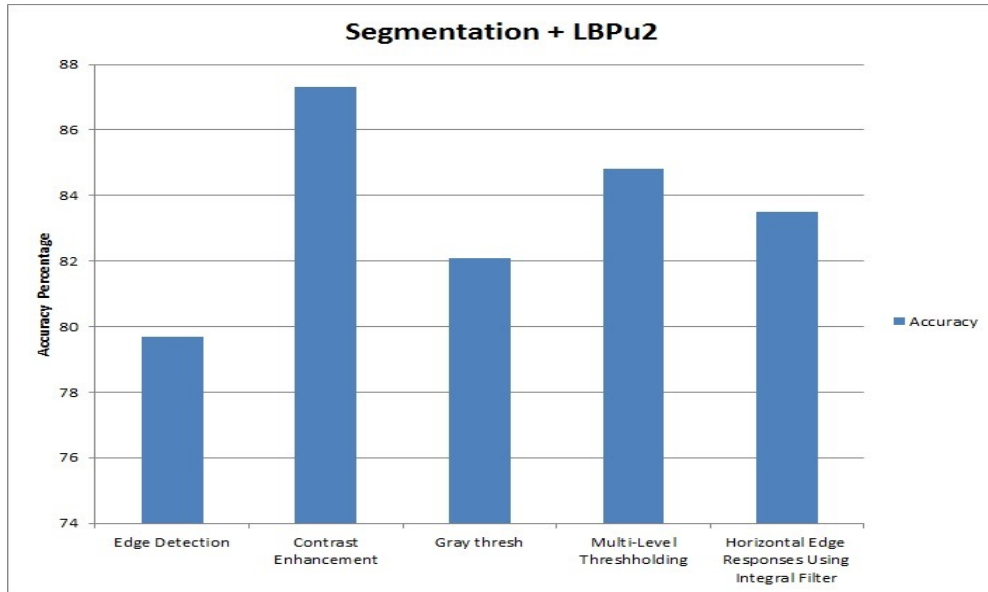| No. Of Features	Segmentation Techniques	Classification Accuracy (in %)	No. of Neurons
36	Edge Detection	73.4	67
36	Contrast Enhancement	83.5	62
36	Gray thresh	79.7	82
36	Multi-Level Thresholding	**84.8**	40
36	Horizontal Edge Responses Using Integral Filter	84.8	33
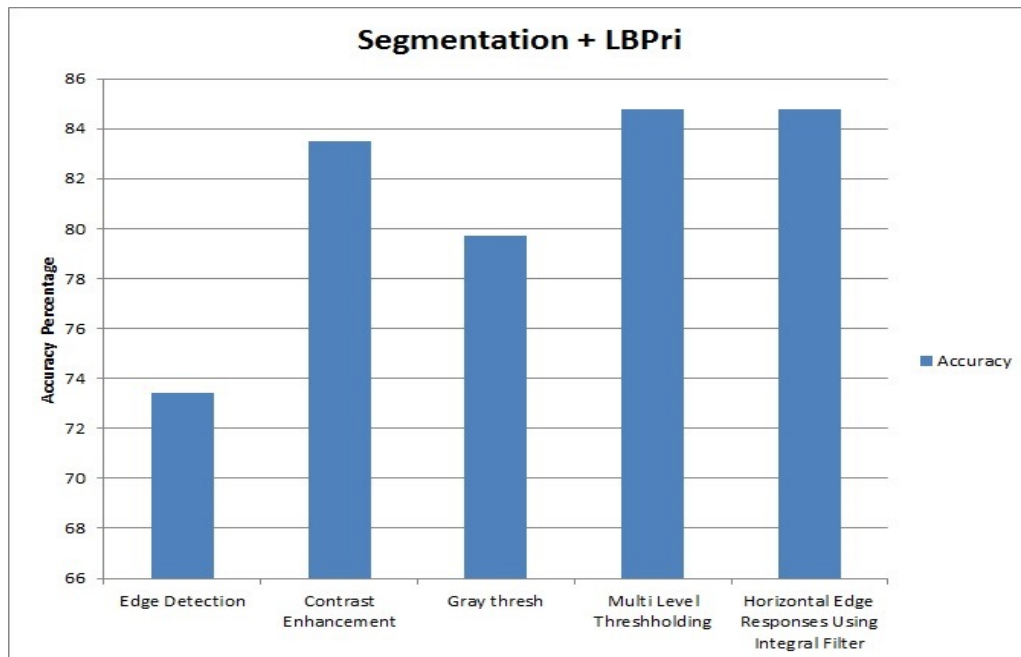
Fig. 4.14: classification accuracy of LBPri after segmentation

Further, another attempt has been made to extracts LBPu2 features from different segmentation techniques. LBPu2 technique produces 59 feature has been extracted to process the algorithm. It is observed from the Table and figures no 4.14, that Contrast Enhancement has an accuracy of 87.5% at 88 neurons. Edge Detection Method performs the least with 79.7% while Gray Threshold gives better results at 82.1%. Hence, it is observed that multi-level thresholding and Horizontal Edge Responses Using the Integral Filter technique yields 84.8% and 83.5% respectively for the selected database. Hence, it is observed that Contrast Enhancement has a maximum accuracy of 87.5% at 88 neurons. The number of neurons gives the exact neuron in which the maximum accuracy was achieved. It is to be kept in mind that the experiment was carried out from 1 neuron to 100 neurons in order to analyze the effect for achieving better accuracy and the optimal neuron is presented in table 4.7.

Table 4.7: % classification accuracy of LBPu2 after segmentation

No. of Features	Segmentation Techniques	% Classification Accuracy	No. of Neurons
59	Edge Detection	79.7	61
59	Contrast Enhancement	**87.3**	88
59	Gray thresh	82.1	80
59	Multi-Level Thresholding	84.8	29
59	Horizontal Edge Responses Using Integral Filter	83.5	4

Fig. 4.15: classification accuracy of LBPu2 after segmentation

Further, an attempt has been made to extracts LBPriu2 features from different segmentation techniques. 10 LBPu2 features have been extracted to process the algorithm. It is observed from the Table and Fig. 4.16, that Contrast Enhancement has the accuracy of 89.9% at 56 neurons. Edge Detection Method performs the least with 69.6% while Gray Threshold gives better results at 88.6%. Hence, it is observed that multi-level thresholding and Horizontal Edge Responses using Integral Filter gives an accuracy of 73.4% and 82.3% respectively for the created database. Hence, it is observed that has the maximum accuracy of 89.9% at 56 neurons is achieved by Contrast Enhancement. It is to be kept in mind that the experiment was carried out from 1 neuron to 100 neurons in order to analyse the effect for achieving better accuracy and the optimal neuron is presented in table 4.8.

Table 4.8: % classification accuracy of LBPriu2 after segmentation

No. of Features	Segmentation	Accuracy	No. of Neurons
10	Edge Detection	69.6	76
10	Contrast Enhancement	**89.9**	56
10	Gray Thresh	88.6	99
10	Multi-Level Thresholding	73.4	88
10	Horizontal Edge Responses Using Integral Filter	82.3	75
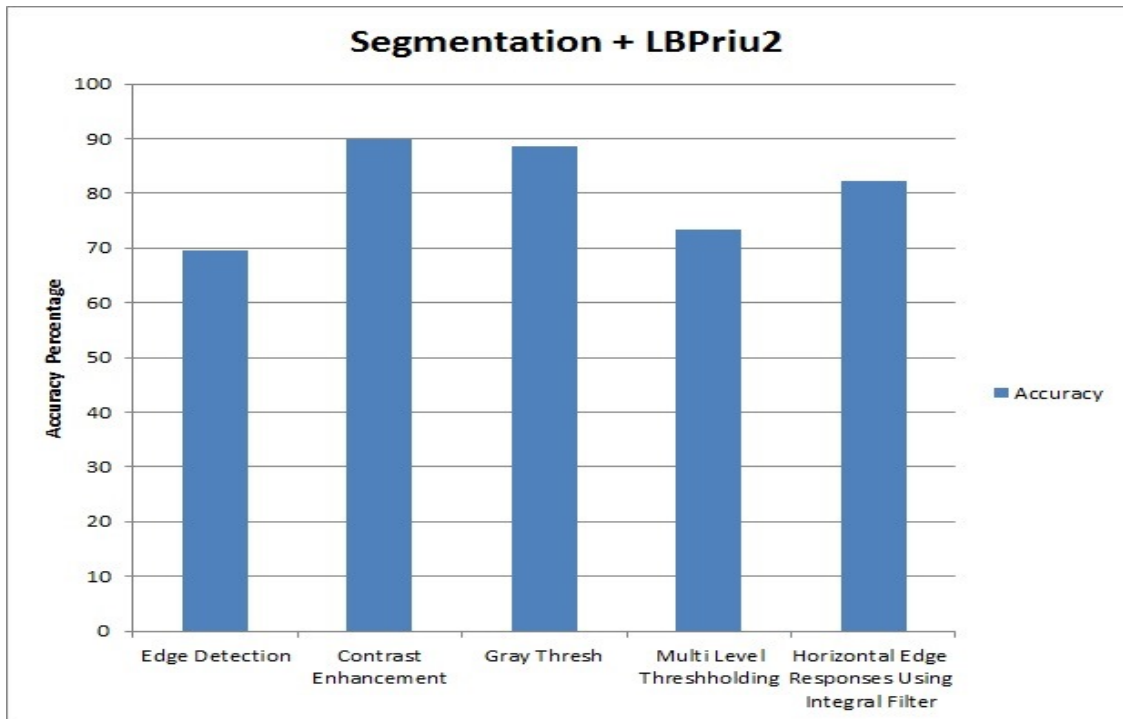
Fig. 4.16: classification accuracy of LBPriu2 after segmentation

In subsequent experiment, an attempt has been made to combine above all three feature vector (LBPri + LBPu2 + LBPriu2) and add it such a way (overlap) on LBP 256 features from the different segmentation techniques so that size of the final feature vector is 256 only. It is observed from Table 4.9 and Fig. 4.17, that Contrast Enhancement has the accuracy of 92.4% at 96 neurons. Edge Detection Method performs the least with 79.7% while Gray Threshold gives better results at 87.3%. It is also observed that multi-level thresholding and Horizontal Edge Responses using Integral Filter gives an accuracy of 82.3% and 84.8% respectively. The number of neurons gives the exact neuron in which the maximum accuracy was achieved. It is again to be kept in mind that the experiment was carried out from 1 neuron to 100 neurons in order to analyze the effect for achieving better accuracy and the optimal neuron is presented in table 4.9.

From the above inference, it is found that the combination of (LBPri + LBPu2 + LBPriu2) with LBP have given the best result. Now, The detailed percentage-wise classification accuracy for the above combination is presented in table 4.9. From the above inference, it is found that the combination of (LBPri + LBPu2 + LBPriu2) with LBP have given the best result. Now, the detailed percentage wise classification accuracy for the above combination is presented below:

Table 4.9: % classification accuracy of (LBPri + LBPu2 + LBPriu2) overlap on LBP

No. of Features	Segmentation Techniques	Classification Accuracy (in %)	No. of Neurons
256	Edge Detection	79.7	86
256	Contrast Enhancement	**92.4**	96
256	Gray Thresh	87.3	95
256	Multi Level Threshholding	82.3	94
256	Horizontal Edge Responses using Integral Filter	84.8	69
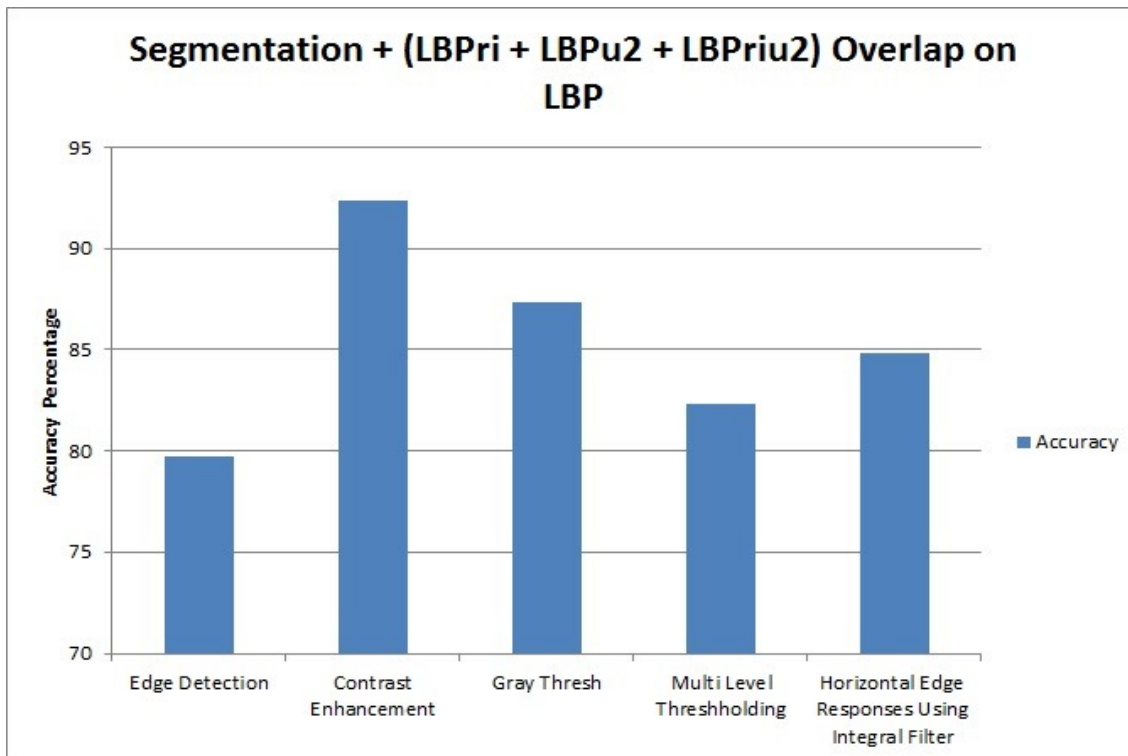
Fig. 4.17: classification accuracy of LBP(LBPri + LBPu2 + LBPriu2) feature

From the above experiment (experiment-2) it is concluded that the feature vector generated by the combination of (LBPri +LBPu2+ LBPriu2) and overlapped on LBP feature having a feature vector dimension of 256 gives the best feature for classification. In the below section the classification accuracy of individual flaws has been discussed for a combined feature and different segmentation techniques.

Table 4.10: % accuracy of LBP(LBPri +LBPu2+ LBPriu2) Feature + Edge Detection

S.No.	Name of Defect	Total No. of Images	No. of Accurately Classified	No. of Images Misclassified	Classification Accuracy (in %)
1	Gas Cavity	8	7	1	87.5
2	Lack of Penetration	20	20	0	100
3	Porosity	7	5	2	71.4
4	Slag	16	11	5	68.75
5	Crack	11	9	2	81.81
6	Lack of Fusion	7	5	2	71.42
7	Wormhole	2	1	2	50
8	Undercut	3	2	1	66.7
9	No Defect	5	3	2	60
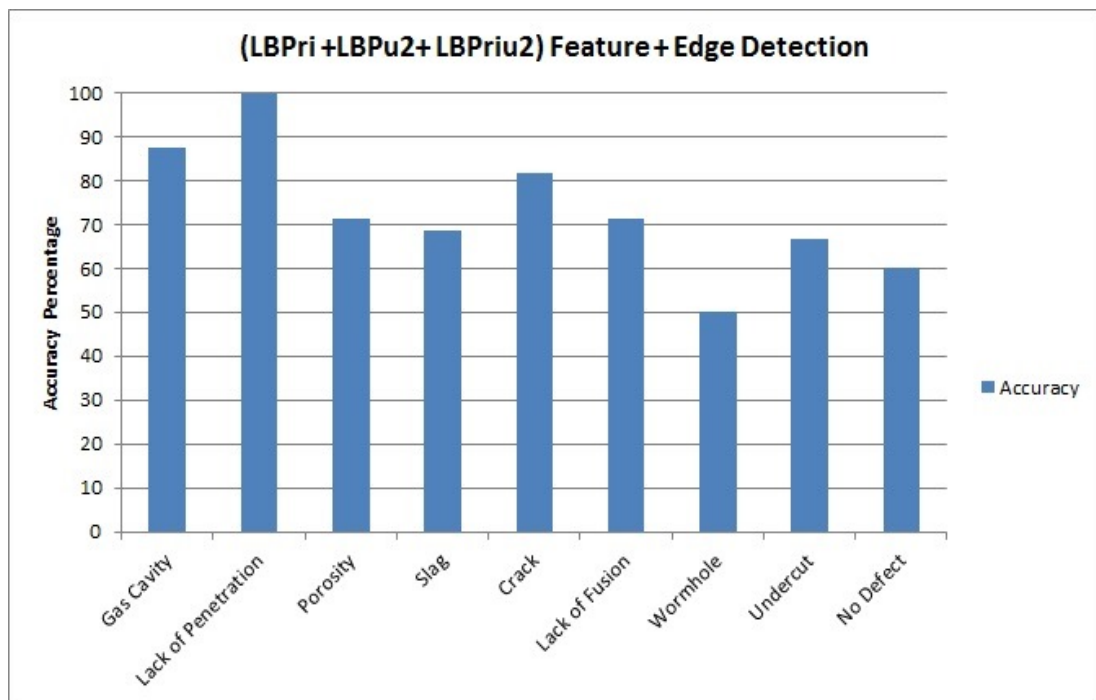
Fig. 4.18:(LBPri +LBPu2+ LBPriu2) Feature + Edge Detection

It is observed that except a lack of penetration, all other defects have not been successfully classified. It seems that the boundary edges haven't been properly identified in this case. The results obtained are not at all promising.

Table 4.11: % accuracy of LBP(LBPri +LBPu2+ LBPriu2) + contrast enhancement

S.No.	Name of Defect	Total No. of Images	No. of images Accurately Classified	No of Images Misclassified	% Classification Accuracy
1	Gas Cavity	8	7	1	**87.5**
2	Lack of Penetration	20	20	0	**100**
3	Porosity	7	6	1	**85.7**
4	Slag	16	14	2	**87.5**
5	Crack	11	11	0	**100**
6	Lack of Fusion	7	7	0	**100**
7	Wormhole	2	2	0	**100**
8	Undercut	3	3	0	**100**
9	No Defect	5	3	2	**100**
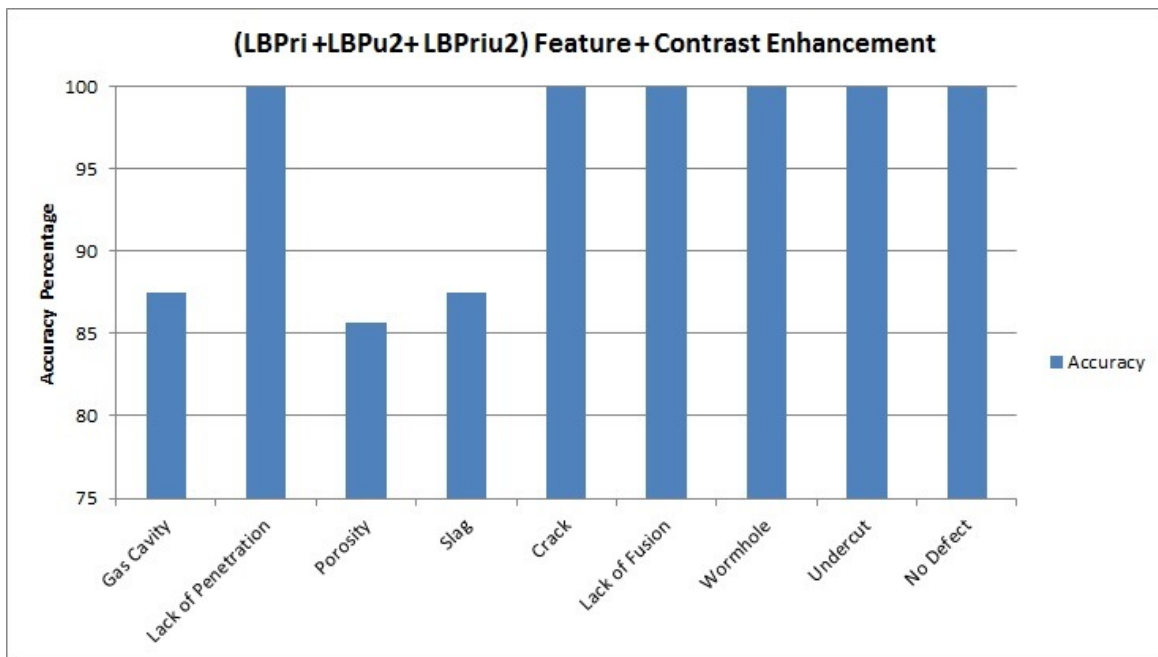
Fig. 4.19: (LBPri +LBPu2+ LBPriu2) Feature + Contrast Enhancement

It is observed that except Gas Cavity, porosity and slag, all other defects have been 100 % classification accuracy. Hence, Contrast enhancement combination with the different LBP variants has fetched the best result.

Table 4.12: % accuracy of LBP(LBPri +LBPu2+ LBPriu2) + Gray Scale Thresholding

S.No.	Name of Defect	Total No. of Images	No. of Accurately Classified	No of Images Misclassified	% Classification Accuracy
1	Gas Cavity	8	7	1	87.5
2	Lack of Penetration	20	19	1	95
3	Porosity	7	6	1	85.7
4	Slag	16	12	4	75
5	Crack	11	11	0	100
6	Lack of Fusion	7	5	2	71.4
7	Wormhole	2	2	0	100
8	Undercut	3	3	0	100
9	No Defect	5	4	1	80

Fig. 4.20:(LBPri +LBPu2+ LBPriu2) Feature + Gray Scale Thresholding

It is observed that except crack, wormhole and undercut, all other defects have not been successfully classified. It seems that the boundary edges haven't been properly identified in grayscale thresholding.

Table 4.13: % accuracy of LBP(LBPri +LBPu2+ LBPriu2) + Multi-Level Thresholding

S. No.	Name of Defect	Total No. of Images	No. of Accurately Classified	No of Images Misclassified	% Classification Accuracy
1	Gas Cavity	8	8	0	100
2	Lack of Penetration	20	18	2	90
3	Porosity	7	5	2	71.4
4	Slag	16	10	6	62.5
5	Crack	11	11	0	100
6	Lack of Fusion	7	5	2	71.4
7	Wormhole	2	2	0	100
8	Undercut	3	3	0	100
9	No Defect	5	3	2	60

Fig. 4.21:(LBPri +LBPu2+ LBPriu2) Feature + Multi – Level thresholding

It is observed that the classification accuracy of lack of penetration, porosity, slag inclusion, lack of fusion and no defects images have very low. It seems that the boundary edges haven't been properly identified in this case too. The results obtained are not promising.

It is observed from Fig 4.18 to Fig 4.21 that the individual classification accuracy of crack, wormhole, undercut and lack of penetration type of flaws are 100% in most of the cases with hybrid feature vector combination of LBP +(LBPri + LBPu2 + LBPriu2) having feature vector dimension of 256.

4.7   Summary

The proposed work of this chapter demonstrated the effectiveness of the different combinations of GLCM features with different direction and LBP variants and their combination in a different possible manner to enhance the classification accuracy of the weld flaws. To achieve this goal, the segmentation of images has also been carried out before applying the feature extraction. The features are extracted from segmented images and then that features are combined and make it a hybrid feature in such a way that each feature have their own merit. Then these hybrid features are fed as input to the neural network classifier because this classifier has shown good result for this weld image data set as proved in chapter 2 but here to evaluate the performance of neural network, two architecture of neural network namely feed-forward algorithm and cascade forward algorithm has been compared and it is found that cascade forward network performed better than fast forward network. In this chapter, all the experiments have been accomplished on 70/30 proportion of randomly divided database. Among the proposed segmentation techniques, the image after contrast enhancement obtained the best classification accuracy of 88.6% on the CF network of ANN. Using GLSM (16 feature in 4 direction = 64). In second experiment feature of variants have combined and observed that classification accuracy of LBP, LBPri, LBPu2, LBPriu2, are 86.1%, 84.8%, 87.3%, 89.9% respectively but when we hybrid these features and form a new feature vector of 256 feature then the CA drastically improved and it archived **92.4%** which is the best among them all techniques performed here. The individual performance of each type of flaws are also described in this chapter and concluded that the individual classification accuracy of crack, wormhole, undercut and lack of penetration type of flaws are 100% in most of the cases with hybrid feature vector combination of LBP +(LBPri + LBPu2 + LBPriu2) having feature vector dimension of 256.

CHAPTER 5:   CONCLUSIONS AND FUTURE SCOPE

5.1   Conclusions

This research work has been carried out to analyze the weld flaws classification of the welding joint on the basis of digitized images of radiographic films of the same. The emphasis has been given to the design and development of some techniques for texture feature extraction for the classification of weld flaws images into nine different categories on their merit. The effectiveness of the proposed techniques has been investigated on the radiographic image database of weld joints collected from the welding research laboratory, department of mechanical and industrial engineering, Indian Institute of Technology Roorkee, Roorkee.

To accomplish the classification task efficiently, a comparative study of the several texture feature extraction techniques have been carried out to find the efficient texture feature extraction techniques for radiographic images of weld flaws. Further, the performance of these techniques has been improved by hybrid these features with many different types as well as extracting these features from multi-resolution images and combining them to form a feature vector data.

The feature vector data extracted by these techniques have been then normalized in the range of 0 to 1 to give equal weightage to all the feature vectors prior to applying it as classifier inputs. The discrete wavelet transforms feature extraction techniques have produced a large number of complex features that may limit the classification accuracy. Therefore there is a need for feature reduction techniques. In the present research principal component analysis (PCA) as a feature reduction technique has been employed to reduce the dimension of feature vector data. Further to analyze the classification accuracy on a fixed feature vector either a full feature or reduced feature, three widely used classification algorithms namely Linear SVM, RBF Kernal SVM, and ANN-based classifier. The Lavenberg Marquardt training method has been employed further to evaluate the performance of the ANN classifier with two sets of the randomly divided database. According to the result obtained the best combination of feature extraction techniques and classification algorithm has been selected.

Performance of Texture Feature Extraction Techniques:

The experimental results accomplished that the full feature vector data (FFVD) and PCA reduced feature selection based feature vector data of the BGP texture feature extraction technique has achieved the best classification accuracy of 91.14% and 89.87%on 80/20 and 70/30 randomly divided data set respectively with ANN classifier. Moreover, these techniques also achieve the same classification accuracy on the PCA reduced feature vector data with very reduced no of features. Amongst several techniques examined here, the GLCM and LBPri produced 2nd and 3rd highest accuracy using the same classifier with both the proportion of training and testing data set. The PCA reduced feature selection hardly affects the performance of the classifier. In all the feature extraction techniques the performance of linear SVM and RBF Kernel SVM classifiers are not up to mark.

Performance of DWT Based Texture Feature Extraction Techniques:

The DWTLBP variants and DWTBGP texture feature extraction techniques have been proposed to enhance the classification accuracy of radiographic weld images. In the proposed techniques, the DWT has been employed to decompose the image up to 5 different levels, followed by texture feature extraction with LBP variants and BGP. The resultant DWT sub-images coefficients obtained using proposed methodologies are distinct at each level and contain valuable information. Extracting texture features by variants of LBP and BGP from several level (L1 – L5) resolutions sub-images have increased the number of significant features. Combining the texture features of several levels (L1 – L5), generate significant feature vector useful in discrimination among the radiographic image of weld flaws. So basically we are combining the different levels for getting the better and the significant outcomes.

The best classification accuracy of 92.4% is obtained for DWTBGP texture features at the 3rd level of image decomposition using the ANN classifier. Further, reduction in feature dimensions is obtained using PCA and it is observed that the same result is obtained even after applying principal component analysis. In all the cases, the best result obtained at the third or fourth level of decomposition and then after the result has been reduced for further decomposition level i.e. at the fifth level.

Performance of Segmentation Based Hybrid Feature Extraction Techniques:

The proposed work demonstrated the effectiveness of the different combinations of GLCM features with different direction and LBP variants to enhance the classification accuracy. To achieve this goal, the segmentation of images has also been carried out before applying the feature extraction. The features are extracted from segmented images and then that features are combined and make it a hybrid feature in such a way that each feature have their own merit. Then these hybrid features are fed as input to the neural network. In order to evaluate the performance of the neural network, two architecture of neural network namely feed-forward algorithm and cascade forward algorithm has been compared and concludes that the cascade forward network performed better than the feed-forward network. All the experiments have been accomplished on 70/30 proportion of randomly divided databases. Among the proposed segmentation techniques, the image after contrast enhancement obtained the best classification accuracy of 88.6% on the CF network of ANN using 16 features of GLCM in four directions. In second experiment feature of LBP and its variants have combined and observed that classification accuracy of LBP, LBPri, LBPu2, LBPriu2, are 86.1%, 84.8%, 87.3%, 89.9% respectively that have also be shown through the tables but when we hybrid these features and form a new feature vector then the CA drastically improved and it achieved 92.4% which is the best among all techniques performed here.

Finally, it is concluded that the segmentation based feature extraction techniques presented here for the classification of radiographic weld flaws have extracted significant features from the image database. Further, it should be stated that employing PCA as a feature vector dimension reduction and selection method has given value addition to the proposed approaches. Among all the proposed methods, the hybridization of suitable segmentation with the combination of LBP LBPri, LBPu2 and LBPriu2 has given the best classification accuracy. Another important finding of this work has been that PCA feature reduction methods do not suffer from information loss compared to full feature vector data. However, it reduced the computational time significantly.

5.2   Scope for Future Work

Even though comprehensive experimental work has been done here, to improve the classification accuracy of weld flaws, following are some of the suggestions for implementation in future research work in this field:

- The proposed approach has used selected mother wavelets to decompose the images by DWT. Several other mother wavelets may be investigated to see their effect on the feature extraction and classification of radiographic images of weld flaws.

- In this study, the PCA (dimensionality reduction) technique has been used to reduce the dimension of feature vector data. Some other techniques such as mRmR, Kernel PCA (dimensionality reduction), genetic algorithm, and correlation-based feature selection may be investigated to reduce the feature vector data.

- Further, to get the multi-resolution images, DWT has been employed. Several other multi-resolution techniques, namely, BWT, Gaussian pyramid (GP), fractional wavelet transform (FRWT) and dual-tree complex wavelet transform (DTCWT) may be investigated to produce significant texture features.

- After compiling the ideas proposed in the present work, an expert system can also be designed and developed to assist the welder for automatic monitoring of the welding process and an indication of flaws in the real-time process.

PUBLICATIONS FROM THE WORK

[1] **Kumar, J.**, Anand,R. S., & Srivastava, S. P., (2014, February). Flaws classification using ANN for radiographic weld images, In IEEE *International Conference on Signal Processing and Integrated Networks (SPIN- 2014), Amity University, Noida,* (pp. 145-150).

[2] **Kumar, J.**, Anand, R. S., & Srivastava, S. P., (2014, January), Multi-class welding flaws classification using texture feature for radiographic images, In IEEE *International Conference on Advances in Electrical Engineering (ICAEE-2014), VIT University, Vellore,* (pp. 1-4).

[3] **Kumar, J.**, Srivastava, S. P., Anand, R. S., & Arvind, P.(2018, December). GLCM and ANN based Approach for Classification of Radiographic weld imagesFlaws classification using ANN for radiographic weld images. In *13th IEEE international conference on Industrial and information system (ICIIS-2018), IIT Roper, 1-2 Dec,2018.*

[4] **Kumar, J.**, Anand, R. S., & Srivastava, S. P., Defect detection using segmentation of radiographic weld images, In International journal of communication networks and distributed systems, (Under review).

[5] **Kumar, J.**, Anand, R. S., & Srivastava, S. P., Classification of radiographic weld images using hybrid wavelet feature extraction techniques, in applied soft computing, Elsevier (Submitted).

REFERENCES

[1]   Smith,B., "Making war on defects. Six-sigma Des," IEEE Spectrum, vol. 30, no. 9, pp. 43-47, 1993.

[2]   Basak, D., "Non-destructive evaluation of drive ropes: a case study," Nondestructive Testing and Evaluation, vol. 20, no. 4, pp. 221 – 229, 2005.

[3]   Grieve,D.   J.,"Welding   Defects,"   www.tech.plym.ac.uk/sme/strc201/ wdefects.htm

[4]   Baumbach, H.,   et   al.,   "Non-destructive   testing   and   quality managementTechnology," Law and Insurance, , vol. 3, no. 3, pp. 191 – 195, 1998.

[5]   Hayes, C., "ABC's of nondestructive weld examination," welding journal, vol.76, no.5, pp. 46-51, 1997.

[6]   Sun, Z., and Karppi.R., "The application of electron beam welding for the joining of dissimilar metals: an overview," *Journal of Materials Processing Technology* vol. 59, no.3, pp. 257-267, 1996.

[7]   Stepinski, T., "Advanced Non destructive methods for inspection of canisters for spent nuclear fuel," Uppsala University. Sweden. Jun 2002.

[8]   "Welding defects to avoid and correct : Solutions with effective, powerful advice,   Description,   search   and   assessment,"www.welding-advisers.com/welding-defects.

[9]   Jebarani, P.N., Sukanesh,R., "Automatic detection of weld defects in pressure vessels using fuzzy neural network,"   International Journal of Computer Applications, vol. 1, no. 21, pp. 119-125, 2010.

[10]   Anouncia, S. M., Saravana,R., "A knowledge model for gray image interpretation with emphasis on welding defect classification," Computer in Industry, vol. 61, pp. 742-749, 2010.

[11]   Daaland, A., "Real time radiography for in service inspection of flexible pipeline system. Trends in NDE science and technology," *InProc. 14th World Conf. Non-Destructive Testing-1996,* New Delhi, vol. 3, pp. 1361-1364.

[12] Rao,B. P. C., "Visual techniques in non-destructive testing," encyclopedia of materials*Science and Technology*, Elsevier Science Ltd, pp. 6043-6046, 2001.

[13] "NDTTechniques",www.ndt.cegelec.com/pages/en/activities/   techniques/ techniques.asp

[14] Valavanis, I., Kosmopoulos, D., "Multiclass defect detection and classification in weld radiographic images using geometric and texture features,"   Expert Systems with Applications, vol. 37, no. 12, pp. 7606-7614, Jul 2010.

[15] Gayer, A., Saya, A., and Shiloh, A., "Automatic recognition of welding defects in real-time radiography", NDT & E International, vol. 23, no.3, pp. 131-136, 1990.

[16] Murakami, K., "Image processing for non-destructive testing," Welding International, vol. 4, no. 2, pp. 144-149, 1990.

[17] Ker, J., and Kengshool, K., "An efficient method for inspecting machined part by a fixtureless machine vision system," In Proc. SME Vision, Detroit, vol. 2, pp. 45-51, 1990.

[18] Nockeman, C., Heidt, H., and Tomsen, N., "Reliability in NDT: ROC study of radiographic weld inspection," NDT & E International, vol. 24, no 5, pp 235-245, 1991.

[19] Kato, Y.,et al.,"Development of an automatic weld defect identification system for radiographic testing," Weld World, vol. 30, no.7/8, pp. 182-188, 1992.

[20] Wu, Z., "Homogeneity testing for unable data: A performance evaluation," CVGIP: Graph. Models Image Process, vol. 55, pp. 370-380, Sept 1993.

[21] Cook,G. E.,et al. "Automated visual inspection and interpretation system for weld quality evaluation," IEEE IAS Annual meeting, pp. 1809-1816, 1995.

[22] Hyatt, R., Kechter,G. E. and Nagashima,S. "A method for defect segmentation in digital radiographs of pipeline girth welds," Materials Evaluations,vol. 54, no.8, pp. 925-928, 1996.

[23] Liao, T. W.   and Ni,J., "An automated radiographic NDT system for weld inspection. Part I. weld extraction," NDT & E International, vol. 29, no. 3, pp. 157-162, 1996.

[24] Liao, T. W. and Tang, K., "Automated extraction of welds from digitized radiographic images based on MLP neural networks,"Applied Artificial Intelligence, vol. 11, no. 3, pp. 197-218, 1997.

[25] Liao, T. W. and Li,Y. M. "An automated radiographic NDT system for weld inspection. Part II. Flaw detection," NDT & E International, vol. 31, no. 3, pp. 183-192, 1998.

[26] Liao,T.W., Li,D.M. and Li, Y.M., "Detection of welding flaws from radiographic images with fuzzy clustering methods," Fuzzy Sets and Systems, vol.108, no. 2, pp. 145–158,1999.

[27] Liao,T. W. Li, D. M. andLi,Y. M. "Extraction of welds from radiographic images using fuzzy classifiers," Information Science, vol. 126, no. 1-4, pp. 21-42, 2000.

[28] Laggoune, H. and Gouton, S. P., "Dimensional analysis of the welding zone," In Proc. 22nd International Conf. Information Technology Interface, 2000, pp. 451-456.

[29] Chan, C. and Grantham, K. H. "Fabric defect detection by fourier analysis,"IEEE transactions on Industry Applications, vol. 36, no. 5, pp. 1267-1275, 2000.

[30] Elewa,I. M. et al., "Assessments of welding defects for gas pipeline radiographs using computer vision," Proc. Third Assuit International Conf. Mech. Engg. Advanced Technol. for Industrial Production, Assiut, Egypt, 2000, pp. 216-223.

[31] Mery, D. andBerti, M. A., "Automatic detection of welding defects using texture features," Insight, vol. 45, pp. 676-681, 2003.

[32] Silva, D. Romeu R., et al. "Estimated accuracy of classification of defects detected in welded joints by radiographic tests," NDT & E International vol. 38, no.5, pp. 335-343, 2005.

[33] Wang, X.,et al. "Image enhancement for radiography inspection,"ThirdInternational Conference on Experimental Mechanics, 2005, Vol. 5852, International Society for Optics and Photonics, 2005.

[34] Silva, R. R., et al. "Pattern recognition of weld defects detected by radiographic test," NDT & E International, vol. 37, no. 6, pp. 461-470, 2004.

[35] Alaknanda, Kumar, P. and Anand, R. S., "Flaw detection in radiographic weld images using Morphological approach," NDT&E International, vol. 39, no. 1, pp. 29-33, 2006.

[36] Nanditha, N.M. and Manoharan, N., "Comparative study on the suitability of feature extraction techniques for tungusten inclusion and hotspot detection from weld thermographs for online weld montoring", International Journal of Engineering and Material science, vol. 17 pp. 20-26, Feb 2010.

[37] Vilar, R. and Zapata, J. "An adaptive-network-based fuzzy inference system for classification of welding defects," NDT & E International, vol. 43, no. 3, pp. 191-199, 2010.

[38] Zapata, J., Vilar, R. and Ruiz, R., "Performance Evaluation of an automatic inspection system of weld defects in radiographic images based on neuro – classifiers," vol. 38, no. 7, pp. 8812 -8824, 2011.

[39] Wang, G.and Liao T. W., Automatic identification of differ-ent types of welding defects in radiographic images," NDT & E International, vol. 35, no. 8, pp. 519–528, 2002.

[40] Liao TW.,"Classification of welding flaw types with fuzzy expert systems," Expert Systems with Applications, vol. 25, no. 1, pp. 101–111, 2003.

[41] Liao TW.,"Improving the accuracy of computer-aided radio-graphic weld inspection by feature selection," NDT & E International, vol. 42, no. 4, pp. 229-239. 2009.

[42] Vilar R, Zapta J, Ruiz R.,"An automatic system of classifi-cation of weld defects in radiographic images," NDT & E International,vol. 42, no. 5, pp. 467-476, 2009.

[43] Kumar G.S., et al.,"Quality level assessment for imperfections in GMAW," Welding Journal. vol. 93, no. 3, pp. 85-97, 2014.

[44] Kumar G.S., Natarajan U., Ananthan S.S.,"Vision inspection system for the identification and classification of defects in MIG welding joints," International Journal of Advanced Manufacturing Technology (IJAMT), vol. 61, no. 9, pp. 923-933, 2012.

[45] Wang Y. et al.,"Detection of line weld defects based onmultiple thresholds and support vector machine," NDT & E International, vol. 41, no. 7, pp. 517-524, 2008.

[46] Shafeek H.I. et al., "Assessment of welding defects for gas pipeline radiographs using computer vision," NDT & E International, vol. 37, no. 4, pp. 291-299, 2004.

[47] Shafeek, H.I., et al., "Automatic inspection of gas pipeline welding defects using an expert vision system,"NDT & E International, vol. 37, no. 4, pp. 301-307, 2004.

[48] Sun Y. et al., "Real-time automatic detection of weld defects in steel pipe" NDT & E International, vol. 38, no. 7, pp. 522-528, 2005.

[49] Tridi M., Belaifa S., Nacereddine N.,"Weld defect classifica-tion using EM algorithm for Gaussian mixture model," 3rd International Conferences: Sciences of Electronic, Technologies of information and Telecommunications. 2005; p. 1-7.

[50] Da Silva R.R. et al. "Radiographics pattern recognition of welding defects using linear classifier," Insight, vol. 43, no. 10, pp. 669-674, 2001.

[51] Da Silva R.R. et al.,"Estimated accuracy of classification of defects detected in welded joints by radiographic tests," NDT & E International, vol. 38, no. 5, pp. 335-343, 2004.

[52] Da Silva R.R. et al.,"Patterns nonlinear classifiers of weld defects in industrial radiographies," American Conferences for Nondestructive Testing, 2003, pp. 1-12.

[53] Lim T.Y., Ratnam M.M., Khalid M.A.,"Automatic classification of weld defects using simulated data and an MLP neural network,"Insight-Non-Destructive Testing and Condition Monitoring, vol. 49, no.3, pp. 154-159, 2007.

[54] Nacereddine N., Hamami L., Ziou D.,"Image thresholding for weld defect extraction in industrial radiographic testing" International Journal of Computer, Electrical, Automation, Control and Information Engineering, vol. 1, no. 7, pp. 2027-35, 2007.

[55] Aoki, L., Suga, Y.,"Application of artificial neural network to discrimination of defect type in automatic radiographic testing of welds" ISIJ International, vol. 39, no. 10, pp. 1081-87, 1998.

[56] Borselli, A., et al. "Surface defects classification in steel products: A comparison between different artificial intelligence-based approaches," 11th IASTED International Conference on Artificial Intelligence and Applications AIA, 2011, pp. 129-134.

[57] Doring, C., et al.,"Improving Surface Defect Detection for Quality Assessment of Car Body Panels," Mathware & Soft Computing, vol.11, no. 4, pp. 163-177, 2004.

[58] Eichhorn, A., et al., "Soft Computing for Automated Surface Quality Analysis of Exterior Car Body Panels," Applied Soft Computing. 2005; 5(3):301-13.

[59] Jelen, L., Fevens, T., Krzyzak, A.,"Classification of Breast Cancer Malignancy Using Cytological Images of Fine Needle Aspiration Biopsies," International Journal of Applied Math and Computer Sciences, vol. 18, no. 1, pp. 75-83, 2008.

[60] Goa, F., Li Z., et al.,"An Online Inspection System of Surface Defects for Copper Strip Based on Computer Vision," 5th International Congress on Image and Signal Processing, 2012; pp. 1200-04.

[61] Kamani, P., Afshar, A., et al.,"Car body paint defect inspec-tion using rotation invariant measure of the local variance and one-against-all support vector machine," 1st IEEE International Conferences on Informatics and Computational Intelligence 2011; pp. 244-49.

[62] Kamani, P., et al.,"Automatic paint defect detection and classification of car body," Machine Vision and Image Processing (MVIP), 2011; pp. 1-6.

[63] Swillo, S.J., Perzyk, M.,"Surface Casting Defects Inspection Using Vision System and Neural Network Techniques," Archives of Foundry Engineering, vol. 13, no. 4, pp. 103-106, 2013.

[64] Sulaiman M., et al., "A 3D Gluing Defect Inspection System Using Shape-Based Matching Application from two Cameras," In International Review on Computers and Software (IRECOS), vol. 8. no. 8, pp.1997-2004, 2013.

[65] Sulaiman M., et al., "Defect Inspection System for Shape-Based Matching Using Two Cameras," Journal of Theoretical and Applied Information Technology (JATIT), vol. 61, no. 2, pp. 288-97, 2014.

[66] Venkatraman, B., Raj, M.A., Vaithiyanathan, V.,"Weld Defect Detection using Iterative Image Reconstruction Methods," Indian Journal of Science and Technology, vol. 6, no. 4, 2013.

[67] Sudheera, K., and Nandhitha, N.M.,"Application of Hilbert Transform for Flaw Characterization in Ultrasonic Signals" Indian Journal of Science and Technology,vol. 8, no. 13, 2015.

[68] Biswas, K. K. and Basu, S. K., "Gesture recognition using Microsoft Kinect®," in 5th International Conference on Automation, Robotics and Applications (ICARA) 2011, pp. 100-103.

[69] Hellwich, O., Laptev, I., and Mayer, H., "Extraction of linear objects from interferometric SAR data," International Journal of Remote Sensing, vol. 23, no. 3, pp. 461-475, 2002.

[70] Jaeger, M., Reigber, A., and Hellwich, O., "A non-parametric texture descriptor for polarimetric sar data with applications to supervised classification," in Proceedings of 10th European Conference on Synthetic Aperture Radar,EUSAR 2014, pp. 1-4.

[71] Klaghstan, M., Haensch, R., Coquil, D., and Hellwich, O., "Impact of hierarchical structures in image categorization systems," in 3rd International Conference on Image Processing Theory, Tools and Applications (IPTA) 2012, pp. 367-370.

[72] Li, W., You, J., and Zhang, D., "Texture-based palmprint retrieval using a layered search scheme for personal identification," *IEEE Transactions on Multimedia,* vol. 7, no. 5, pp. 891-898, 2005.

[73] Patil, H. A., Dutta, P. K., and Basu, T., "Comparison of performance of different speech features for identification of professional mimics in Hindi and Urdu languages," in National Symposium on Acoustics, 2004, pp. 25-27.

[74] Sarfraz, M. S., and Hellwich, O., "Probabilistic learning for fully automatic face recognition across pose," Image and Vision Computing, vol. 28, no. 5, pp. 744-753, 2010.

[75] You, J., Li, W., and Zhang, D., "Hierarchical palmprint identification via multiple feature extraction," *Pattern recognition,* vol. 35, no. 4, pp. 847-859, 2002.

[76] Zhang, D., Kong, W.-K., You, J., and Wong, M., "Online palmprint identification," *IEEE Transactions on Pattern Analysis and Machine Intelligence,* vol. 25, no. 9, pp. 1041-1050, 2003.

[77] Bhuyan, M., Ghosh, D., and Bora, P., "Feature extraction from 2D gesture trajectory in dynamic hand gesture recognition," in IEEE Conference on Cybernetics and Intelligent Systems, 2006 pp. 1-6.

[78] Haralick, R. M., Shanmugam, K., and Dinstein, I. H., "Textural features for image classification," *IEEE Transactions on Systems, Man and Cybernetics*, no. 6, pp. 610-621, 1973.

[79] Daugman, J. G., "Uncertainty relation for resolution in space, spatial frequency, and orientation optimized by two-dimensional visual cortical filters," *JOSA A,* vol. 2, no. 7, pp. 1160-1169, 1985.

[80] Soh, L.K., and Tsatsoulis, C., "Texture analysis of SAR sea ice imagery using gray level co-occurrence matrices," *IEEE Transactions on Geoscience and Remote Sensing,* vol. 37, no. 2, pp. 780-795, 1999.

[81] Mu, T., Nandi, A. K., and Rangayyan, R. M., "Classification of breast masses using selected shape, edge-sharpness, and texture features with linear and kernel-based classifiers," *Journal of digital imaging,* vol. 21, no. 2, pp. 153-169, 2008.

[82] Galloway, M. M., "Texture analysis using gray level run lengths," *Computer graphics and image processing,* vol. 4, no. 2, pp. 172-179, 1975.

[83] Ojala, T., Pietikainen, M., and Harwood, D., "Performance evaluation of texture measures with classification based on Kullback discrimination of distributions," in Proceedings of the 12th IAPR International Conference on Pattern Recognition, Vol. 1-Conference A: Computer Vision & Image Processing, 1994, pp. 582-585.

[84] Ojala, T., Pietikäinen, M., and Harwood, D., "A comparative study of texture measures with classification based on featured distributions," *Pattern recognition,* vol. 29, no. 1, pp. 51-59, 1996.

[85] Nanni, L., Brahnam, S., and Lumini, A., "Combining different local binary pattern variants to boost performance," *Expert Systems with Applications,* vol. 38, no. 5, pp. 6209-6216, 2011.

[86] Nanni, L., Lumini, A., and Brahnam, S., "Local binary patterns variants as texture descriptors for medical image analysis," *Artificial intelligence in medicine,* vol. 49, no. 2, pp. 117-125, 2010.

[87] Nanni, L., Lumini, A., and Brahnam, S., "Survey on LBP based texture descriptors for image classification," *Expert Systems with Applications,* vol. 39, no. 3, pp. 3634-3641, 2012.

102

[88]   Ojala, T., Pietikainen, M., and Maenpaa, T., "Multiresolution gray-scale and rotation invariant texture classification with local binary patterns," *IEEE Transactions on Pattern Analysis and Machine Intelligence,* vol. 24, no. 7, pp. 971-987, 2002.

[89]   Pietikäinen, M., Hadid, A., Zhao, G., and Ahonen, T., "Computer vision using local binary patterns," *Computational Imaging and Vision*, 2011.

[90]   Mäenpää, T., *The local binary pattern approach to texture analysis: extenxions and applications*: Oulun yliopisto, 2003.

[91]   Pietikäinen, M., Ojala, T., and Xu, Z., "Rotation-invariant texture classification using feature distributions," *Pattern Recognition,* vol. 33, no. 1, pp. 43-52, 2000.

[92]   Ahonen, T., Matas, J., He, C., and Pietikäinen, M., "Rotation invariant image description with local binary pattern histogram fourier features," *Image Analysis*, pp. 61-70: Springer, 2009.

[93]   Zhao, G., Ahonen, T., Matas, J., and Pietikainen, M., "Rotation-invariant image and video description with local binary pattern features," *IEEE Transactions on Image Processing,* vol. 21, no. 4, pp. 1465-1477, 2012.

[94]   Guo, Z., Zhang, D., and Zhang, S., "Rotation invariant texture classification using adaptive LBP with directional statistical features," in 17th IEEE International Conference on Image Processing (ICIP), 2010, pp. 285-288.

[95]   Guo, Z., and Zhang, D., "A completed modeling of local binary pattern operator for texture classification," *IEEE Transactions on Image Processing* vol. 19, no. 6, pp. 1657-1663, 2010.

[96]   Zhang, L., Zhou, Z., and Li, H., "Binary Gabor pattern: An efficient and robust descriptor for texture classification," in 19th IEEE International Conference on Image Processing (ICIP), 2012, pp. 81-84.

[97]   Canuto, A. M., Vale, K. M., Feitos, A., and Signoretti, A., "ReinSel: A class-based mechanism for feature selection in ensemble of classifiers," *Applied Soft Computing,* vol. 12, no. 8, pp. 2517-2529, 2012.

[98]   Yaghouby, F., Ayatollahi, A., and Soleimani, R., "Classification of cardiac abnormalities using reduced features of heart rate variability signal," *World Applied Sciences Journal,* vol. 6, no. 11, pp. 1547-1554, 2009.

[99] Yaghouby, F., Ayatollahi, A., Bahramali, R., and Yaghouby, M., "Robust genetic programming-based detection of atrial fibrillation using RR intervals," *Expert Systems,* vol. 29, no. 2, pp. 183-199, 2012.

[100] Yaghouby, F., Ayatollahi, A., Bahramali, R., Yaghouby, M., and Alavi, A. H., "Towards automatic detection of atrial fibrillation: A hybrid computational approach," *Computers in biology and medicine,* vol. 40, no. 11, pp. 919-930, 2010.

[101] Camastra, F., "Data dimensionality estimation methods: a survey," *Pattern recognition,* vol. 36, no. 12, pp. 2945-2954, 2003.

[102] Jack, L., and Nandi, A., "Support vector machines for detection and characterization of rolling element bearing faults," *Proceedings of the Institution of Mechanical Engineers, Part C: Journal of Mechanical Engineering Science,* vol. 215, no. 9, pp. 1065-1074, 2001.

[103] Bond, B., *Wood Identification for hardwood and softwood species native to Tennessee*: Agricultural Extension Service, University of Tennessee, 2002.

[104] Brazier, J., and Franklin, G., "Identification of hardwoods: a microscopic key," *For. Prod. Res. Bull,* vol. 46, 1961.

[105] Chowdhury, S., Sing, J. K., Basu, D. K., and Nasipuri, M., "Face recognition by generalized two-dimensional FLD method and multi-class support vector machines," *Applied Soft Computing,* vol. 11, no. 7, pp. 4282-4292, 2011.

[106] Coussement, K., and Van den Poel, D., "Churn prediction in subscription services: An application of support vector machines while comparing two parameter-selection techniques," *Expert systems with applications,* vol. 34, no. 1, pp. 313-327, 2008.

[107] Khadtare, M. S., and Sahambi, J., "ECG arrhythmia analysis by multicategory support vector machine," *Applied Computing*, pp. 100-107: Springer, 2004.

[108] Liu, M., Wang, M., Wang, J., and Li, D., "Comparison of random forest, support vector machine and back propagation neural network for electronic tongue data classification: Application to the recognition of orange beverage and Chinese vinegar," *Sensors and Actuators B: Chemical,* vol. 177, pp. 970-980, 2013.

[109] Lyle, J. R., Miller, P. E., Pundlik, S. J., and Woodard, D. L., "Soft biometric classification using local appearance periocular region features," *Pattern Recognition,* vol. 45, no. 11, pp. 3877-3885, 2012.

[110] Malhotra, R., "Comparative analysis of statistical and machine learning methods for predicting faulty modules," *Applied Soft Computing,* vol. 21, pp. 286-297, 2014.

[111] Xu, H., Caramanis, C., and Mannor, S., "Robustness and regularization of support vector machines," *The Journal of Machine Learning Research,* vol. 10, pp. 1485-1510, 2009.

[112] Yaghouby, F., and Ayatollahi, A., "An arrhythmia classification method based on selected features of heart rate variability signal and support vector machine-based classifier," in World Congress on Medical Physics and Biomedical Engineering, September 7-12, 2009, Munich, Germany, 2010, pp. 1928-1931.

[113] Cortes, C., and Vapnik, V., "Support-vector networks," *Machine learning,* vol. 20, no. 3, pp. 273-297, 1995.

[114] Fan, R. E., et al., "LIBLINEAR: A library for large linear classification," *The Journal of Machine Learning Research,* vol. 9, pp. 1871-1874, 2008.

[115] Platt, J. C., Cristianini, N., and Shawe-Taylor, J., "Large margin DAGs for multiclass classification," in Proceedings of Neural Information Processing Systems (NIPS), 1999, pp. 547-553.

[116] Crammer, K., and Singer, Y., "On the learnability and design of output codes for multiclass problems," *Machine Learning,* vol. 47, no. 2-3, pp. 201-233, 2002.

[117] Ben-Hur, A., et al., "Support vector machines and kernels for computational biology," *PLoS computational biology,* vol. 4, no. 10, pp. e1000173, 2008.

[118] Yuan, G.-X., Ho, C.-H., and Lin, C.-J., "Recent advances of large-scale linear classification," *Proceedings of the IEEE,* vol. 100, no. 9, pp. 2584-2603, 2012.

[119] Shan, C., Gong, S., and McOwan, P. W., "Facial expression recognition based on local binary patterns: A comprehensive study," *Image and Vision Computing,* vol. 27, no. 6, pp. 803-816, 2009.

[120] Alexandre, L. A., "Gender recognition: A multiscale decision fusion approach," *Pattern Recognition Letters,* vol. 31, no. 11, pp. 1422-1427, 2010.

[121] Heikkilä, M., Pietikäinen, M., and Schmid, C., "Description of interest regions with local binary patterns," *Pattern recognition,* vol. 42, no. 3, pp. 425-436, 2009.

[122] Chu, W.-S., Huang, C.-R., and Chen, C.-S., "Gender classification from unaligned facial images using support subspaces," *Information Sciences,* vol. 221, pp. 98-109, 2013.

[123] Apatean, A., Rogozan, A., Emerich, S., and Bensrhair, A., "Wavelets as features for objects recognition," *Acta Tehnica Napocensis,* vol. 49, no. 2, 2008.

[124] Nikam, S. B., and Agarwal, S., "Wavelet energy signature and GLCM features-based fingerprint anti-spoofing," in International Conference on Wavelet Analysis and Pattern Recognition (ICWAPR'08), 2008, pp. 717-723.

[125] Anand, C. S., and Sahambi, J. S., "Wavelet domain non-linear filtering for MRI denoising," *Magnetic Resonance Imaging,* vol. 28, no. 6, pp. 842-861, 2010.

[126] Jain, V., and Sahambi, J., "Neural network and wavelets in arrhythmia classification," *Applied Computing*, pp. 92-99: Springer, 2004.

[127] Bruce, L. M., Koger, C. H., and Li, J., "Dimensionality reduction of hyperspectral data using discrete wavelet transform feature extraction," *IEEE Transactions on Geoscience and Remote Sensing,* vol. 40, no. 10, pp. 2331-2338, 2002.

[128] Koenderink, J. J., "The structure of images," *Biological cybernetics,* vol. 50, no. 5, pp. 363-370, 1984.

[129] Mallat, S. G., "A theory for multiresolution signal decomposition: the wavelet representation," *IEEE Transactions on Pattern Analysis and Machine Intelligence,* vol. 11, no. 7, pp. 674-693, 1989.

[130] Prasad, G. K., and Sahambi, J., "Classification of ECG arrhythmias using multi-resolution analysis and neural networks," in Conference on Convergent Technologies for the Asia-Pacific Region TENCON 2003, 2003, pp. 227-231.

[131] Pujara, C., Bhardwaj, A., Gadre, V. M., and Khire, S., "Secure watermarking in fractional wavelet domains," *IETE Journal of Research,* vol. 53, no. 6, pp. 573-580, 2007.

[132] Sengar, R. S., Upadhyay, A. K., Singh, M., and Gadre, V. M., "Segmentation of two dimensional electrophoresis gel image using the wavelet transform and the watershed transform," in National Conference on Communications (NCC), 2012, pp. 1-5.

[133] Sharma, M., Gadre, V. M., and Porwal, S., "An eigenfilter-based approach to the design of time-frequency localization optimized two-channel linear phase biorthogonal filter banks," *Circuits, Systems, and Signal Processing,* vol. 34, no. 3, pp. 931-959, 2015.

[134] Sharma, M., Kolte, R., Patwardhan, P., and Gadre, V., "Time-frequency localization optimized biorthogonal wavelets," in International Conference on Signal Processing and Communications (SPCOM), 2010, pp. 1-5.

[135] You, J., and Bhattacharya, P., "A wavelet-based coarse-to-fine image matching scheme in a parallel virtual machine environment," *IEEE Transactions on Image Processing,* vol. 9, no. 9, pp. 1547-1559, 2000.

[136] Deka, B., and Bora, P. K., "Wavelet-based despeckling of medical ultrasound images," *IETE Journal of Research,* vol. 59, no. 2, pp. 97-108, 2013.

[137] Gupta, R. D., Dash, J. K., and Mukhopadhyay, S., "Rotation invariant textural feature extraction for image retrieval using eigen value analysis of intensity gradients and multi-resolution analysis," Pattern Recognition, vol. 46, no. 12, pp. 3256-3267, 2013.

[138] Livens, S., Scheunders, P., Van de Wouwer, G., and Van Dyck, D., "Wavelets for texture analysis, an overview," in 6th International Conference on Image Processing and Its Applications, 1997, pp. 581-585.

[139] Mukhopadhyay, S., Dash, J. K., and Gupta, R. D., "Content-based texture image retrieval using fuzzy class membership," *Pattern Recognition Letters,* vol. 34, no. 6, pp. 646-654, 2013.

[140] Nirmala, S., Dandapat, S., and Bora, P., "Wavelet weighted blood vessel distortion measure for retinal images," *Biomedical Signal Processing and Control,* vol. 5, no. 4, pp. 282-291, 2010.

[141] Nirmala, S., Dandapat, S., and Bora, P., "Wavelet weighted distortion measure for retinal images," *Signal, Image and Video Processing,* vol. 7, no. 5, pp. 1005-1014, 2013.

[142] Sharma, L., Tripathy, R., and Dandapat, S., "Multiscale energy and eigenspace approach to Detection and Localization of Myocardial Infarction," *IEEE Transactions on Biomedical Engineering*, vol. 62, no. 7, pp. 1827-1837, 2015.

[143] Jain, V., and Sahambi, J., "Neural network and wavelets in arrhythmia classification," *Applied Computing*, pp. 92-99: Springer, 2004.

[144] Kumar. D,P. d. Carvalho, M. Antunes, J. Henriques, M. Maldonado, R. Schmidt, J. Habetha, "Wavelet transform and simplicity based heart murmur segmentation in computer in cardiology,2006, IEEE, pp-173-176

[145] Sharma, H., Zerbe, N., Heim, D., Wienert, S., Behrens, H.-M., Hellwich, O., and Hufnagl, P., "A multi-resolution approach for combining visual information using nuclei segmentation and classification in histopathological images," in Proceedings of the International Conference on Computer Vision Theory and Applications (VISAPP 2015), Berlin Germany, 2015, pp. 37-46.

[146] Pan, S., and Kudo, M., "Recognition of wood porosity based on direction insensitive feature sets," *Transactions on Machine Learning and Data Mining,* vol. 5, no. 1, pp. 45-62, 2012.

[147] Sripath, D., "Efficient implementations of discrete wavelet transforms using FPGAs," Open Access, Department of Electrical and Computer Engineering, The Florida State University, 2003.

[148] Wang, J. Z., Wiederhold, G., Firschein, O., and Wei, S. X., "Content-based image indexing and searching using Daubechies' wavelets," International Journal on Digital Libraries, vol. 1, no. 4, pp. 311-328, 1998.

[149] Dixon, S., Edwards, C. and Palmer, S. B., "A laser–EMAT system for ultrasonic weld inspection," Ultrasonics, vol.37, no.4, pp.273-281, 1999.

[150] Liao, T. W. and J. Ni, J., "An automated radiographic NDT system for weld inspection: part I—weld extraction," NDT & EInternational , vol. 29, no. 3, pp.157-162, 1996.

[151] Liao, T. W. and Li, Y., "An automated radiographic NDT system for weld inspection: Part II—Flaw detection," NDT & EInternational, vol. 31, no. 3, pp.183 - 192, 1998.

[152] Barai, V. and Reich, Y., "Weld classification in radiographic images: data mining approach," Proceedings of National Seminar on Non Destructive Evaluation, Chennai, 2002.

[153] Yin, Y. and Tian, G. Y. "Feature extraction and optimisation for x-ray weld image classification." Proceedings of 17th World Conference on Nondestructive Testing, Shanghai, 2008.

[154] Mekhalfa F. and Nacereddine, N.,"Multiclass classification of weld defects in radiographic images based on support vector machines," IEEE Tenth
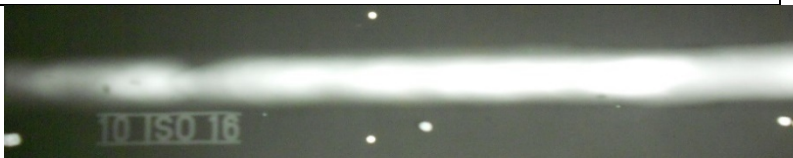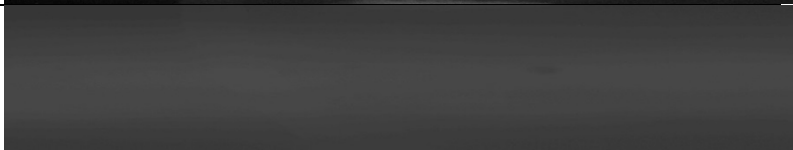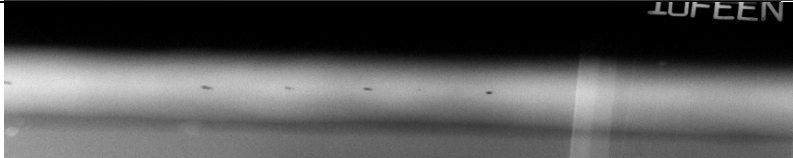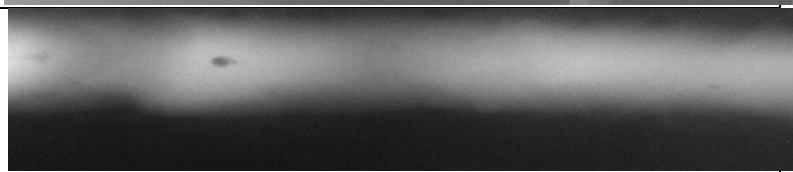
International Conference on Signal-Image Technology and Internet-Based Systems (SITIS), Washington, 2014.
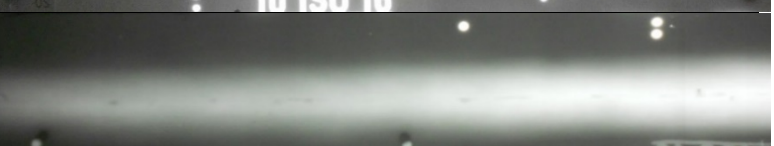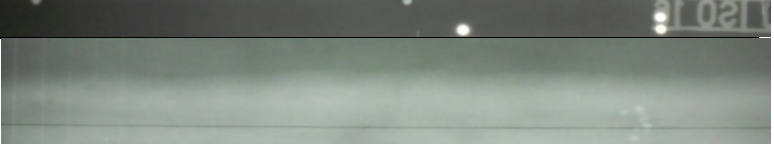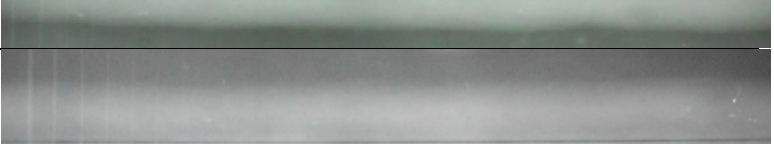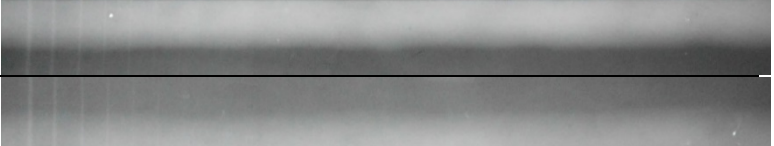
[155] Azari, A., Moghaddam, and Rangarajan,L. "Classification of welding defects in radiographic images," Pattern Recognition and Image Analysis, vol. 26, no. 1, pp. 54 - 60, 2016.

[156] Matlab 2017a, The Mathworks, Inc.

[157] DaSilva,R. R. andMery, D. "Radiographic Testing: Part I, Image Processing,"Materials Evaluation, vol. 643, pp. 1 - 9, 2007.

[158] Changying,D. et al., "Multi-step radiographic image enhancement conforming to weld defect segmentation," IET Image Processing, vol. 9, no. 11, pp.943 - 950, 2015.

[159] Yadav,G.,Maheshwari, S. and A. Agarwal., "Contrast limited adaptive histogram equalization based enhancement for real time video system," International Conference on Advances in Computing, Communications and Informatics (ICACCI-2014), pp. 2392 - 2398.

[160] Rathod, V. R., & Anand, R. S., "A comparative study of different segmentation techniques for detection of flaws in NDE weld images" Journal of Nondestructive Evaluation, vol. 31, no. 1, pp.1-16, 2012.

[161] Kumar, J., Anand R. S.and Srivastava,S. P. "Multi - Class welding flaws classification using texture feature for radiographic images," 2014 International Conference on Advances in Electrical Engineering (ICAEE), Vellore, 2014, pp. 1-4.
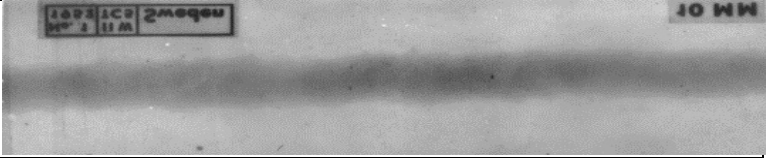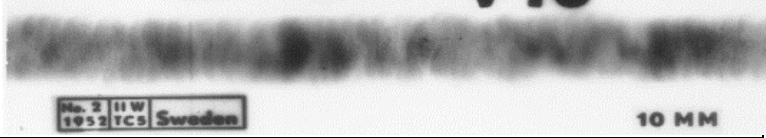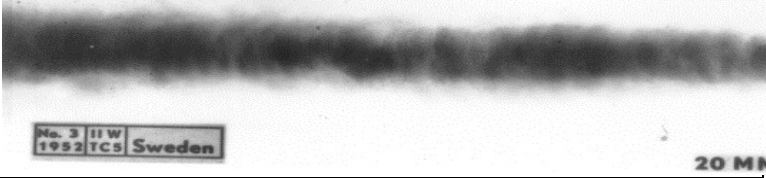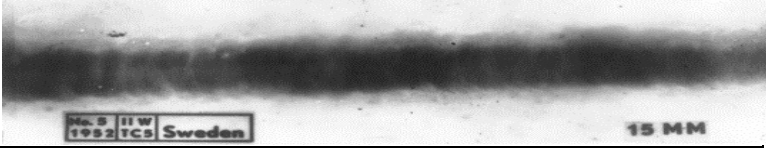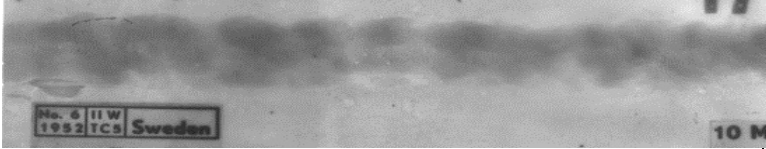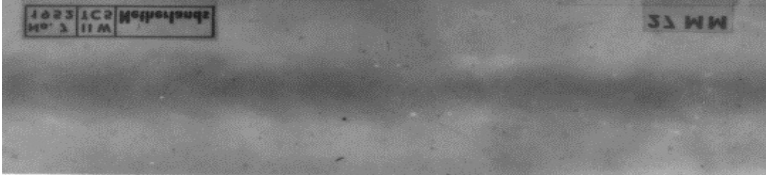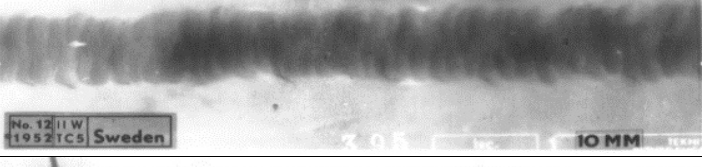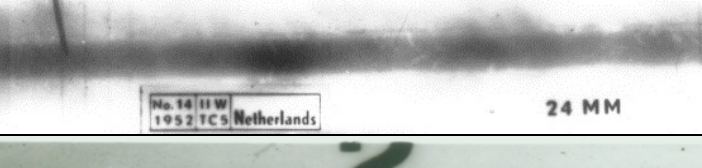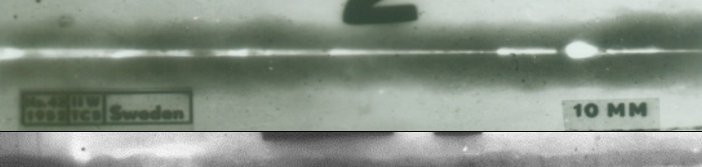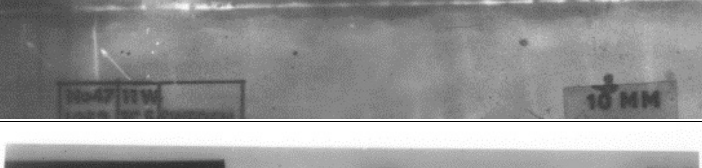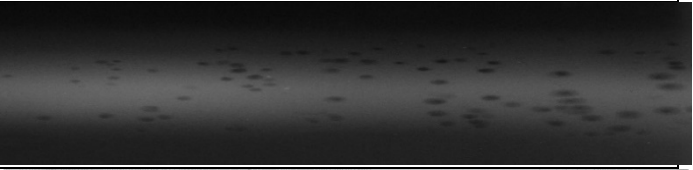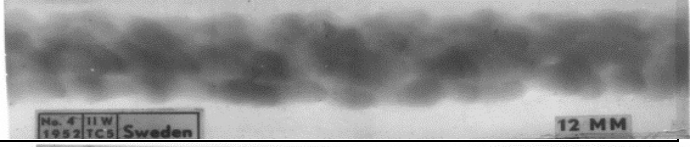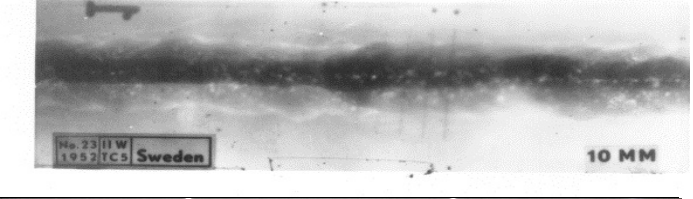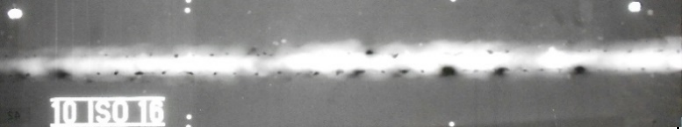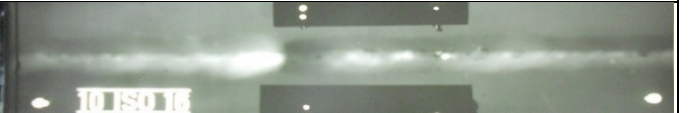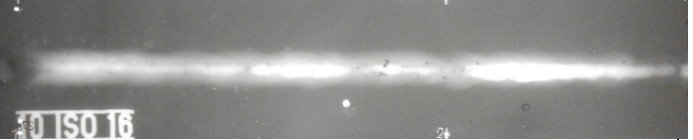
IMAGE DATABASE

In total 79 images have been considered. The image has been collected from Welding Research Laboratory, Department of Mechanical and Industrial Engineering, Indian Institute of Technology Roorkee. This database consists of 09 types of weld flaws images.
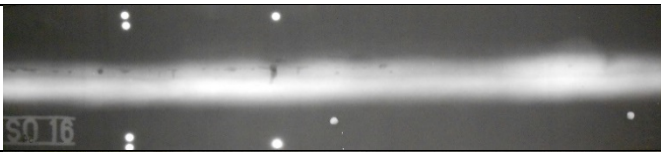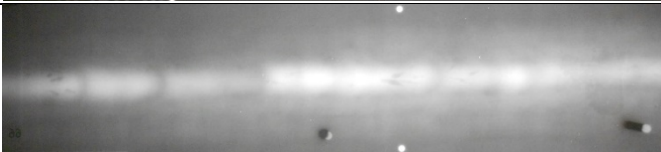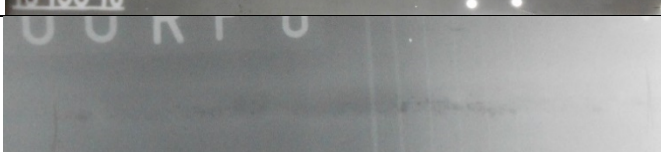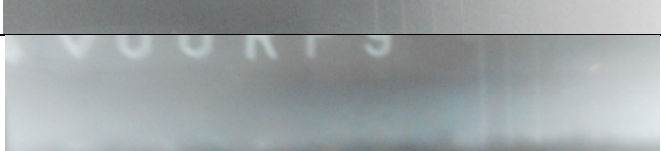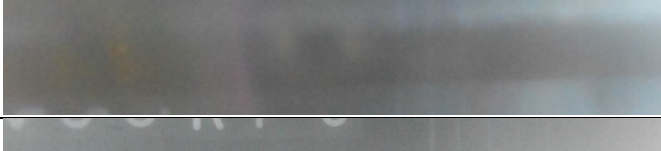
S. No	Type of Flaws	Image
1.		
2		
3		
4	Gas Cavity	
5		
6		
7		
S. No	Type of Flaws	Image
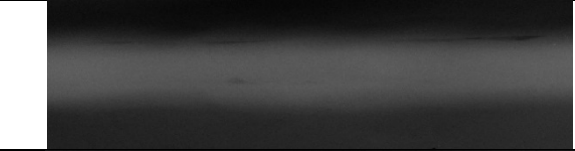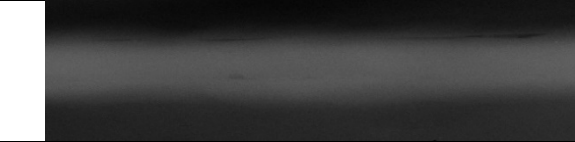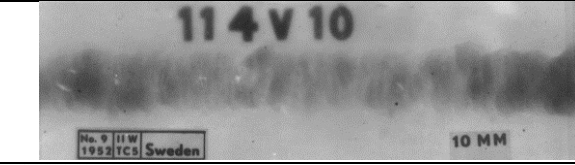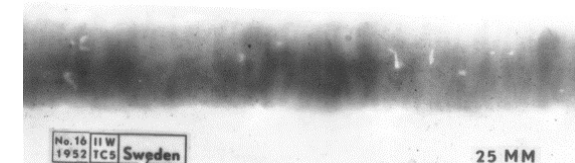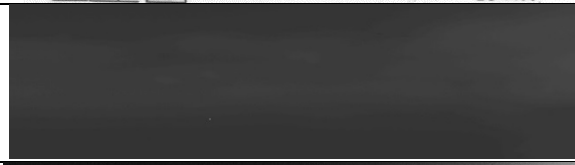
8	**Gas Cavity**		
9			
10			
11	**Lack of Penetration**		
12			
13			
14			
15			
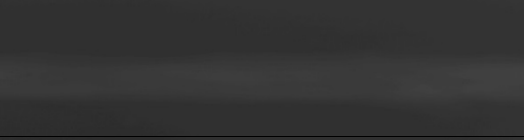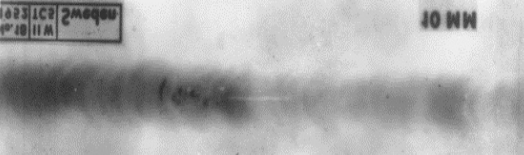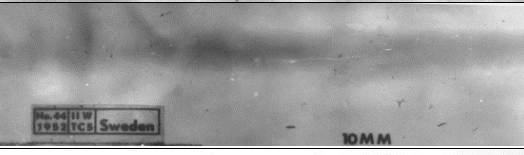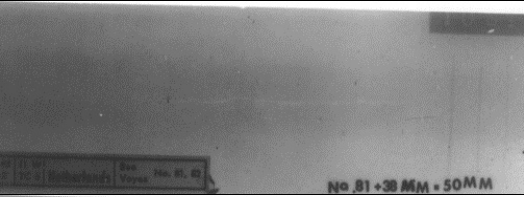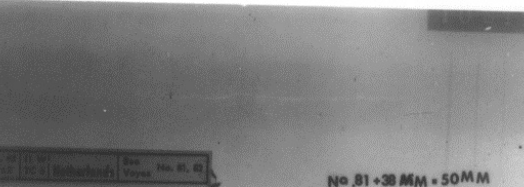
S. No	Type of Flaw	Image
16		
17		
18	**Lack of**	
19	**Penetration**	
20		
21		
22		
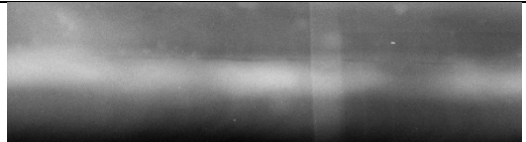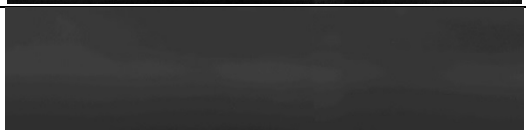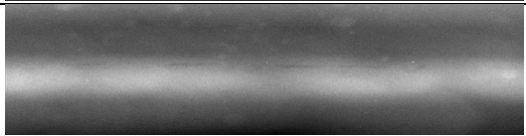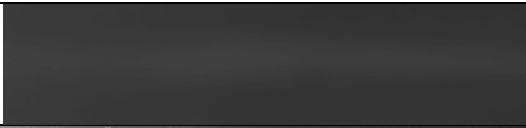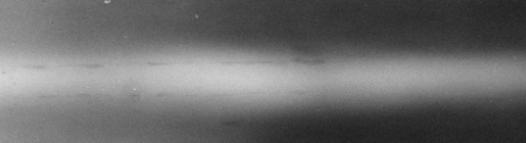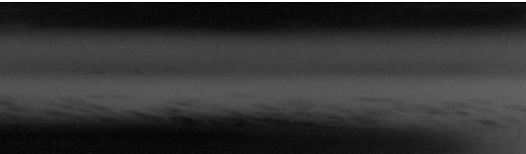
S. No	Type of Flaw	Image
23		
24		
25	Lack of Penetration	
26		
27		
28		
29	Porosity	
30		
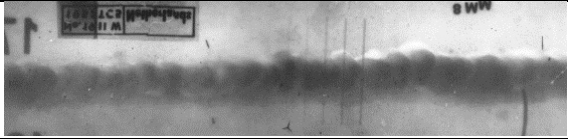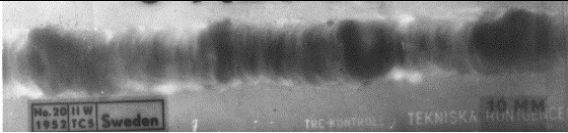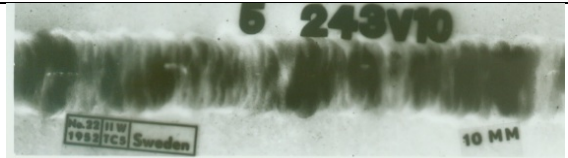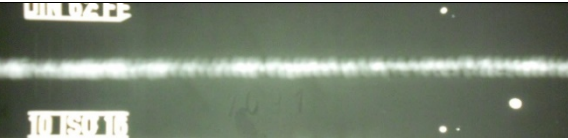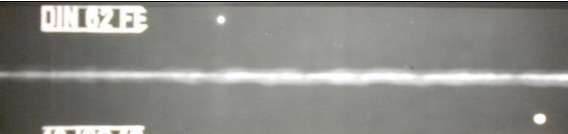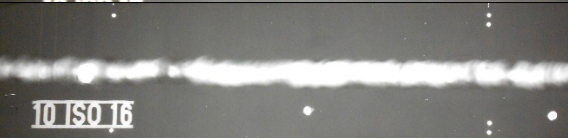
S. No	Type of Flaw	Image
31	Porosity	
32		
33		
34		
35		
36	Slag	
37		
38		
39		

S. No	Type of Flaw	Image
40		
41		
42		
43		
44	Slag	
45		
46		
47		

S. No	Type of Flaw	Image
48		
49	**Slag**	
50		
51		
52	**Crack**	
53		
54		

S. No	Type of Flaw	Image
55		
56		
57		
58		
59	Crack	
60		
61		
62		

S. No	Type of Flaw	Image
63		
64		
65	Lack of Fusion	
66		
67		
68		
69		
70	Worm Hole	
71		

S. No	Type of Flaw	Image
72	**Under Cut**	
73		
74		
75	**No Defect**	
76		
77		
78		
79		